STATE OF THE CALIFORNIA CURRENT 2018–19: A NOVEL ANCHOVY REGIME AND A NEW MARINE HEATWAVE?

Article · January 2019

CITATION
1

READS
270

41 authors, including:

Andrew Richard Thompson
Southwest Fisheries Science Center
76 PUBLICATIONS **1,253** CITATIONS
SEE PROFILE

Isaac D. Schroeder
National Oceanic and Atmospheric Administration
43 PUBLICATIONS **1,256** CITATIONS
SEE PROFILE

Steven Bograd
University of California, Santa Cruz
260 PUBLICATIONS **10,736** CITATIONS
SEE PROFILE

Elliott Lee Hazen
National Oceanic and Atmospheric Administration
183 PUBLICATIONS **5,100** CITATIONS
SEE PROFILE

STATE OF THE CALIFORNIA CURRENT 2018–19: A NOVEL ANCHOVY REGIME AND A NEW MARINE HEAT WAVE?

ANDREW R. THOMPSON*
National Marine Fisheries Service
Southwest Fisheries Science Center
8901 La Jolla Shores Drive
La Jolla, CA, 92037-1509
andrew.thompson@noaa.gov

ISAAC D. SCHROEDER[1,2], STEVEN J. BOGRAD[1], ELLIOTT L. HAZEN[1], MICHAEL G. JACOX[1,3], ANDREW LEISING[1], AND BRIAN K. WELLS[4]
[1]Southwest Fisheries Science Center
National Marine Fisheries Service
99 Pacific Street, Suite 255A
Monterey, CA 93940-7200
[2]Institute of Marine Sciences
University of California
Santa Cruz, CA
and
Southwest Fisheries Science Center
NOAA
Monterey, CA
[3]Earth System Research Laboratory
NOAA
Boulder, CO 80305
[4]Southwest Fisheries Science Center
National Marine Fisheries Service
NOAA
Santa Cruz, CA 95064

JOHN LARGIER
Bodega Bay Marine Laboratory
University of California, Davis
Bodega Bay, CA 94923

JENNIFER L. FISHER[1,2], KYM C. JACOBSON[2], AND SAMANTHA M. ZEMAN[1]
[1]Cooperative Institute for
Marine Resources Studies
Oregon State University
Hatfield Marine Science Center
Newport, OR 97365
[2]Northwest Fisheries Science Center
Hatfield Marine Science Center
Newport, OR 97365

ERIC P. BJORKSTEDT[1] AND ROXANNE R. ROBERTSON[2]
[1]Southwest Fisheries Science Center
National Marine Fisheries Service
NOAA
Santa Cruz, CA 95064
[2]Cooperative Institute for
Marine Ecosystems and Climate
Humboldt State University

MATI KAHRU
AND RALF GOERICKE
Scripps Institution of Oceanography
University of California, San Diego
La Jolla, CA 92093

CLARE E. PEABODY
National Marine Fisheries Service
Southwest Fisheries Science Center
8901 La Jolla Shores Drive
La Jolla, CA 92037-1509

TIMOTHY R. BAUMGARTNER, BERTHA E. LAVANIEGOS, LUIS E. MIRANDA, ELIANA GOMEZ-OCAMPO, AND JOSE GOMEZ-VALDES
Oceanology Division
Centro de Investigación Científica y
Educación Superior de Ensenada
Carretera Ensenada-Tijuana No. 3918
Zona Playitas C.P. 22860
Ensenada, Baja California, Mexico

TOBY D. AUTH[1], ELIZABETH A. DALY[2], CHERYL A. MORGAN[2], AND BRIAN J. BURKE[3]
[1]Pacific States Marine Fisheries Commission
Hatfield Marine Science Center
2030 Marine Science Drive
Newport, OR 97365
[2]Cooperative Institute for
Marine Resources Studies
Oregon State University
Hatfield Marine Science Center
Newport, OR 97365
[3]Fish Ecology Division
Northwest Fisheries Science Center
National Marine Fisheries Service
National Oceanic and
Atmospheric Administration
2725 Montlake Boulevard E
Seattle, WA 98112

JOHN C. FIELD AND KEITH M. SAKUMA
Southwest Fisheries Science Center
National Marine Fisheries Service
NOAA
Santa Cruz, CA 95064

EDWARD D. WEBER
AND WILLIAM WATSON
National Marine Fisheries Service
Southwest Fisheries Science Center
8901 La Jolla Shores Drive
La Jolla, CA 92037-1509

JESSICA M. PORQUEZ[1], JANE DOLLIVER[1], DONALD E. LYONS[1,2], AND RACHAEL A. ORBEN[1]
[1]Department of Fisheries and Wildlife
Oregon State University
Hatfield Marine Science Center
Newport, OR 97365
[2]National Audubon Society
104 Nash Hall
Corvallis, OR 97331

JEANNETTE E. ZAMON
Northwest Fisheries Science Center
Point Adams Research Station
520 Heceta Place
Hammond, OR 97121

PETE WARZYBOK
AND JAIME JAHNCKE
Point Blue Conservation Science
3820 Cypress Drive, Suite 11
Petaluma, CA 94954

JARROD A. SANTORA[1], SARAH ANN THOMPSON[2], BRIAN HOOVER[2], AND WILLIAM SYDEMAN[2]
[1]Department of
Applied Mathematics and Statistics
Center for Stock Assessment Research
University of California, Santa Cruz
Santa Cruz, CA 95060
[2]Farallon Institute for
Advanced Ecosystem Research
Petaluma, CA 94952

SHARON R. MELIN
National Marine Fisheries Service
Alaska Fisheries Science Center
Marine Mammal Laboratory
NOAA
7600 Sand Point Way N. E.
Seattle, WA 98115

ABSTRACT

The California Current Ecosystem (CCE) has been in a primarily warm state since 2014, and this pattern largely continued into 2019. The CCE experienced a mild El Niño from late 2018 into 2019, and basin-scale indicators reflected this condition (elevated Oceanic Niño Index and Pacific Decadal Oscillation; table 1). Despite the El Niño, spring upwelling was above average between southern California and Washington but below average in Baja California. Sea surface temperature (SST) was mostly near the long-term average between Washington and southern California, while surface chlorophyll *a* was above average in Oregon/Washington and slightly below average in most of California in spring/early summer 2019. SST changed dramatically by fall 2019, however, as a marine heat wave (MHW) that formed in May 2019 in the Gulf of Alaska impinged upon the West Coast of the United States. The expansion of the 2019 MHW followed a similar pattern to the 2014–15 MHW.

Off Oregon, the zooplankton assemblage was in a mixed state as southern copepods were close to average while northern copepod abundances were positively anomalous in 2019. Off northern California, *Euphausia pacifica* body size was smaller than average. Euphausid abundances were well below average in both central and southern California in 2019.

In the north, winter 2019 larval fish abundances were high and dominated by offshore taxa that are associated with warm conditions; spring larval and post-larval biomass were close to average; and spring surface trawls observed record-high market squid (*Doryteuthis opalescens*) abundances. The single most important finding in 2019 was that northern anchovy (*Engraulis mordax*) adults and larvae were at record-high abundances in central and southern California. In central California, market squid and Pacific sardine (*Sardinops sagax*) were also abundant. In southern California warm-water mesopelagic fishes have been very abundant since 2014, and this trend continued into 2019.

Indicators for future salmon returns were mixed in 2019. The abundance of northern copepods, which correlate positively with returns, was high. However, abundances of yearling Chinook salmon (*Oncorhynchus tshawytscha*) and coho salmon (*O. kisutch*), which also correlate positively with returns, were slightly below average. Winter ichthyoplankton was comprised mostly of southern or offshore taxa, which bodes poorly for future salmon returns.

Seabird (common murre [*Uria aalge*]; Brandt's cormorant [*Phalacrocorax penicillatus*]; and pelagic cormorant [*Phalacrocorax pelagicus*]) productivity off Oregon was the highest in years in both 2018 and 2019. In 2018, common murre chicks in Oregon consumed large amounts of young-of-the-year flatfish, a prey item known to be conducive to chick survival. Despite the prevalence of northern anchovy in central California, common murre and Brand's cormorant production was low in Southeast Farallon Island as these birds were unable to feed optimally on northern anchovy, and there was a scarcity of more appropriate prey such as young-of-the-year flatfishes or rockfishes.

California sea lions (*Zalophus californianus*), by contrast, benefitted greatly from the large northern anchovy forage base. In 2018, live pup count, weight, and growth rate were anomalously high, and northern anchovy remains occurred in >85% of scat samples. Humpback whale (*Megaptera novaeangliae*) sightings were also very high in 2019, likely because humpback whales congregated near shore to feed on northern anchovy.

INTRODUCTION

The past 6 years were extraordinarily warm in the California Current Ecosystem (CCE) (Thompson et al. 2018). The warming began in the Gulf of Alaska in late 2013 when slack winds resulted in strong stratification and anomalous heating of surface waters. This "blob" of warm water expanded south throughout 2014 and impinged on the southern parts of the California Current by late 2014 (Bond et al. 2015). The warm pattern continued into 2015 when a strong El Niño brought warm water to both shallow and deep areas throughout the CCE (Jacox et al. 2016). Conditions remained warm throughout most of 2016, and 2014–16 turned out to be the warmest 3-year period in the CCE since records began in 1920 (Jacox et al. 2018a). This 3-year stretch was termed a "marine heat wave" (MHW) (Frölicher et al. 2018). Conditions in 2017 reverted to more of an average state, but many biological remnants of the MHW lingered throughout much of the CCE (Wells et al. 2017; Thompson et al. 2018). In 2018, oceanographic conditions north of Point Conception remained close to average, but anomalously warm water returned to the southern CCE in summer, and the single warmest daily water temperature since measurements began in 1931 occurred at the Scripps Pier on August 1, 2018 (Thompson et al. 2018). From a broad perspective, the Pacific Decadal Oscillation Index (PDO) was almost exclusively positive and the North Pacific Gyre Oscillation negative since 2014; both measurements are consistent with warm conditions in the eastern north Pacific (Thompson et al. 2018).

The post-2013 record-high water temperatures induced some major ecological surprises. For example, a near-paradigm based on data from roughly 1950 to 2002 was that Pacific sardine (*Sardinops sagax*; Sardine) thrive under warm and northern anchovy (*Engraulis mordax*) under cool ocean conditions (Chavez et al. 2003). However, northern anchovy recruitment was very high and

TABLE 1

Overview of conditions throughout the California Current in 2019. For basin indices and physical conditions, blue font suggests that conditions are cool, pink font that conditions are moderately warmer than average, and red that conditions are much warmer than normal. For biological indices, green indicates that conditions are conducive for high production, pink moderately below average production, and red well below average.

Indicator	Basin	Oregon/ Washington	Central/Northern California	Southern California	Northern Baja California
ONI	slightly above average				
PDO	slightly above average				
NPGO	very, very low				
NPH	below average				
Upwelling (spring 2019)		above average	above average	above average	below average
Cumulative upwelling (2019)		average	average	average	
SST (spring 2019)		average	average	average	
SST (fall 2019)		far above average	far above average	far above average	
Chlorophyll *a* (spring 2019)		above average	slightly below average	slightly below average	
Copepods/krill		southern species above average; northern species above average	*Euphausia pacifica* smaller than average at Trinidad Head Line. Euphausid abundances well below average in central CA.	Euphausid abundance well below average.	
Forage fish and squid (2019)		larval fish abundance high in winter 2018 but dominated by southern taxa; larval fish abundance average in June 2019; post-larval biomass average in spring 2018	anchovy record high, market squid high, sardine high; juvenile rockfish, sanddabs, and hake low	anchovy record high; subtropical mesopelagics very high	
Salmon survival (2019)		yearling Chinook and yearling coho slightly below average; northern copepod biomass suggests better than average return; larval fish prey assemblage dominated by southern, offshore species which suggests poor salmon survival and adult return			
Seabird productivity (summer 2019)		above average reproductive success for murre, Brandt's cormorant and pelagic cormorant	below average production for murre and pelagic cormorant average production for Brandt's cormorant		
Seabird at-sea abundance (summer 2019)		sooty shearwater and common murre observtions close to the long-term average	Brandt's cormorant, murre, pink-footed shearwater and sooty shearwater above average. black-footed albatros, and Cassin's auklet below average	Sabine's gull, Cook's petrel, pink-footed shearwater above average, sooty shearwater, murre and elegant tern slightly below average, black-footed albatross and Leach's storm petrel below average	
Sea lions (2018)				pup number, weight, and growth high	
Whales (2019)			high encounters of humpback		

sardine recruitment low during the 2014–16 MHW (Zwolinski et al. 2017). In addition, rockfishes (*Sebastes* spp.), which typically recruit highly during cool, productive conditions (Ralston et al. 2013), had very high recruitment from 2013–18 in central and southern California (Thompson et al. 2018; Schroeder et al. 2019). In some cases, long-term fish abundance ~ environment correlations broke down during the past 6 years. For example, there was a highly significant, positive correlation between water oxygen concentration and larval abundance of many mesopelagic fishes between 1951 and 2008 but these mesopelagic fishes were very abun-

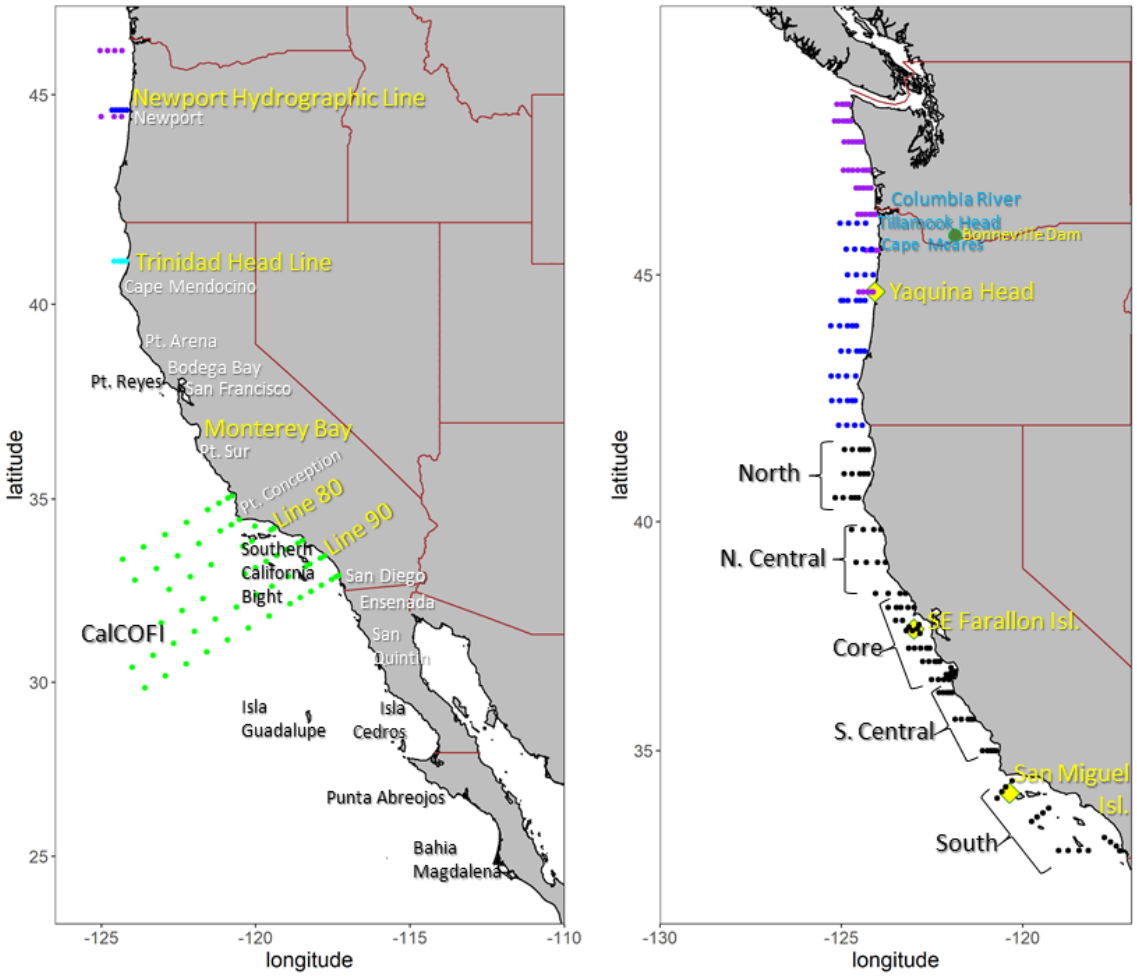

Figure 1. Maps depicting surveys that included bongo tows (left) versus rope trawls and fixed observations for birds or marine mammals (right). Left) Maps where bongo tows were conducted. From north, (purple) pre-larval surveys taken in summer, (blue) pre-larval survey from winter, (cyan) Trinidad head taken year-round, and (green) core CalCOFI stations sampled quarterly. Right) from north: purple) Juvenile Salmon and Ocean Ecosystem Survey (JSOES) in the upper 20 m, blue) post-larval midwater trawl, and (black) Rockfish Recruitment and Ecosystem Assessment Survey (RREAS); bracket define the five regions of the RREAS. Yellow diamonds define land-based locations of bird (Yaquina Head, Southeast Farallon Islands) and sea lion (San Miguel Island) surveys.

dant during the MHW even though mean oxygen was low (Koslow et al. 2019). Similarly, in the Pacific Northwest, returns of 1- or 2-year old salmon to the Columbia River correlated positively with the biomass of winter ichthyoplankton that juveniles encounter and consume when first leaving the river prior to the MHW (Daly et al. 2013). During the MHW, subsequent returns were low even though overall winter ichthyoplankton biomass was high (Daly et al. 2019). These and other unexpected events during the last six years challenged our capacity to understand mechanistically the processes that control population and assemblage dynamics in the CCE.

Three years past the 2014–16 MHW, it is possible that the proverbial MHW seeds would begin to bear fruit. For example, Northern Anchovy become sexually mature at one year old, reach peak maturity at ages 3–4, and typically do not live past 6 years (Schwartzlose et al. 1999). As such, larval abundance of northern anchovy may be high in 2019. The high rockfish recruitment during the MHW may have also resulted in augmented adult populations by 2019. In this year's State of the California Current, a variety of ongoing monitoring efforts are analyzed to evaluate how the extreme events of 2014–16, coupled with current oceanographic condition impact species at multiple trophic levels throughout the CCE (fig. 1).

BASIN-SCALE CONDITIONS

North Pacific Climate Indices

The Oceanic Niño Index[1] (ONI), a three-month running mean of SST anomalies averaged over 5°S–5°N and 120°W–170°W (NIÑO3.4 region), is a measure of El Niño–Southern Oscillation (ENSO) variability. The

[1]The ONI, PDO, and NPGO indices can be downloaded at: http://upwell.pfeg.noaa.gov/erddap/.

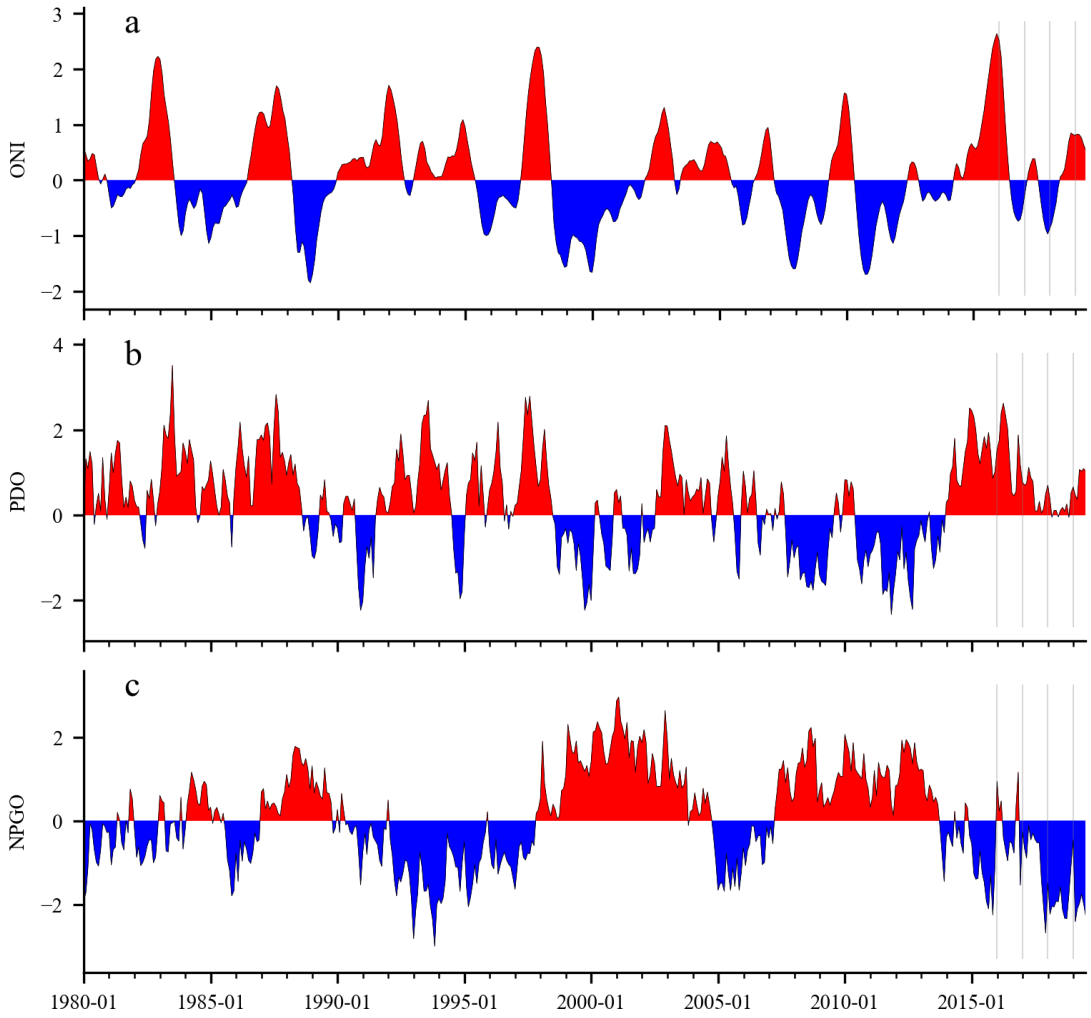

Figure 2. Time series of monthly values for three ocean indices especially relevant to the California Current: a) Oceanic Niño Index (ONI), b) Pacific Decadal Oscillation (PDO), and c) North Pacific Gyre Oscillation (NPGO). Vertical lines mark January 2016–19.

ONI marks an El Niño event when three-month averages reach a threshold of 0.5°C. The ONI indicated a transition from La Niña conditions during fall 2017 to winter 2017–18 to weak El Niño conditions over September 2018 to June 2019 (fig. 2a). The values of the ONI during the 2018–19 El Niño event only reached a high of 0.9°C, which is relatively low compared to the 2.6°C anomaly experienced during the strong 2015–16 El Niño event (fig. 2a). NOAA's Climate Prediction Center (CPC) reported El Niño neutral conditions as of August 2019[2] and forecasted El Niño-neutral conditions to persist through spring 2020 (55%–60% chance). In general, El Niño impacts on the CCE include weaker upwelling (or stronger downwelling), lower nutrient supply from upwelled waters, warmer temperatures, and lower productivity (Jacox et al. 2015). However, there is considerable variability in the CCE response to ENSO (Fiedler and Mantua 2017), and the CCE does not respond predictably to weak ENSO events (Jacox et al. 2018a).

The Pacific Decadal Oscillation (PDO) index describes the temporal evolution of dominant spatial patterns of SST anomalies over the North Pacific (Mantua et al. 1997). Positive PDO values are associated with a shallower upwelling cell in the northern CCE, resulting in less vertical mixing of nutrient-rich deep waters into the surface (Chhak and Di Lorenzo; 2007, Di Lorenzo et al. 2008). Since December 2018, the PDO exhibited positive values with values over 1 from April–June 2019 (fig. 2b). PDO values during 2019 were high, but not nearly as high as during past El Niño events of 1982, 1998, and 2016.

The North Pacific Gyre Oscillation (NPGO) is a low-frequency signal of sea surface height (SSH) variations across the North Pacific, indicating variations in the circulation of the North Pacific Subtropical Gyre and

[2]https://www.cpc.ncep.noaa.gov/products/analysis_monitoring/enso_advisory

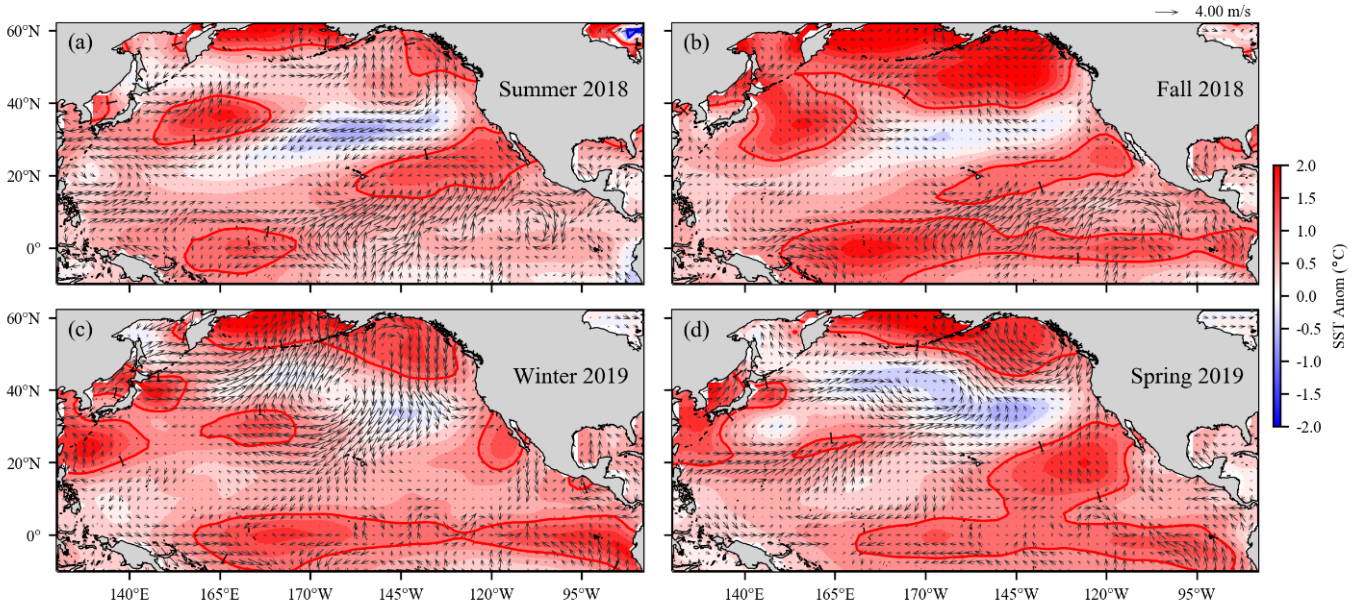

Figure 3. Anomalies of surface wind velocity and sea surface temperature (SST) in the North Pacific Ocean for summer (June–August) 2018, fall (September–November) 2018, winter (December–February) 2019, and spring (March–May) 2019. Arrows denote magnitude and direction of wind anomaly (scale arrow at top). Contours denote SST anomaly. Shading interval is 0.25°C and contour intervals at plus/minus 1°C are shown. Negative (cool) SST anomalies are shaded blue. Wind climatology period is 1968–96. SST climatology period is 1950–79.

Alaskan Gyre (Di Lorenzo et al. 2008). Positive NPGO values are linked with increased equatorward flow in the California Current, along with increased surface salinities, nutrients, and chlorophyll in the southern-central CCE (Di Lorenzo et al. 2009). Negative NPGO values are associated with a shallower upwelling cell in the southern CCE resulting in less vertical mixing of nutrient rich deep waters into the surface (Di Lorenzo et al. 2008). The NPGO during 2019 continued an extended period of negative values since December 2016 (fig. 2c). The negative NPGO values From October 2017 to June 2019, the NPGO reached some of the strongest negative values observed over the entire time-series (since 1950).

North Pacific Climate Patterns

A basin-scale examination of seasonal SST and surface wind anomalies[3] allows for the interpretation of the spatial evolution of climate patterns and wind forcing over the North Pacific related to trends in the basin-scale and upwelling indices (fig. 3). From fall 2018 to spring 2019 El Niño conditions were present in the equatorial Pacific (fig. 2a), with temperature anomalies above 1°C in the Niño3.4 region (fig. 3). Since summer 2018, there has been a general expansion of positive 1°C anomalies in the Bering Sea and Gulf of Alaska (fig. 3), with the largest spatial extent of these anomalies occurring in fall 2018. In the eastern Pacific, north of Hawaii, negative (≤ –0.5°C) to near-zero SST anomalies occurred over the four seasons. Along the North American west coast, SST anomalies were slightly positive (≤0.5°C) between Vancouver Island and the Southern California Bight, while coastal SST anomalies in the Gulf of Alaska and along the Baja Peninsula were over 1°C for the four seasons. The SST patterns of 2018–19 showed positive anomalies with spatial coverage similar to that seen during the 2015–16 El Niño event (McClatchie et al. 2016b), but the magnitude of the positive anomalies during 2015–16 were much higher, with some areas of seasonal anomalies over 2°C.

During the 2018–19 El Niño event, the trade winds over the western equatorial Pacific were weaker in fall 2018 and winter 2019, with westerly wind anomalies at 160°E (fig. 3). Spring 2019 trade winds strengthened with zero to positive easterly wind anomalies located between 165°E–120°W. Anticyclonic wind anomalies in the North Pacific and Gulf of Alaska were evident during summer 2018, winter 2019, and spring 2019. Along the West Coast, upwelling winds were near the climatological average for the four seasons, especially north of Point Conception.

COAST-WIDE CONDITIONS

Upwelling in the California Current

Anomalies of coastal SST[4] (averaged from the coast to 100 km offshore), upwelling, and upwelled nitrate

[3]NOAA Extended Reconstructed SST V5 and wind NCEP/NCAR Reanalysis data were obtained from http://www.esrl.noaa.gov.

[4]Daily optimum AVHRR SST data obtained from https://coastwatch.pfeg.noaa.gov/erddap/griddap/ncdcOisst2Agg.

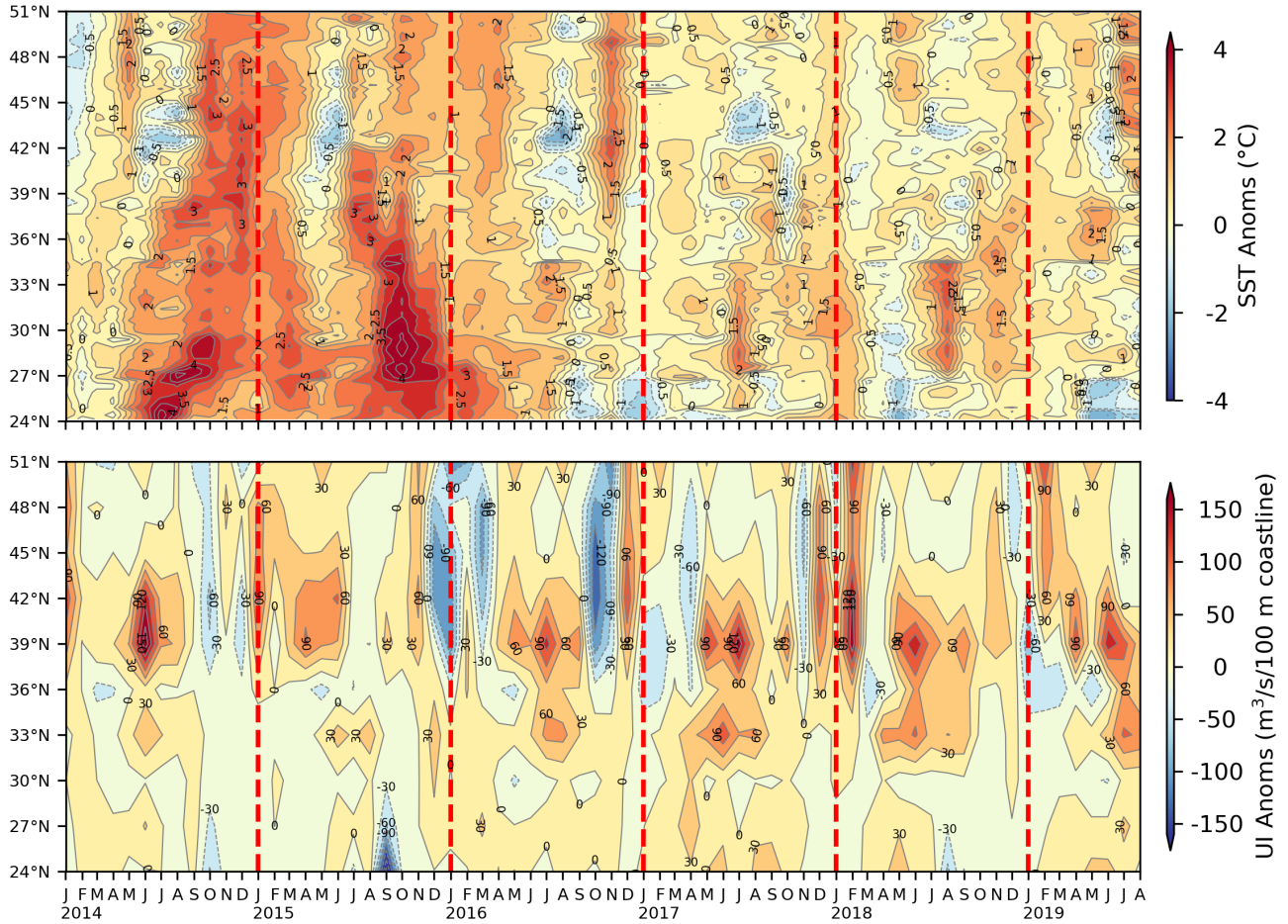

Figure 4. Monthly sea surface temperature (SST) anomalies (top) and Bakun upwelling index (UI) anomalies (bottom) for January 2014–August 2018. The SST anomalies were averaged from the coast to 75 km offshore. Positive and negative upwelling anomalies denote greater than average upwelling or downwelling (usually during the winter), respectively. Anomalies were relative to 1982–2010 monthly means.

were used to examine anomalous coastal upwelling conditions within the CCE from January 2014 to July 2019 (figs. 4, 5). Upwelling estimates came from two sources: the Bakun upwelling index[5] (UI; fig. 4; Schwing et al. 1996) and the Coastal Upwelling Transport Index[6] (CUTI; fig. 6; Jacox et al. (2018b)). In addition, The Biological Effective Upwelling Transport Index[7] (BEUTI; fig. 5; Jacox et al. 2018b) gives estimates of vertical nitrate flux into the surface layer. Both CUTI and BEUTI were derived from a data-assimilative regional ocean model (Neveu et al. 2016). Multiple upwelling indices are evaluated as the UI has long been used in studies of the California Current, but in some places, particularly south of 39°N, it is a less reliable indicator of upwelling due to relatively poor estimation of the wind stress and modulation of upwelling by the cross-shore geostrophic flow (Bakun 1973; Jacox et al. 2018b). In addition, the UI does not provide information on the nutrient content of upwelled water.

High SST anomalies during the 2014–16 marine heat wave (MHV) extended coastwide from fall 2014 to spring 2016, with anomalies exceeding 2°C (fig. 4). Since summer 2016, SST anomalies were generally weaker (with magnitude less than 1°C), and spatially dependent. However, during winter 2019, positive SST anomalies of 1°C occurred from 32° to 50°N. In May and June 2019 SST anomalies were large (>1°C) for Monterey Bay and Gulf of Farallones, though to the north, between 38° and 44°N, SST anomalies were negative (–0.5°C). This pattern reversed during July and August 2019, with positive anomalies (>1°C) in the north and negative anomalies (–0.5°C) in the south.

Despite warm temperatures during the 2014–16 MHW, spring upwelling in 2014 and 2015 was relatively strong, especially in the northern CCE (figs. 4, 5). Upwelling during winter 2015–16, during the El Niño event, was below average to average for latitudes

[5]Six-hourly upwelling index data obtained from http://oceanview.pfeg.noaa.gov/erddap/tabledap/.

[6]Data obtained from http://upwell.pfeg.noaa.gov/erddap/.

[7]SST output obtained from https://oceanmodeling.ucsc.edu and BEUTI from https://oceanview.pfeg.noaa.gov/products/upwelling/.

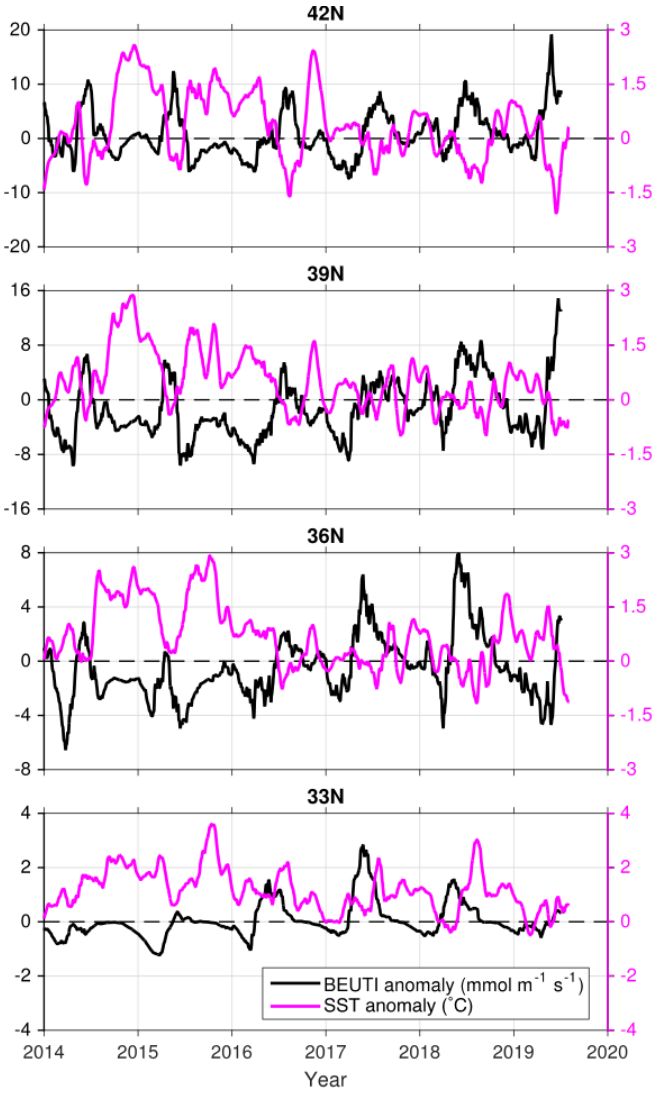

Figure 5. Daily anomalies over January 2014 to July 2019 of Biologically Effective Upwelling Transport Index (BEUTI; black) and sea surface temperature (SST; magenta) relative to 1980–2010 climatology, derived from a data assimilative ocean reanalysis of the California Current System at four latitudes off the US West Coast. Values were averaged from the coast to 75 km offshore. SST was smoothed with a 30-day running mean and BEUTI was smoothed with a 60-day running mean.

north of 39˚N. Upwelling anomalies during the winter and spring of 2019 were mostly average to positive for latitudes north of 42˚N. Slightly negative anomalies (–30 m^3/s/100 m coastline) occurred in the Monterey Bay region (36.5˚N), with lowest values during May 2019. During July and August 2018, upwelling anomalies north of 39˚N were average to slightly negative, while positive upwelling anomalies occurred between 30˚ and 39˚N.

Vertical nitrate fluxes during the MHW were extremely low as indicated by the negative BEUTI anomalies from fall 2014 to winter 2015–16, with the largest negative anomalies at 36˚N and 39˚N (fig. 5). BEUTI values increased from 2016 to 2018 with higher values in each subsequent spring. This trend halted in spring 2019, which saw BEUTI values as low as during 2014–15, especially off central California. These low nitrate fluxes were the result of both weak upwelling and relatively low nitrate concentrations in upwelled waters. However, in June–July 2019 the highest BEUTI values in over a decade were observed near and to the north of Cape Mendocino (40˚N), and, correspondingly, the cold, upwelled water produced strongly negative nearshore SST. This strong upwelling appeared to be keeping a thin strip of ocean next to the coast cool while there was a broad region of anomalously warm water farther offshore.

The cumulative Coastal Upwelling Transport Index (CCUTI) is the cumulative sum of daily CUTI values starting January 1 and ending December 31, and it provides an estimate of the net influence of upwelling on ecosystem structure and productivity over the course of the year (Bograd et al. 2009; Jacox et al. 2018b). In general, winter and spring upwelling was stronger during 2018–19 than the previous two years (fig. 6). Cumulative upwelling during 2016–17 was mostly average over the year for all latitudes except for the locations of 39˚N and 42˚N, which had low yearly values. Upwelling during 2019 was stronger in the north, with 45˚N and 47˚N experiencing strong upwelling in the spring. However, upwelling at 39˚N was low, similar to 2018, with low CUTI values starting in January. The yearly range of upwelling at 33˚N was not as large as the northern latitudes and the CCUTI values have been average over the past 4 years.

During winter, storm-driven mixing typically deepens the mixed layer and serves to elevate nutrient concentrations in surface waters, particularly in the northern CCS. However, in some years, periods of sustained calm and stratification (in the north) or even mild upwelling favorable winds (more so in the south) can occur in mid- to late-winter, and allow bursts of primary productivity and successful reproduction in copepod and krill populations well in advance of the typical spring transition (Feinberg and Peterson 2003; Feinberg et al. 2010). Such events serve to precondition the ecosystem for increased production in the spring (Schroeder et al. 2009; Black et al. 2010). The area of sea level atmospheric pressure associated with the North Pacific High (NPH)[8] can be used as an index of this winter preconditioning (Schroeder et al. 2013). Since 2014 there has been a continually weak NPH during the winter (January–February; fig. 7). The 2019 area was similar to 2018, but the area was considerably smaller compared to high area years that were common from 1999–2013.

[8]Six-hourly data used to define the area of the NPH is located at https://coastwatch.pfeg.noaa.gov/erddap/.

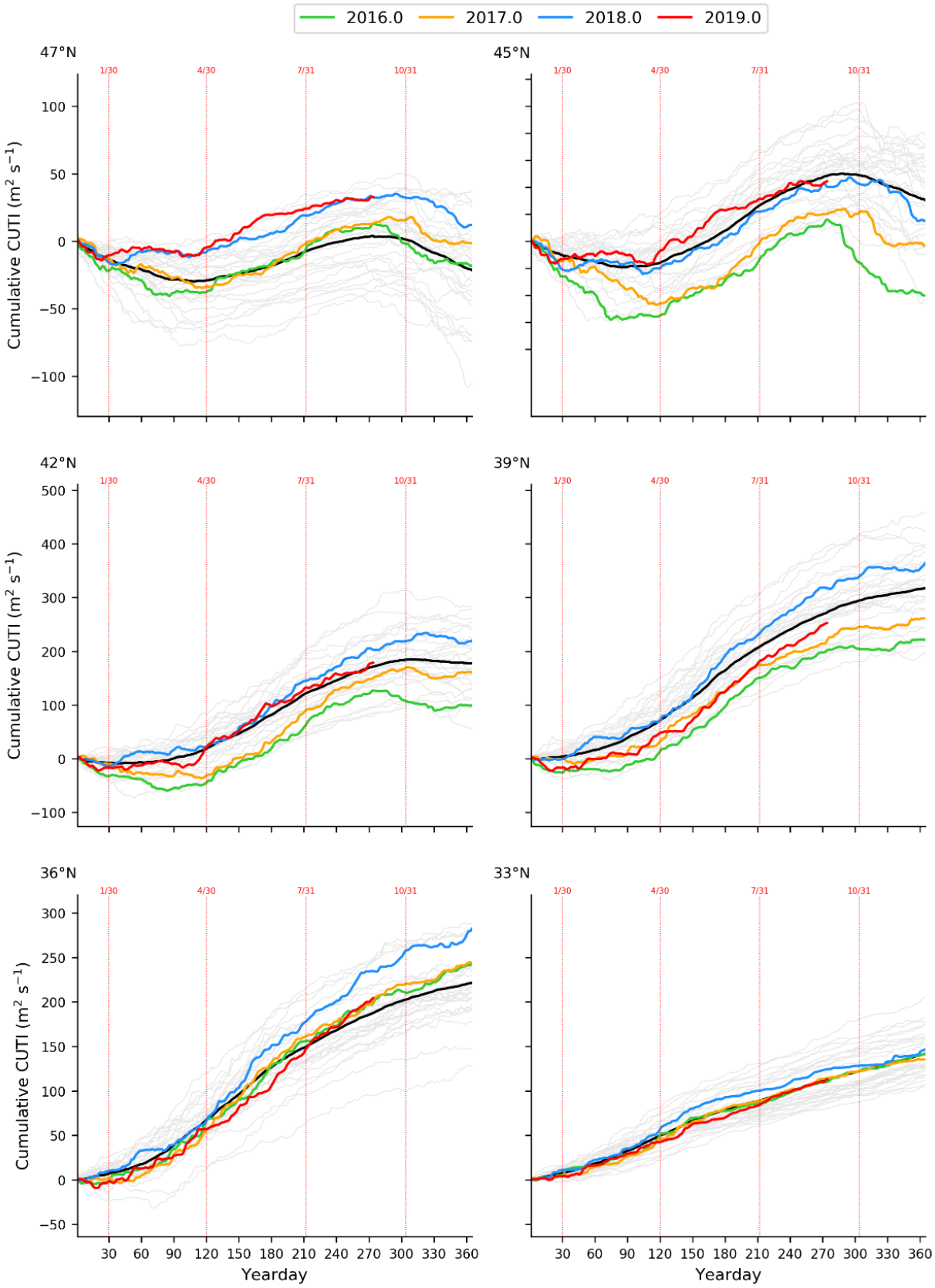

Figure 6. Yearly curves of the cumulative Coastal Upwelling Transport Index (CCUTI) starting on January 1 calculated from daily CUTI at locations along the west coast of North America. Grey lines are all yearly CCUTI for the years 1988–2015, colored curves are for the years 2016–19. The black line is the climatological mean. The red dashed vertical lines mark the end of January, April, July, and October.

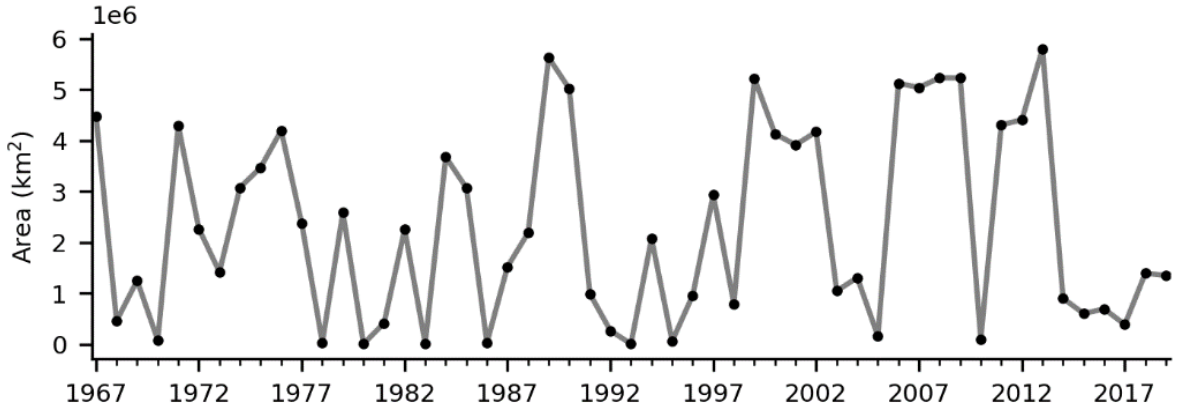

Figure 7. Area of high atmospheric pressure of the North Pacific High averaged over January and February each year. The area is the areal extent of the 1020 hPa isobar located in the eastern North Pacific.

Coastal sea surface and subsurface temperatures

Daily sea surface temperature (SST) time series, measured by National Data Buoy Center (NDBC) buoys[9], showed periods of above temperatures over July 2018 to August 2019 (fig. 8). During this period, buoys in the Southern California Bight had the highest temperatures during summer and fall 2018, while buoys off Washington State had the highest temperatures over July to September 2019. However, temperature extremes over the last two years have not exceeded the magnitude and duration observed during the 2014–16 MHW. Alongshore winds during winter 2018–19 were similar to the 2015–16 El Niño event, with periods of strong downwelling winds (positive values of alongshore winds) especially during January 2019 (fig. 8). The two northern buoys (46041 and 46029) experienced strong northerly winds during May and June 2019, while the buoys to the south had weak upwelling during May 2019.

Subsurface ocean temperature anomalies derived from a data assimilative ocean reanalysis had the largest surface (0–50 m) positive anomalies during the 2014–15 marine heat wave (fig. 9). Positive anomalies extended from the surface down to 250 m during the two El Niño events of 2015–16 and 2018–19 for locations between 33°N–39°N. Cooling occurred by spring 2019, with negative temperature anomalies ranging from the surface to below 100 m; this cooling started several weeks earlier for locations 39°N and 42°N.

Primary production in the CCE

Spring (April–May) averages of chlorophyll *a* anomalies during 2019 showed a general pattern of northern (north of Monterey Bay) positive anomalies and southern negative anomalies (fig. 10). Positive anomalies spanned coastal areas between 43°–44°N and north of Pt. Reyes during 2019.

[9]Data provided by NOAA NDBC, http://www.ndbc.noaa.gov/.

Currents in the CCE

During spring 2018, surface currents were predominantly southward throughout the domain, including within the Southern California Bight[10]. In general, currents continued southward through summer, however there were marked offshore orientations, specifically between Point Sur and Point Conception, and poleward currents in the Santa Barbara Channel (fig. 11). In fall 2018, alongshore flow was variable with weak means throughout the domain, with the persistence of offshore-orientated surface currents. In winter 2019, flows were predominantly poleward, specifically north of Point Reyes and well organized north of Cape Blanco. Persistent mesoscale eddies were not observed in 2018–19, but enhanced offshore flows near headlands (Point Conception, Point Arena, Cape Mendocino) were observed as in prior years due to separation of alongshore flows.

A new marine heat wave

Although the coastal region remained relatively cool[11] during spring and early summer of 2019 (fig. 9), a new, large MHW formed off the Gulf of Alaska in mid-May 2019 (fig. 12). By late August 2019, this MHW extended to the coast of Washington, Oregon, and central and northern CA where surface temperatures were up to 3°C above average. In mid-September 2019, anomalously warm water impinged most of the coast north of Monterey Bay and was seaward of the shelf break off southern California and Baja California (fig. 13). In mid-

[10]Data on surface currents were obtained from high frequency (HF) radar, with vectors calculated hourly at 6 km resolution using optimal interpolation. Real-time displays can be viewed at www.sccoos.org/data/hfrnet/ and www.cencoos.org/sections/conditions/Google_currents/. HF-radar data are available thanks to the initial investment of the State of California in establishing the array in California and to the National Science Foundation for establishing elements of the array in Oregon and California. NOAA-IOOS and participating universities (listed at http://cordc.ucsd.edu/projects/mapping/) provide ongoing funds/support for operation and management.

[11]SST anomaly data from 1982–Aug 2019 NOAA OISST: https://www.ncdc.noaa.gov/oisst.

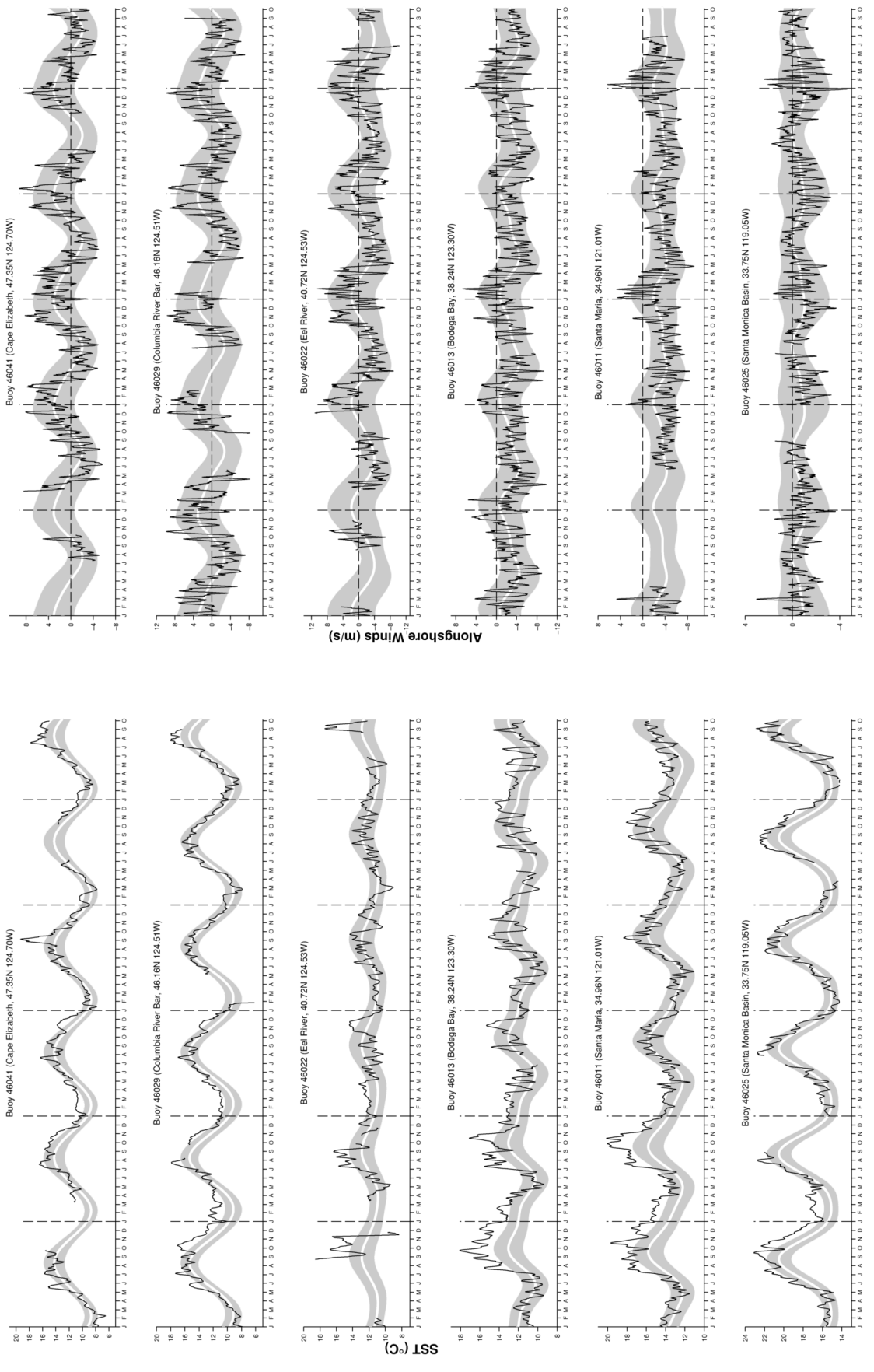

Figure 8. Time series of daily sea surface temperatures (left) and alongshore winds (right) from various National Data Buoy Center (NDBC) coastal buoys along the CCS for January 2014 to September 2019. The wide white line is the biharmonic annual climatological cycle at each buoy. Shaded areas are the standard errors for each Julian day. Series were smoothed with a 7-day running mean.

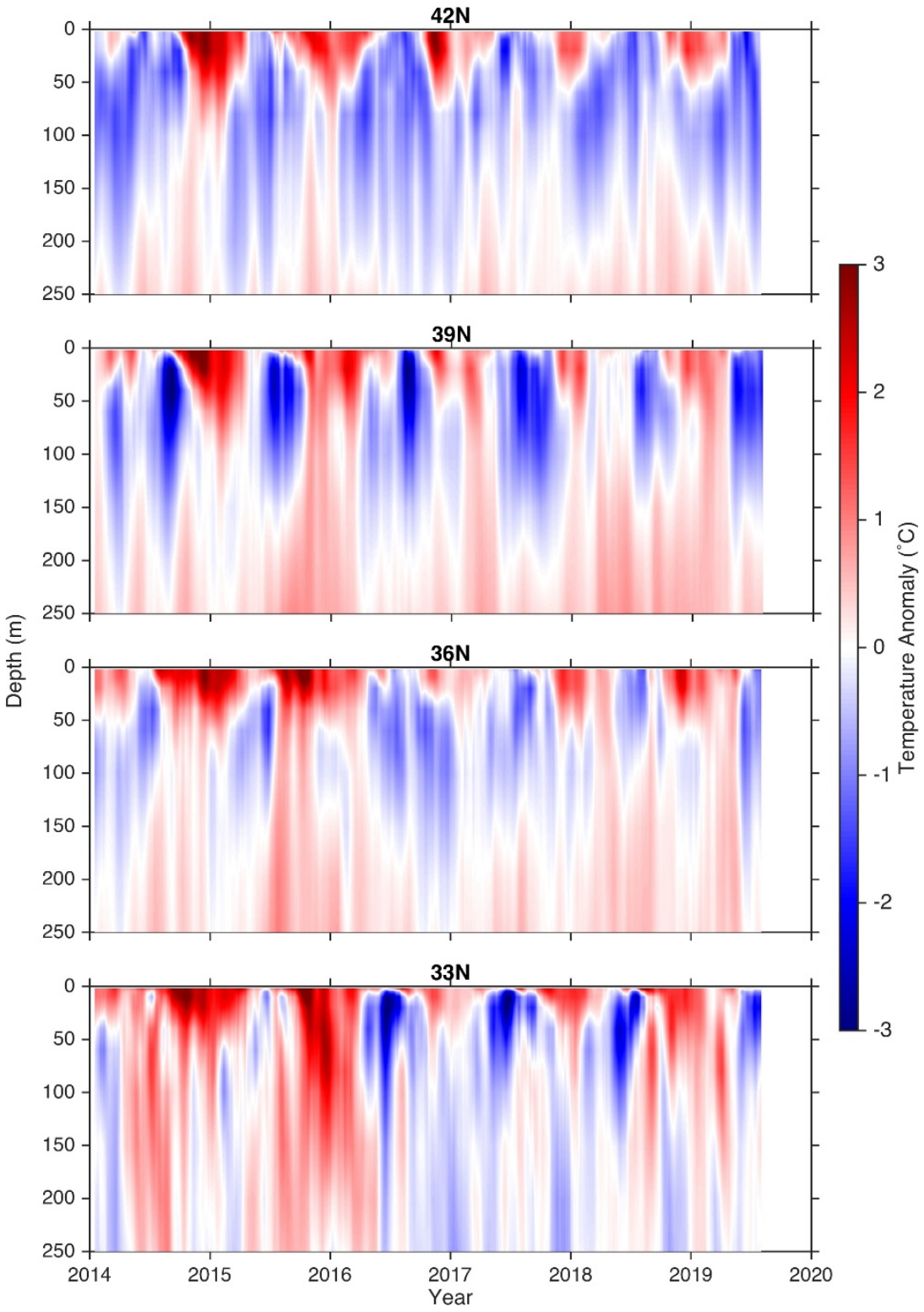

Figure 9. Temperature anomalies relative to the 1999–2011 climatology, derived from a data assimilative ocean reanalysis of the California Current System at four latitudes off the US West Coast. Temperatures were averaged from the coast to 75 km offshore and smoothed with a 30-day running mean.

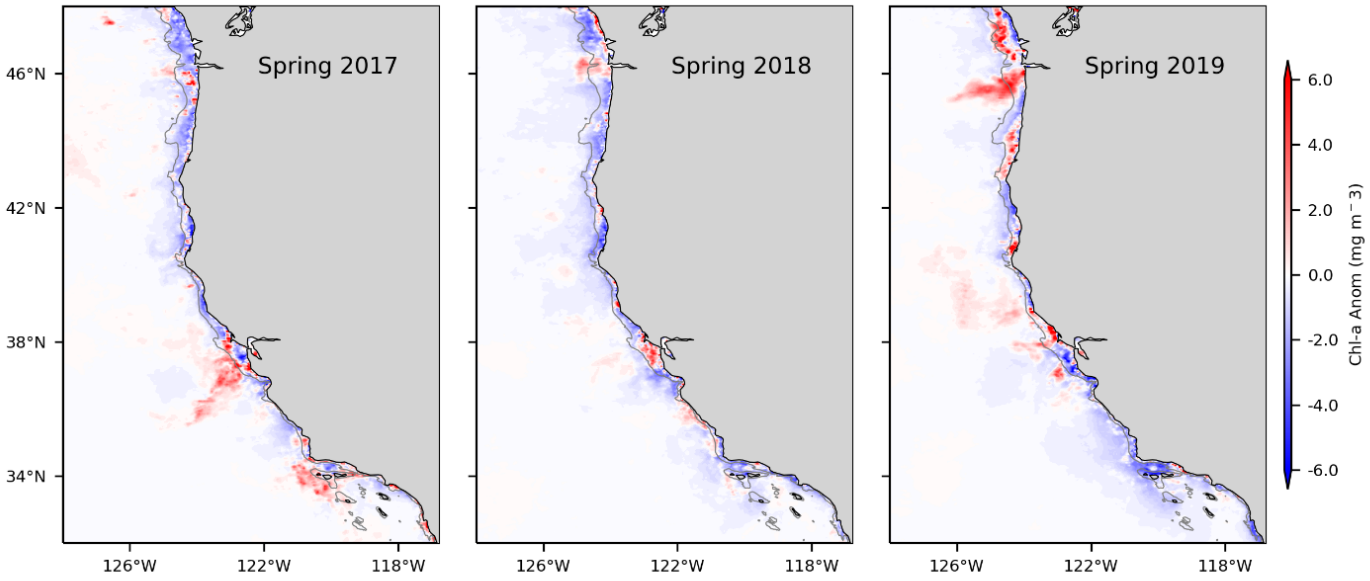

Figure 10. Chlorophyll *a* anomalies from Aqua MODIS over spring (March– May) 2017–19. Monthly anomalies were averaged onto a 0.1° x 0.1° grid and the climatology was based on the 2003–19 period.

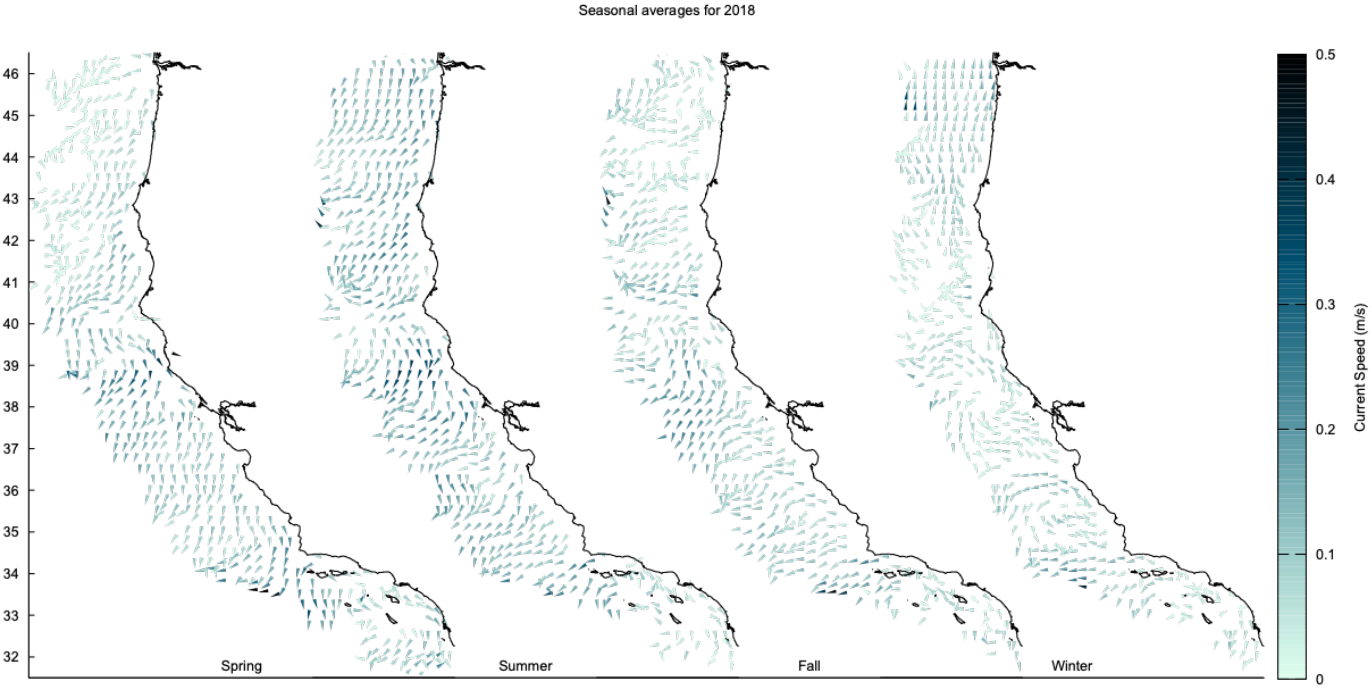

Figure 11. Seasonal mean surface currents observed in the CCE with HF radar. From left to right, the panels present data for spring (March–May 2018), summer (June–August 2018), fall (September–November 2018), and winter (December–February 2019). Current speed is indicated by shading and direction given by orientation of arrow extending from observation location. Currents are displayed with spatial resolution of 0.25o (i.e., nearshore flows are not well represented here).

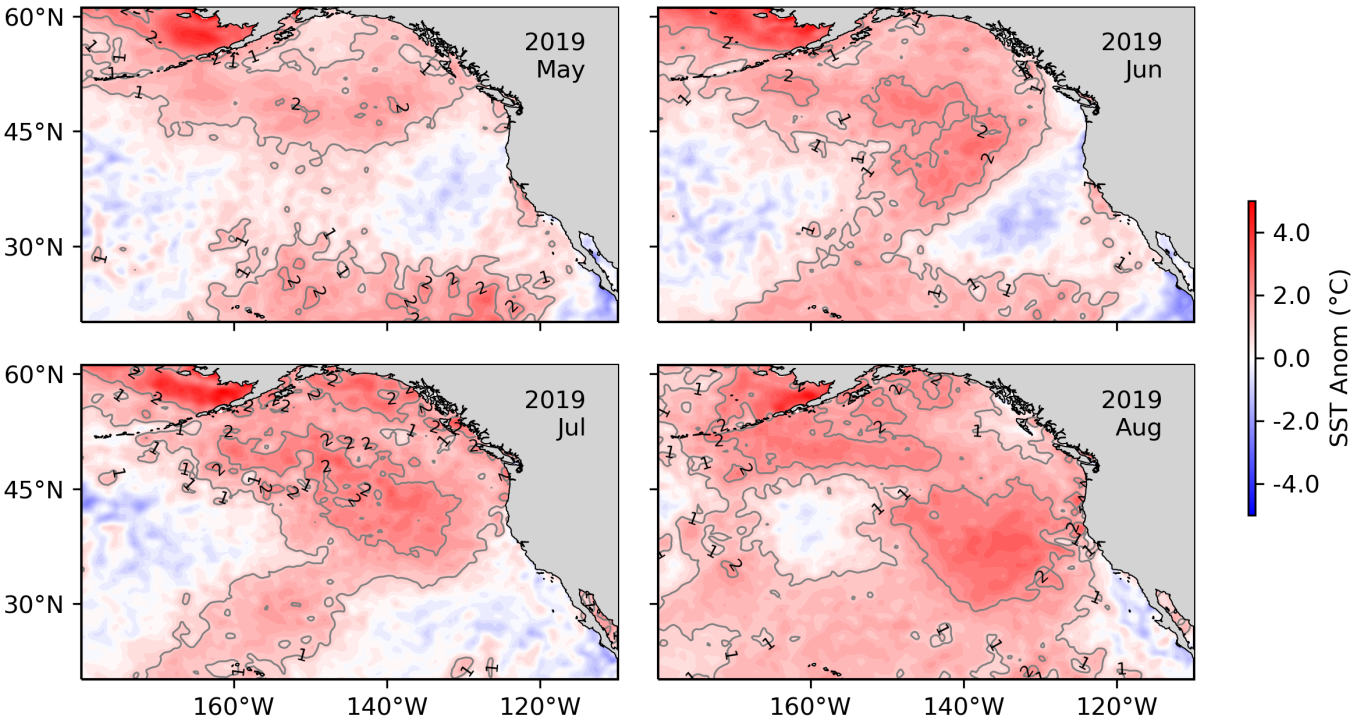

Figure 12. Monthly sea surface temperature anomalies from May to August 2019 relative to 1982–2010 climatology. Contour intervals depict 1°C and 2°C values.

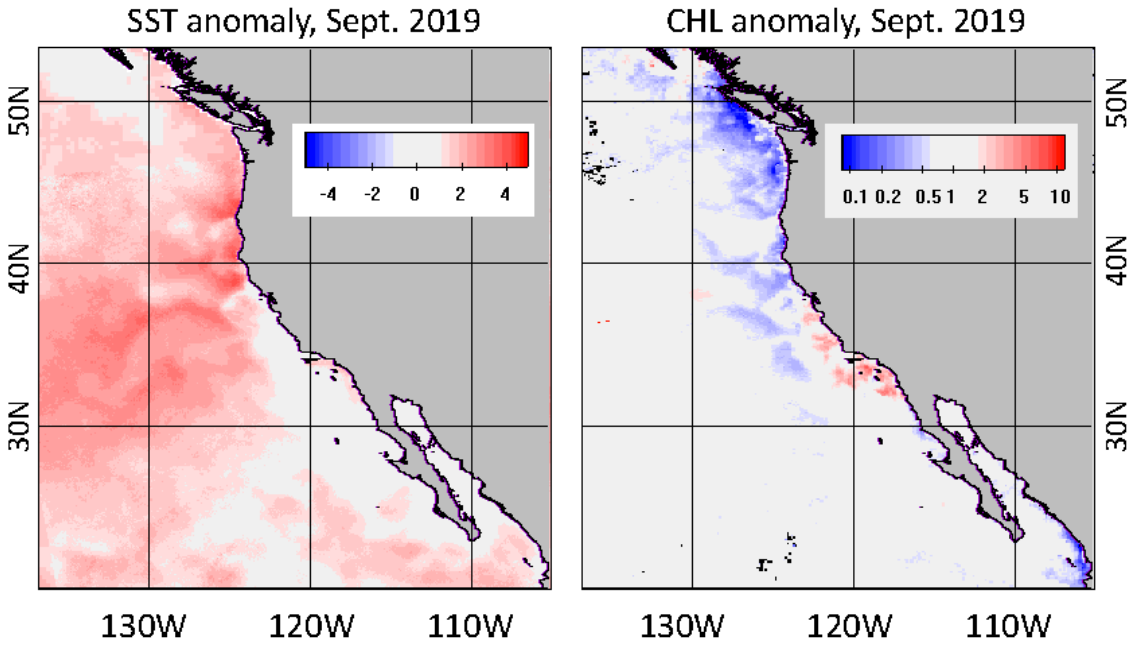

Figure 13. Spatial patterns of September, 2019 anomalies in SST and chlorophyll *a*. The SST anomaly was computed as difference from the long-term mean (1981–2019) in °C. The chlorophyll *a* anomaly was expressed as ratio to the long-term mean (1996–2019).

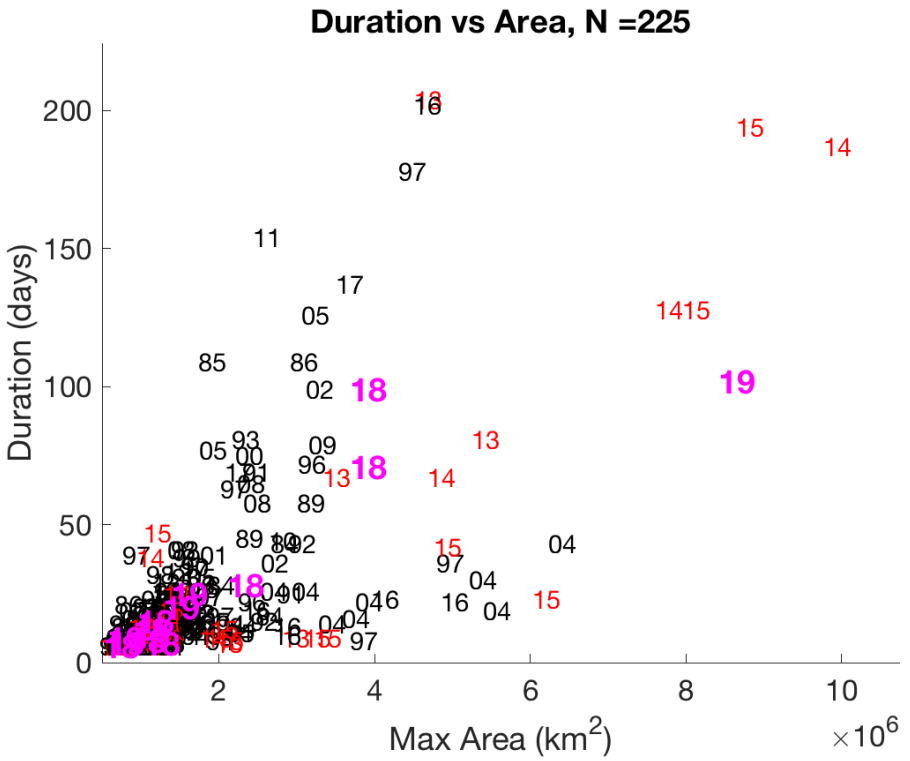

Figure 14. Duration of all marine heat waves (MHW)s >5 days long vs maximum area of each MHW, with the year of the feature initiation labeled. Highlighted are the main "blob" years of 2013–14 in red, and the most recent MHW of 2018 and 2019 in magenta.

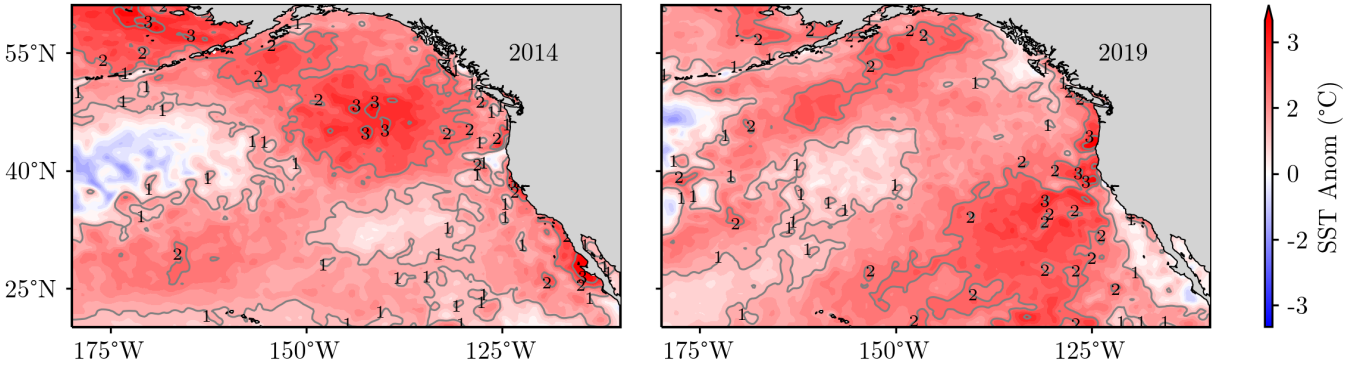

Figure 15. Monthly sea surface temperature anomalies from September 2014 (left) and September 2019 (right). Contour intervals depict 1°C and 2°C values.

September 2019, chlorophyll *a* was well above average in both central and southern California but below average off Oregon and Washington (fig. 13).

As of August 31, 2019, this large MHW, defined following criteria similar to those applied by Hobday et al. (2016), became the third-largest event out of 223 identified MHWs since 1982. The 2019 MHW lagged only slightly behind the MHWs tracked during 2014 and 2015 On August 31, 2019 the MHW was present for 104 days (fig. 14).

Comparison of SST anomalies towards the beginning of the 2014–16 MHW in September 2014 versus September 2019 indicated that elevated SST were prevalent in many of the same areas between years (fig. 15). In both years, anomalously warm SST occurred in most of the offshore area off the United States, Baja California, and Canada. Similarly, SST was elevated close to shore in both years north of approximately Monterey Bay. However, while SST was anomalously high between Monterey Bay and southern Baja California in September 2014, SST was closer to average south of Monterey Bay in September 2019.

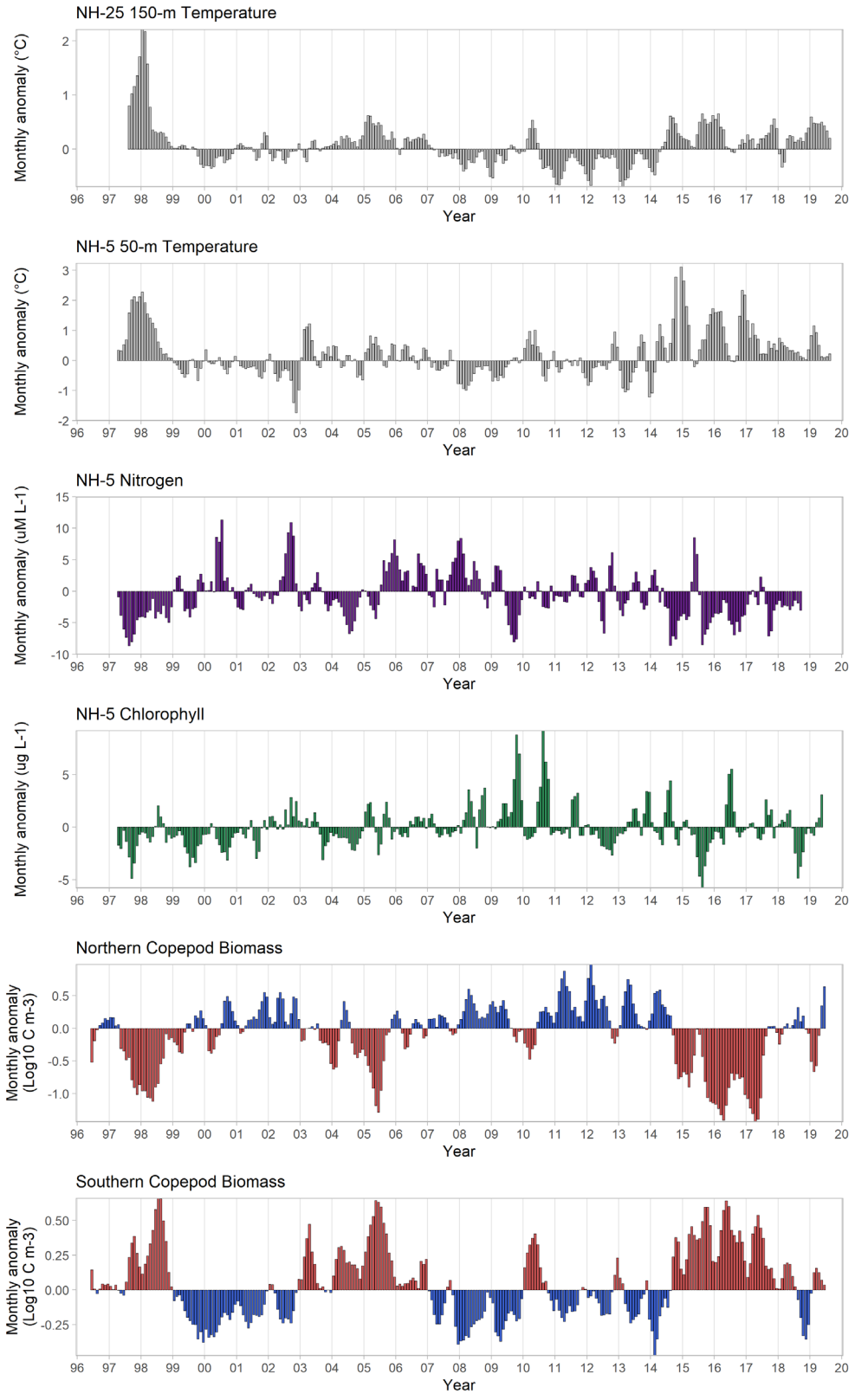

Figure 16. Time series plots of local physical and biological anomalies (monthly climatology removed) from 1996–present at NH-25 (Latitude: 44.6517 N Longitude: 124.65 W) and NH-5 (Latitude: 44.6517 N Longitude: 124.1770 W) along the Newport Hydrographic Line. Temperature and salinity are from 150 m and 50 at NH-25 and NH-5 respectively, NO2 + NO3 from the surface, and copepod biomass anomalies integrated over the upper 60 m. All data were smoothed with a 3-month running mean to remove high frequency variability.

REGIONAL OBSERVATIONS OF ENVIRONMENT AND LOWER TROPHIC LEVELS

Northern California Current: Oregon (Newport Hydrographic Line)

Water temperature anomalies on the shelf (50 m) and slope (150 m) off Newport, Oregon (44.5°N, fig. 1), were strongly positive from the spring of 2014 until summer 2017 (fig. 16). During 2018 and 2019, temperature anomalies returned to weakly positive to near neutral on the shelf but remained strongly positive on the slope (fig. 16). The 2014–17 warm ocean conditions were associated with a southern copepod community, which persisted from fall 2014 through spring 2018 (Peterson et al. 2017)[12]. The near-neutral temperature anomalies on the shelf during the summers of 2018 and 2019 were accompanied by an increased biomass of northern copepods, yet southern copepods were still abundant during that time, signaling a pelagic ecosystem still in flux. During September 2019, nearshore surface waters were +3°C above the long-term mean (figs. 13, 15), signaling the arrival of another MHW to continental shelf waters off Oregon.

In 2018 and 2019, the onset of upwelling followed the long-term mean. (figs. 4–6). Although the Bakun upwelling index indicated average upwelling during summer 2018, positive SST anomalies (+2.5°C) occurred for much of the summer, with brief periods of negative surface temperatures during the end of May, July, and the beginning of September (figs. 8, 16). Hypoxic oxygen concentrations below 1.4 ml/L were observed on the shelf from July–September 2018, and during August 2019 (data not shown). Following the upwelling season in 2018, positive temperature anomalies occurred on the shelf and slope (fig. 16). With the exception of two months during the 2015 and 2017 upwelling season, nitrogen concentrations on the shelf remained below average since fall 2015, and continued to be below average throughout 2018 (fig. 16). Chlorophyll *a* was well below average in mid-2018, became average in late 2018/early 2019, and was above average by mid-2019 (fig. 16).

The zooplankton community was dominated by southerly, lipid-poor species from September 2014 until the summer of 2017. The copepod community then transitioned to a more neutral state (fig. 16). During 2015 and 2016, the copepod community did not transition from a warm-water winter copepod community to a cold-water summer community (data not shown). This ecologically important biological transition to a lipid-rich, cold-water community also did not occur in 1998, when warm ocean conditions occurred in the NCC. However, this transition did occur in late June 2017, 52 days later than the 21-year average. In 2018, this biological transition occurred in late May, 22 days later than the climatology. In 2019, the transition occurred on June 5, which is later than the long-term climatology, and similar to 2018.

During the spring and summer of 2018 and 2019, the abundance of southern copepods was still higher than average accompanied by positive biomass anomalies of the northern copepods, indicating that the pelagic ecosystem is in a state of flux between a warm copepod community and a cold upwelling community. During winter of 2018–19, negative biomass anomalies of northern copepods and positive anomalies of southern copepods occurred, signaling a warm water zooplankton community off central Oregon. In general, northern copepods have been scarce and southern copepods copious since mid-2014 off Newport (fig. 16).

Northern California Current: Northern California (Trinidad Head Line: THL)

Coastal waters off THL in northern California (station TH02, 41°N, fig.1) were relatively cool and salty throughout the first half of 2018, but warmed in response to relaxation from upwelling in late summer (fig. 17). Relatively high temperatures and low salinity persisted in shelf and near surface waters throughout early 2019 prior to the onset of moderate upwelling that cooled coastal waters in spring and early summer. Chlorophyll *a* concentrations were relatively high for a brief period in early summer, but otherwise remained low throughout the first half of 2019. There were no observed hypoxic events.

Throughout 2018, the euphausiid community continued to shift towards a composition similar to that observed prior to the 2014–16 marine heat wave, but this trend appears to have reversed in 2019 (fig. 18). Densities of adult *Thysanoessa spinifera* increased in abundance relative to the low abundances observed during the 2014–16 warm period (figure not shown). *Nyctiphanes simplex* (a warm-water species most commonly observed in the southern CC) were absent throughout 2018, but reappeared in early 2019 and persisted into April before disappearing with the intensification of spring upwelling. Likewise, *Euphausia recurva*, a warm-water species first detected in association with the arrival of "warm blob" waters in 2014, were again detected during winter 2019. Mean length of *Euphausia pacifica* adults continued to increase in 2018, reaching size distributions comparable to those observed prior to the warm anomaly, though still including a relatively high fraction of small adults (fig. 18). This trend appears to have reversed in 2019; the seasonal increase in mean length of

[12]Copepod data were based on samples collected with a 0.5 m diameter ring net of 202 μm mesh, hauled from near the bottom to the sea surface. A TSK flowmeter was used to estimate volume of water sampled.

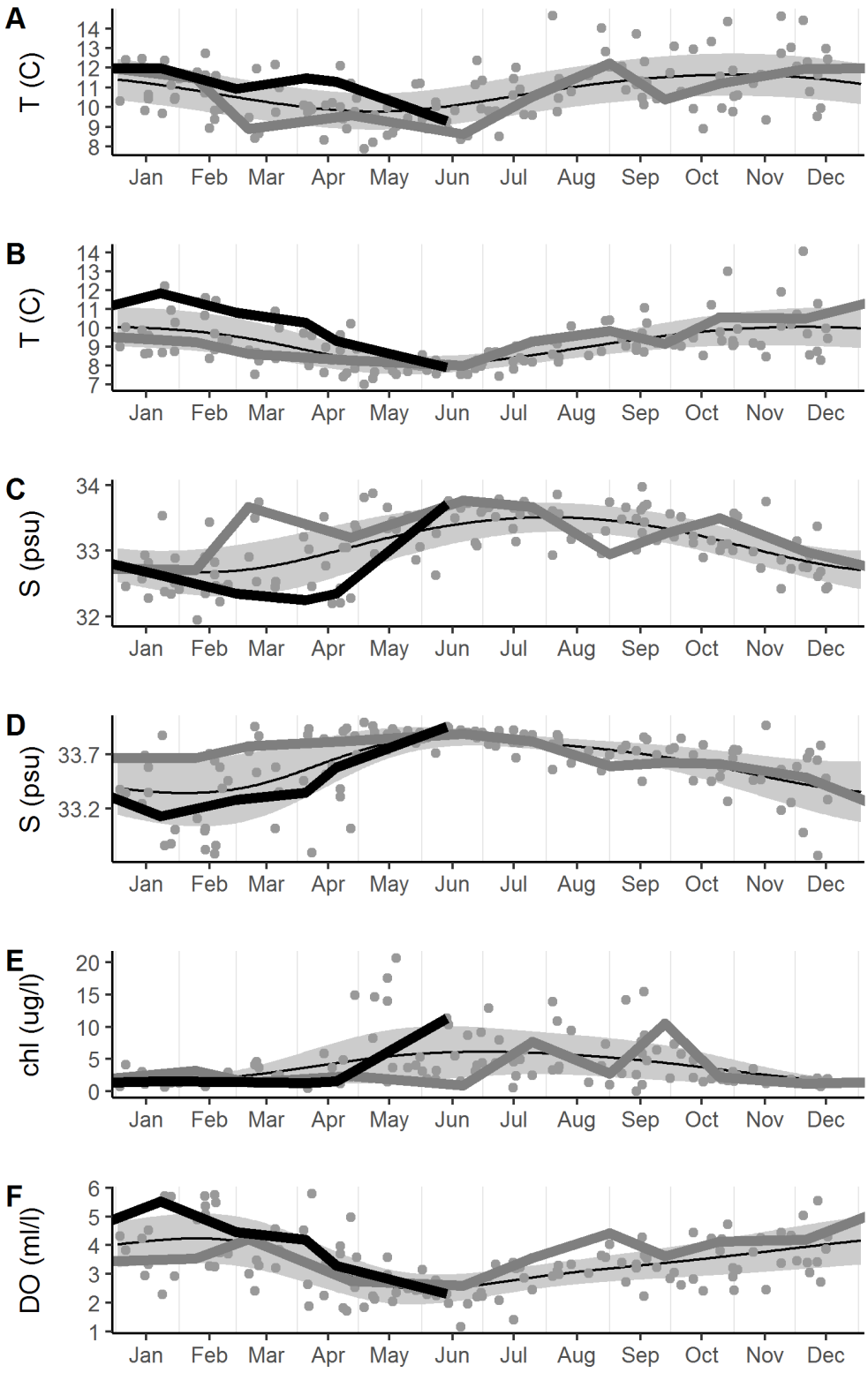

Figure 17. Hydrographic observations at station TH02 (mid-shelf) along the Trinidad Head Line in context of seasonal climatology. Panels from top to bottom show A) temperature at 15 m, B) temperature at 65 m, C) salinity at 15 m, D) salinity at 65 m, E) mean (uncalibrated) chlorophyll concentration from 2–30 m, and F) dissolved oxygen concentration at 65 m. Grey points indicate individual cruise observations. Thin black line indicates climatology derived from GAM of environmental parameter on day-of-year; light grey ribbon about this mean indicates range of mean residual around this climatology (based on GAM of absolute residuals on day of year). Dark grey line indicates observations during 2018. Black line indicates observations during 2019.

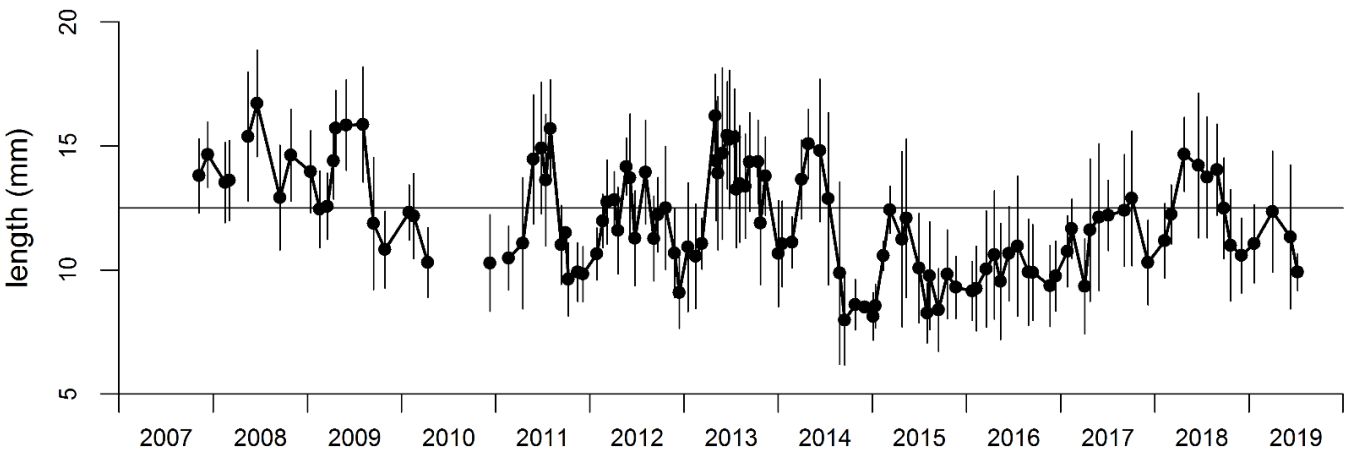

Figure 18. Density-weighted mean (points) and standard deviation (whiskers) of rostral-dorsal length of adult *Euphausia pacifica* collected along the Trinidad Head Line (aggregated over stations TH01 to TH05). Horizontal line indicates mean length taken over entire time series.

adult *E. pacifica* appears to have been cut short early in the year, so that mean lengths were comparable to during 2015–17 (fig. 18).

In conjunction with the observed shifts in euphausiid assemblage and size structure, pyrosomes (*Pyrosoma atlanticum*), which were prevalent in recent years (Brodeur et al. 2018), were absent during the first half of 2019.

Central and Southern California: Remotely Sensed SST and Chlorophyll *a*

After the period of extreme anomalies in 2014–16 that in many areas resulted in all-time highest SST and all-time lowest chlorophyll *a* (Kahru et al. 2018) and minima in the frequency of surface fronts, satellite readings[13] revealed that the conditions in 2018 and the first half of 2019 were close to long-term averages. From 2017 to mid-2019, SST was mostly slightly above the long-term average (fig. 19). After the deep declines in 2014–16, chlorophyll *a* values in 2018 and in the first half of 2019 were close to the long-term averages (fig. 19). However, starting in July and particularly in August and September 2019, a new warm anomaly developed that produced SST anomalies about +2°C in offshore and transition zones (fig. 19, areas 1 and 2). In California the warm SST anomaly was primarily offshore and less than +1°C in areas affected by upwelling (fig. 13). However, a separate narrow band of warm water developed along the coast of southern California. In contrast with the 2014–16 anomalies, warm SST in mid-2019 did not suppress chlorophyll *a* along the California coast. A steep decrease in chlorophyll *a*, however, was evident further north (e.g., off Vancouver Island (fig. 13).

Southern California: CalCOFI Survey

From spring 2018–spring 2019, mixed layer (ML) temperature anomalies averaged over the 66 standard CalCOFI stations[14] (29°N to 35°N, fig. 1) were slightly, but significantly, above the long-term average (fig. 20a) except during fall 2018. Over the last two years, ML temperatures were similar to the 1984 to 1998 period. Mixed layer salinity increased rapidly from spring to summer 2018, peaked in winter 2019 and declined (but remained relatively high) in spring 2019 (fig. 20b). Temporal trends of ML salinity were similar in all four regions of the CalCOFI domain. Salinity maxima were observed during summer 2018 in the offshore and California Current regions[15] (see footnote 14 for definition of which stations make up each region) and subsequently observed in the upwelling region and the Southern Cali-

[13]Time series of SST and chlorophyll *a* concentration were extended to September 20, 2019, using methods described in Kahru et al. (2018). SST data were derived from the version 2.0 daily data sets of optimally interpolated global blended AVHRR temperatures (Reynolds et al. 2007); https://podaac.jpl.nasa.gov/dataset/AVHRR_OI-NCEI-L4-GLOB-v2.0?ids=Platform&values=NOAA-18). High-resolution SST data were merged from MODIS-Terra, MODIS-Aqua, and VIIRS-SNPP. Chlorophyll *a* data were derived from the merged multisensor regionally optimized data set (Kahru et al. 2012; Kahru et al. 2015a; Kahru et al. 2015b); http://www.wimsoft.com/CC4km.htm). Anomalies were calculated relative to the long-term (1981–2019 for SST, 1996–2019 for Chlorophyll *a*) mean monthly values. For SST these were difference anomalies; for chlorophyll *a* the anomalies were reported as ratio anomalies expressed as % (100*[Ratio – 1]). The time series is shown in six subareas, namely the offshore, transition and coastal zones of central and southern California (fig. 18).

[14]Methods used to collect and analyze samples from CalCOFI cruises were described in detail at calcofi.org/ccpublications/calcofi-methods.html. Results were presented as time series of properties averaged over all 66 standard CalCOFI stations covered during a cruise or as anomalies of such values with respect to the 1984–2012 period. The calculation of standard errors for such averages is not straightforward due to spatial autocorrelation of properties across the CalCOFI grid. To correct for this bias, standard errors for cruise means were calculated from the residuals of objectively mapped data and actual data.

[15]Averages from selected regions were based on a subset of the 66 standard CalCOFI stations. These regions (and corresponding CalCOFI stations) were: offshore (L77St100, L80St100, L83St100, L87St100-110, L90St90-120, L93St80-120), Southern California Current (L77St70-90, L80St70-90, L83St70-90, L87St70-90, L90St60-80), upwelling (L77St49-60; L80St51-60; St82.46, L83St51-60, L87St45-55) and Southern California Bight (L83St41-42, L87St33-40, L90St28-45, L93St27-45).

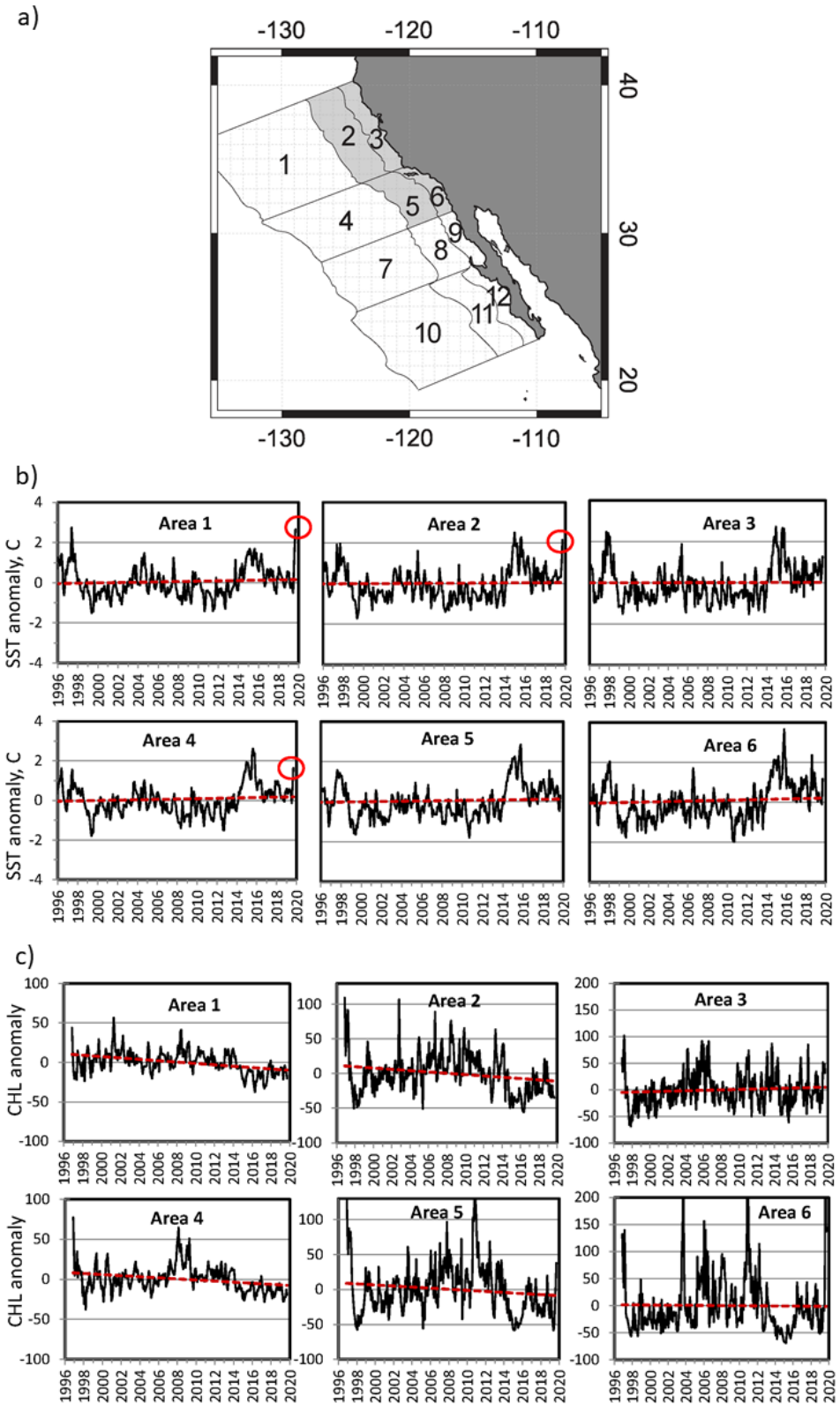

Figure 19. a) Map of the selected offshore (300–1000 km from coast, areas 1, 4), transition (100–300 km from coast, areas 2, 5) and coastal (0–100 km from coast, areas 3, 6) off central and southern California. b) Anomalies in monthly mean sea surface temperature off central and southern California. Anomalies were calculated relative to monthly means of Sept. 1981–September 2019. The dashed line is the long-term linear trend. Circles point to the +2 °C anomalies in August–September, 2019. Anomalies in monthly mean surface chlorophyll-*a* concentration off central and southern California (fig. 18a). Anomalies were calculated relative to monthly means from November 1996 to September 2019. The dashed line is the long-term linear trend.

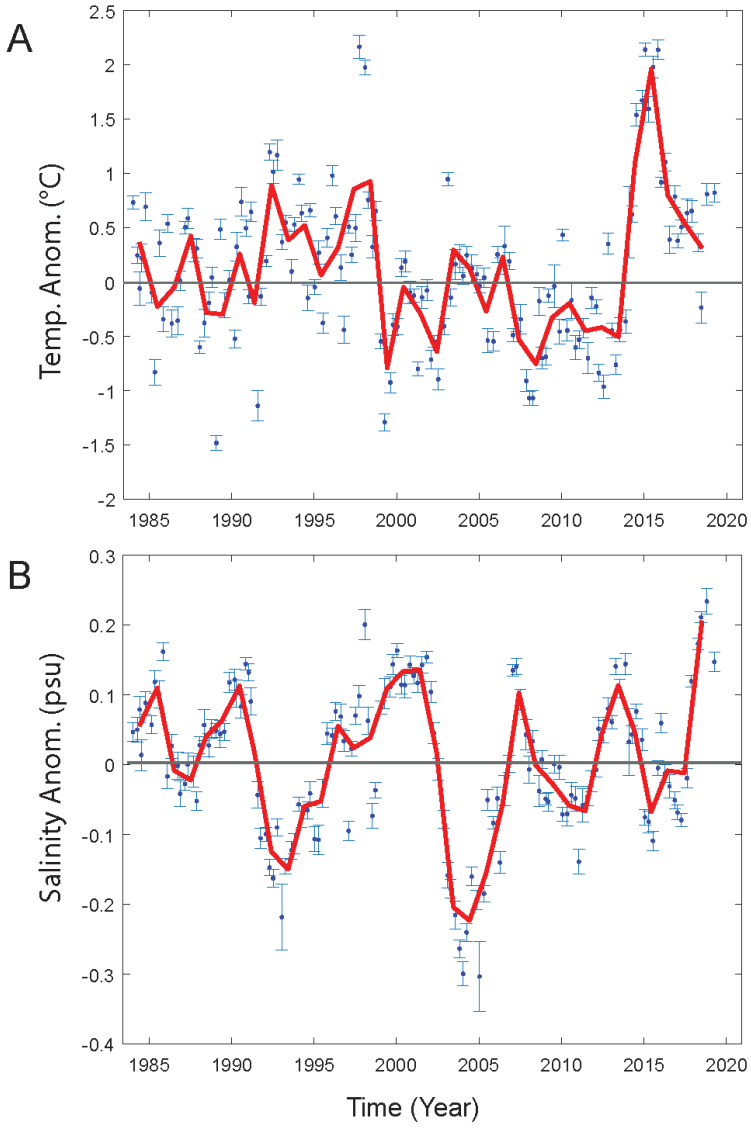

Figure 20. Cruise averages of ML temperature anomalies A) and ML salinity anomalies B) for the 66 standard CalCOFI stations (fig. 1) for 1984 to the spring of 2019. Whiskers indicate the 95% confidence intervals for the means. Red solid lines represent annual averages, grey horizontal lines the climatological mean, which is zero in the case of anomalies. Anomalies were based on the 1984 to 2012 period.

fornia Bight in fall 2018, suggesting that the signal took no more than 3 months to propagate to those areas. Absolute changes of salinity were highest in the offshore and California Current regions that are closest to the likely source of the high salinity water, the open northeast Pacific (Thompson et al. 2018).

In 2017 and 2018, the σ–26.2 isopycnal, which has a long-term average depth of 151 m, shoaled by almost 20 m relative to the high values observed during the MHW of 2014–16 (fig. 21a). Over the last year, this isopycnal was only slightly deeper than its long-term average with the exception of the spring of 2019 when it was 19 m deeper than average, likely due to the effects of the 2018–19 El Nino (fig. 21a). Patterns of spiciness (warm and salty versus cool and fresh) on the σ–26.2 isopycnal largely mirrored isocline depth during 2018–19 with values being close to average through winter 2019 and then rising by spring 2019 (fig. 21b). Oxygen on the isopycnal decreased significantly by about 10% between ~1995 and ~2005 (Bjorkstedt et al. 2012). Subsequent to 2005, however, oxygen on the isopycnal did not vary significantly over the long-term, and only short-term variations were observed (fig. 21c). A GAM fit to the data shows an increase of oxygen concentrations between 2010 and 2019, although this increase was not significant over the short time period. An analogous

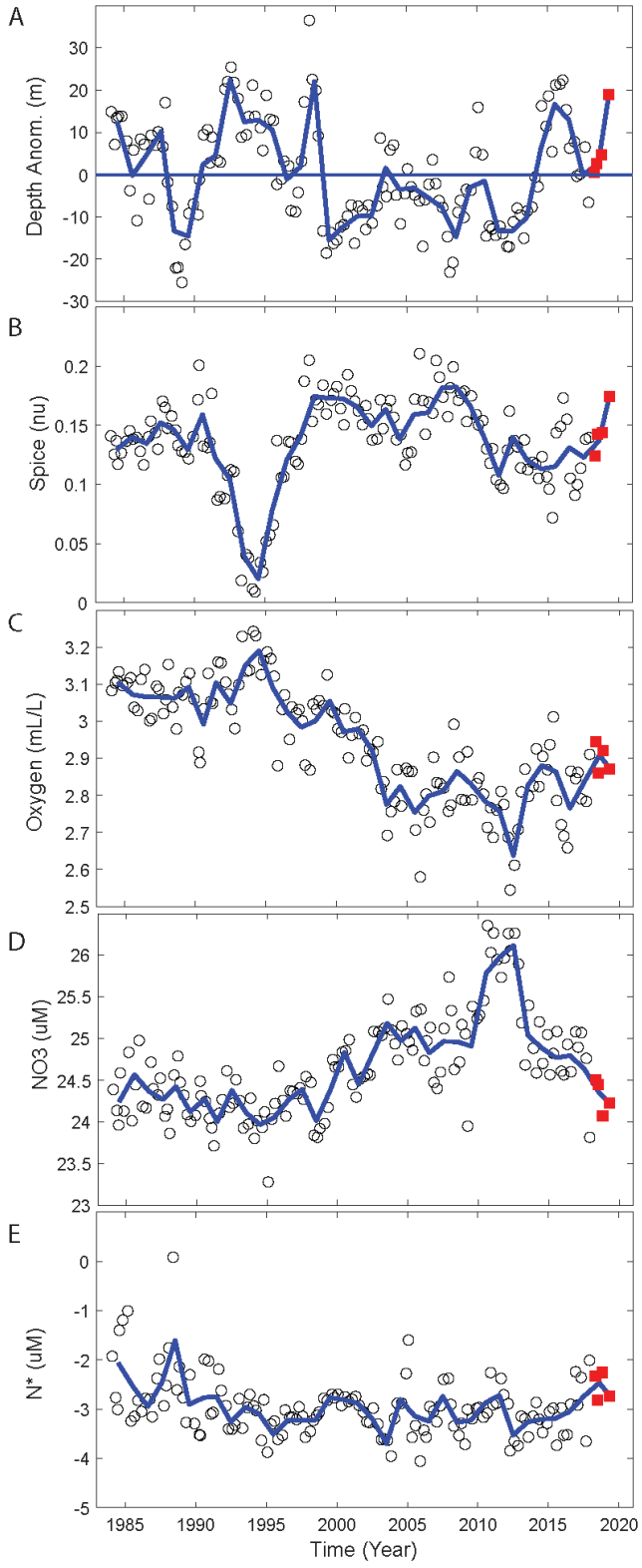

Figure 21. Anomalies of hydrographic properties at the σ_θ-26.2 isopycnal (open circles) averaged for each cruise over the 66 standard CalCOFI stations. Shown are anomalies of A) isopycnal depth, B) spiciness, C) oxygen, D) concentrations of nitrate and E) N*, a biogeochemical indicator that reflects nitrate deficit relative to concentrations of phosphate. The solid blue line connects annual averages. Summer and fall 2018 and winter and spring 2019 cruises are in red.

analysis of oxygen in the CalCOFI domain at depths of 100 to 200 m yielded almost identical results, except that the oxygen increased significantly between 2010 and the present. Nitrate concentration on the isopycnal fell steadily since the 2015 peak, and this trend continued through spring 2018 (fig. 21d). By contrast, N⋆, a biogeochemical indicator that reflects nitrate deficit relative to concentrations of phosphate (Gruber and Sarmiento 1997), on the isopycnal increased since 2014 (fig. 21e).

To determine if regional processes drove CalCOFI domain trends, region-specific concentrations of oxygen were analyzed at σ_θ–26.2 and the σ_θ–26.8 isopycnals. There was no evidence of region-specific trends as both isopycnals displayed patterns that were similar in all four regions over the past two decades (fig. S4). Oxygen at the σ_θ–26.2 isopycnal in all regions began declining significantly between 1995 and 2000 and continued to fall until about 2005. Oxygen did not decline significantly in any of the four regions after 2005; indeed, an increase of oxygen was observed for the California Current region. The patterns at the σ_θ–26.8 isopycnal, which is at a depth of 387 m on average, were similar in general, except that the large decline of oxygen lasted until about 2010, declining by 12% on average. Oxygen subsequently increased significantly in the California Current and upwelling regions.

Observations of oxygen dynamics are consistent with larger-scale analyses of oxygen in the North Pacific that show a rapid decline of oxygen concentrations at 300 m from about 1992 until 2003, stable oxygen from 2003 to 2013, and no significant long-term trend over the last 70 years (Schmidtko et al. 2017). These results do not support a hypothesis that global warming directly causes oxygen concentrations to decline in the CCE, nor do they suggest that this trend to will continue monotonically over the coming decades. Concentrations of oxygen in the thermocline of the CCE are likely related to subsurface salinity variability in the North Pacific Current and controlled by ocean circulation dynamics linking the CCE to the North Pacific (Pozo Buil and Di Lorenzo 2017). A modeling study suggest that anthropogenically-forced trends in oxygen at the σ_θ=26.5 isopycnal will be small in the CalCOFI domain and not detectable until decades from now (Long et al. 2016).

Mixed layer chlorophyll *a* was close to the long-term average over the last three years (fig. 22a); with values significantly lower than those observed during the 1999 to 2013 cool period. The exception was spring 2019 when chlorophyll *a* was as low as during the 2015–16 El Niño. These patterns were particularly strong in the California Current and upwelling regions (fig. S2). The depth distribution of chlorophyll *a* in the offshore and the California Current regions was similar to the warm period of 1984 to 1998, with subsurface maxima

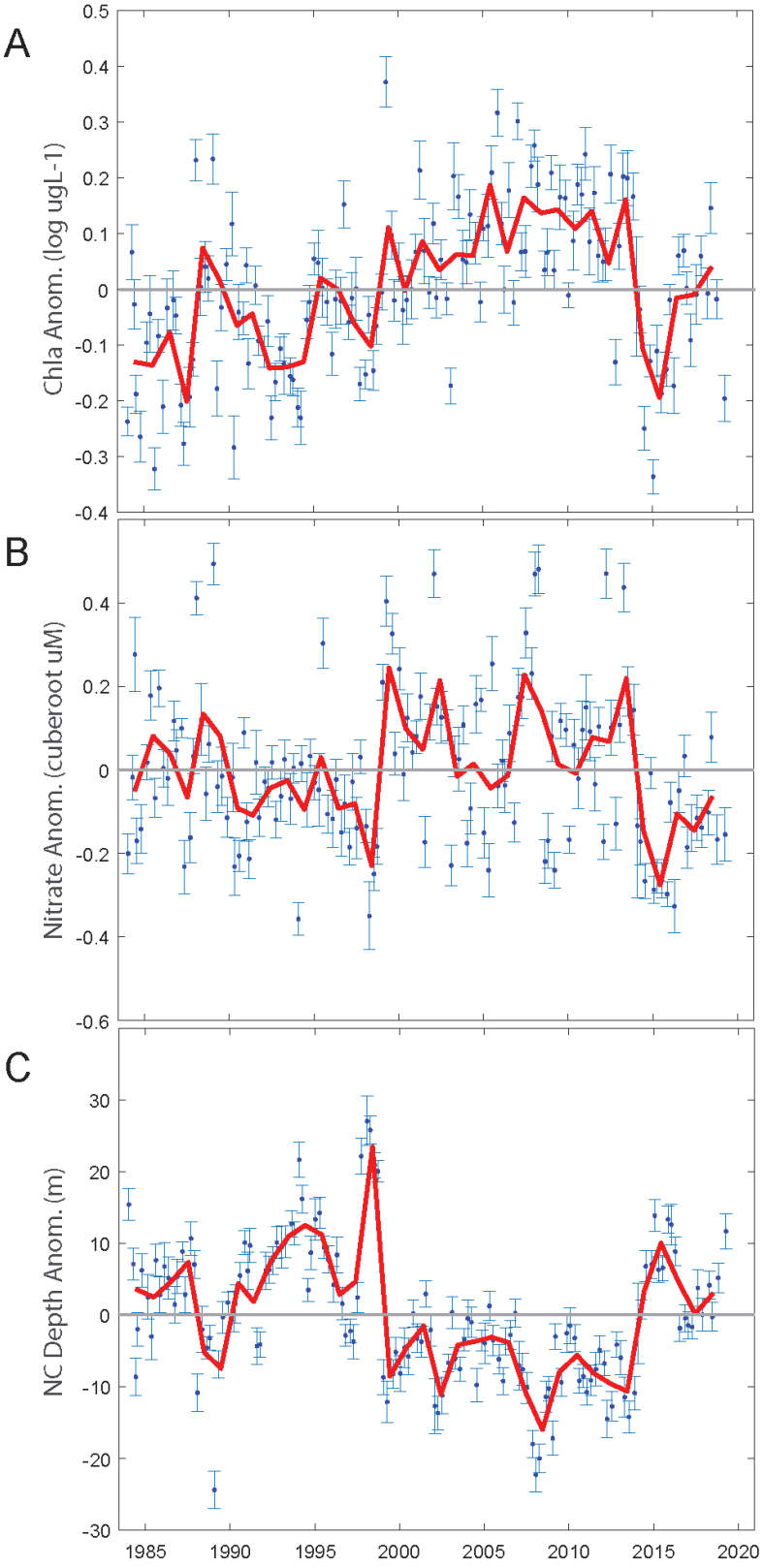

Figure 22. Cruise averages of mixed layer properties for the 66 standard CalCOFI stations. A) the $\log_{10}$ of chlorophyll *a*, B) the cube root of nitrate, and C) nitracline depth.

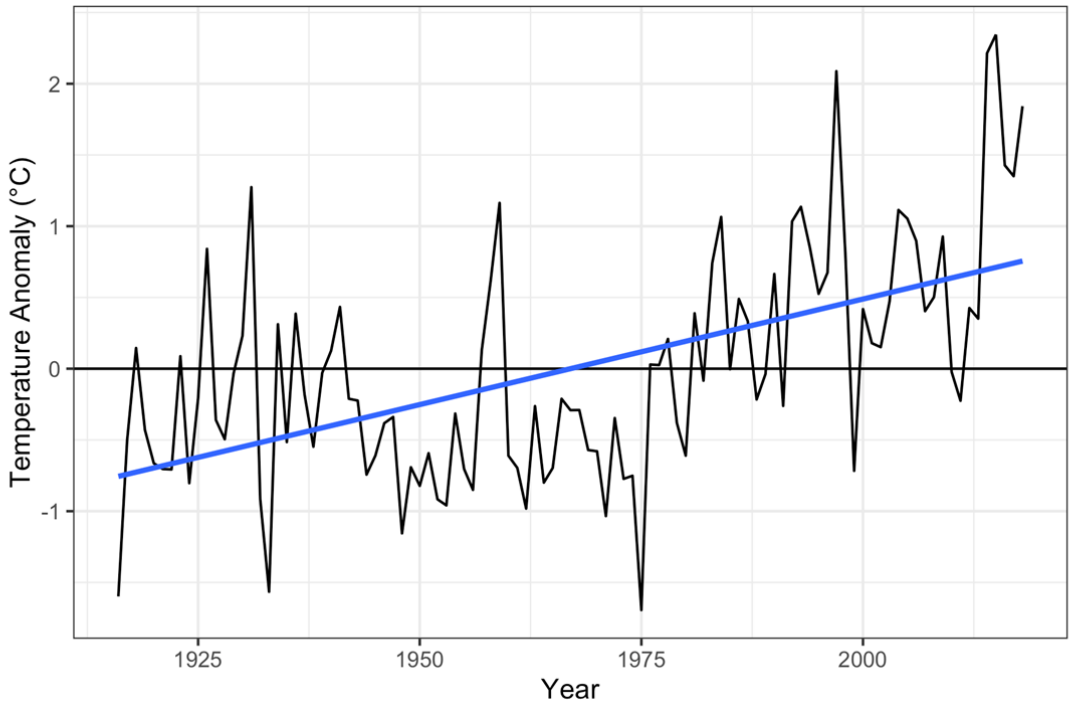

Figure 23. Annual mean SST anomalies taken from the Scripps Pier, La Jolla, California.

20 m below those observed during the 1999 to 2013 cool period.

Recent concentrations of mixed nitrate were significantly below long-term averages since the 2015–16 El Niño (fig. 22b). Nitracline depths[16] mirror those of mixed layer nitrate: values over the last two years were close to long-term averages and significantly lower than during the 1999 to 2013 cool period (fig. 22c). The exception was the spring of 2019 with significantly higher nitracline depths. The changes of mixed layer chlorophyll *a* and nitracline depth in 2018–19 mirror each other. The anomalies observed during the spring of 2019 may well be due to El Niño conditions (fig. 2)

Overall, conditions over the last 12 to 36 months strongly resemble conditions observed during the 1984 to 1998 warm period and are unlike those observed during the 1999 to 2013 cool period. This statement holds for the mixed layer properties of temperature, chlorophyll *a*, nitrate and nitracline depth and the water column distribution of chlorophyll *a* (the subsurface chlorophyll *a* maximum shifted, fig. S2) and nitrate (fig. S3) in most regions of the study domain. It is unknown if these conditions will persist over the next decade as they did from 1984 to 1997.

[16]Nitracline depth was defined as the depth where concentrations of nitrate reach values of 1 μM, calculated from measurements at discrete depths using linear interpolation. Statistical analyses were carried out in Matlab except for trend analyses that were carried out using R's mgcv gam-package.

Southern California:
Scripps Pier Water Temperature

Daily measurements of water temperature at the Scripps Pier in La Jolla, CA (32.5°N), began on August 22, 1916, and continue to the present[17]. On August 1, 2018, daily water temperature exceeded the previous record high from July 30, 1931 (Thompson et al. 2018). Water temperature continued to be anomalously warm through the remainder of 2018 as the mean annual temperature was ~1.5° above the long-term average (fig. 23). There was a significant trend ($r^2 = 0.30$) of rising water temperature through time with a ~0.148°C increase per year since 1916. Mean annual temperature was anomalously warm from 2012–18 and in 16 of 18 years since 2000 (fig. 23).

Baja California:
Satellite Imagery for Summer 2018

SST[18] ranged from 16° to 28°C and SST anomalies from –1.4° to 2.4°C throughout waters off Baja California (22.5°N to 32.3°N; fig. 22). SST anomalies were mostly positive in summer, 2018 but cooler water occurred off Punta Abreojos and just south of

[17]Scripps Pier temperature data was obtained from: https://scripps.ucsd.edu/programs/shorestations/shore-stations-data/data-sio. The Scripps Pier was lengthened in 1988 resulting in increased rip current transport of warmer water from the shore. Following (Checkley and Lindegren 2014), 0.45°C was subtracted from measurements taken after 1988.

[18]Temperature was obtained from https://podaac.jpl.nasa.gov/Multi-scale_Ultra-high_Resolution_MUR-SST.

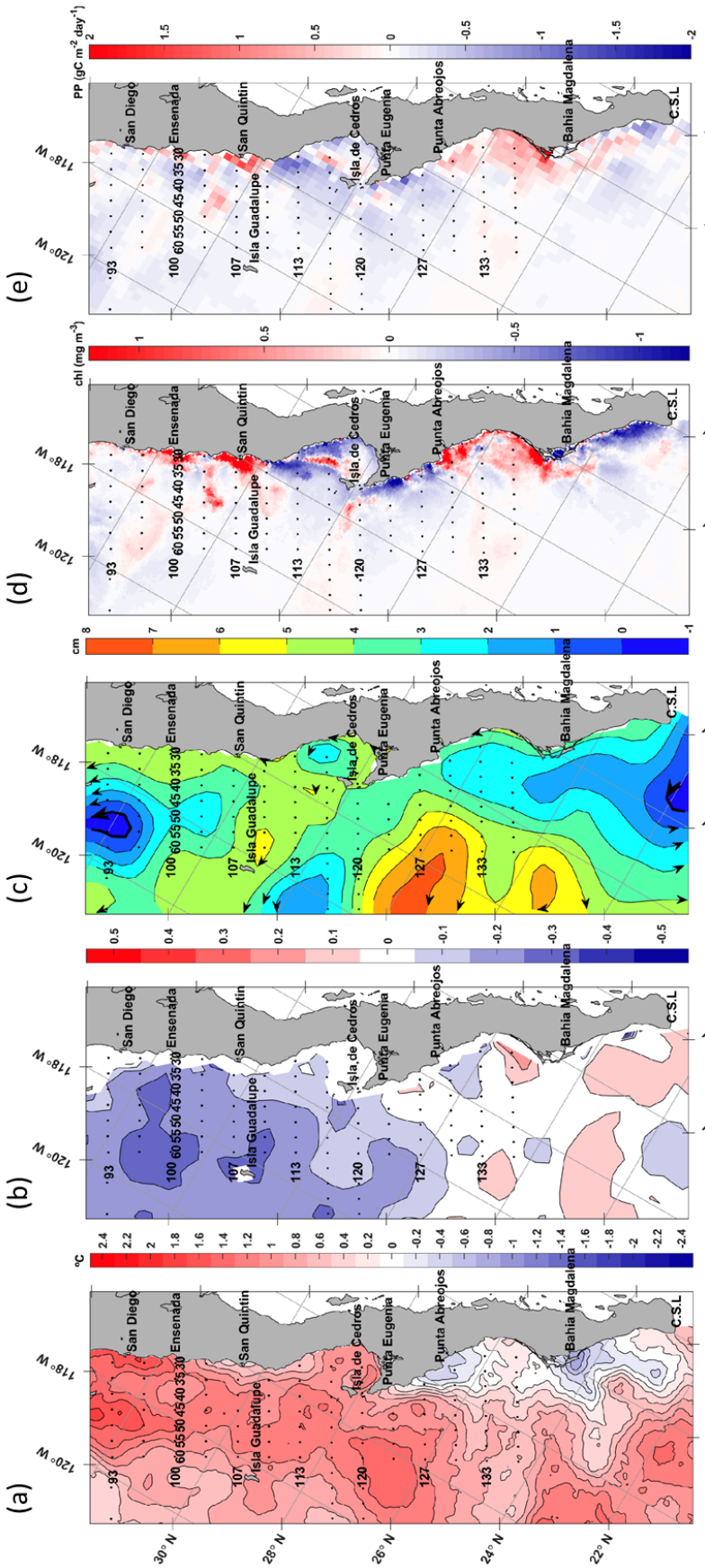

Figure 24. Satellite readings of a) SST, b) salinity, c) sea surface height, d) chlorophyll a and e) primary production off the coast of southern California and Baja California in summer 2018. Dots depict standard IMECOCAL stations.

Bahia Magdalena (fig. 24a). This cool coastal water suggested high upwelling at these two sites. Surface salinity[19] ranged from 33.4 to 35 and salinity anomalies from –0.5 to 0.2 (fig. 24b). Overall, salinity was negatively anomalous in northern Baja California and patchy to the south. Although upwelled water typically is relatively saline (McClatchie 2014), the spatial distribution of anomalously cool and anomalously saline water did not perfectly overlap. Rather, the cool water just south of Punta Abreojos was relatively fresh. South of Bahia Magdalena the cool water was mostly relatively saline.

SSH[20] anomalies (fig. 24c) ranged from –1 to just under 8 cm throughout the entire region. The SSH anomaly field depicted mesoscale eddies and gyres. There was a cyclonic gyre in the northern area, centered on line 93. This was the gyre of the Southern California Bight that extended southward roughly to a line between Isla Guadalupe and San Quintin. The cyclonic flow created a frontal system known as the Ensenada Front since it was generally most prominent off Ensenada (Peláez and McGowan 1986). The large anticyclonic eddy centered roughly 320 km southwest of Punta Eugenia measured approximately 7.5 cm in height, the highest point in the anomaly field. Further inshore, the flow reversed from generally equatorward to poleward (Lynn and Simpson 1987). This inshore poleward flow intruded from the south and was associated with broad cyclonic flow centered off Cabo San Lucas and stretching to Punta Abreojos (a distance of around 560 kilometers). The poleward flow appeared to be similar to that described by Durazo and Baumgartner (2002) in October 1997 at the beginning of the 1997–98 El Niño when warm, salty subtropical surface waters comprised much of the system.

Chlorophyll *a*[21] concentrations during summer 2018 ranged from <0.1 to almost 10 mg m^{-3} and anomalies from approximately –1.2 to1.2 mg m^{-3} (fig. 24d). The Ensenada Front was captured by a weak, offshore, positive anomaly between San Diego and Ensenada. There were strong, positive anomalies off Ensenada and San Quintin with filaments jutting offshore. Negative anomalies predominated south of San Quintin, from line 110 through line 127, with only patches of positive anomalies west and northeast of Isla Cedros. Positive anomalies from Punta Abreojos to just south of Bahia Magdalena mostly overlapped areas with cool water, suggesting that upwelling and production were high here in summer 2018. Primary production[22] varied from <0.3 to roughly 6 $gCm^{-2}day^{-1}$ with anomalies ranging between approximately –1.5 to 1.5 $gCm^{-2}day^{-1}$ (fig. 24e). Primary production anomalies largely mirrored chlorophyll *a* anomalies with mostly positive anomalies from approximately San Diego to Isla Guadalupe, negative anomalies from Isla Guadalupe to Punta Abreojos, positive anomalies from Punta Abreojos to just south of Bahia Magdalena, and negative anomalies at the southern tip of the peninsula.

REGIONAL EPIPELAGIC MICRONEKTON AND SALMON OBSERVATIONS

Northern California Current

The Northwest Fisheries Science Center and Oregon State University have conducted multiple surveys over the last two decades to measure the status of various biota at multiple trophic levels. Although the main goal is to examine ocean conditions that correlate to salmon survival, other elements of the surveys examine prey composition, abundance, and availability, competitors, and predators of the salmon. Since these surveys target different life stages, they occur at different times of the year but are relatively consistent in timing among years. Each of these seasonal datasets represents a unique ecosystem state that, taken as a whole, can help us understand the phenology of the Northern California Current (NCC).

Winter salmon forage indicators in the northern California Current Juvenile Chinook salmon feed primarily on late-larval and early-juvenile fishes when they enter coastal waters (Daly and Brodeur 2015). The late-larval and early-juvenile life stage of most marine fishes is difficult to sample effectively (Brodeur et al. 2011), which led us to explore alternative indices of potential prey fish abundance. The majority of marine fishes in the NCC spawn in late winter and early spring (Brodeur et al. 2008). Winter–spawned fish larvae that grow and survive through spring provide a food base for juvenile steelhead and coho and Chinook salmon during their first marine summer. Therefore, winter ichthyoplankton biomass was used as a proxy for potential salmon food availability during the spring critical growth period. This biomass included five of the most commonly eaten fish prey (Daly et al. 2013). During cold and productive periods in October–December from 1997 to 2013, ichthyoplankton biomass was relatively high, and coastal fish larvae such as Pacific sandlance (*Ammodytes personatus*), smelts (Osmeridae), and

[19]Salinity was obtained from https://podaac.jpl.nasa.gov/dataset/SMAP_JPL_L3_SSS_CAP_MONTHLY_V42.

[20]Sea surface height anomalies were obtained at https://www.aviso.altimetry.fr/en/data/products/sea-surface-height-products/global/gridded-sea-level-anomalies-mean-and-climatology.html.

[21]Chlorophyll *a* concentration was obtained at https://esa-oceancolour-cci.org/ and ttps://rsg.pml.ac.uk/thredds/dods/CCI.

[22]Primary productivity was obtained from the VGPM model (Behrenfeld and Falkowski 1997) that is available from Oregon State University https://www.science.oregonstate.edu/ocean.productivity/ using data from MODIS Aqua. The model estimates net primary production as a function of chlorophyll concentration, available light, and the temperature-dependent photosynthetic efficiency.

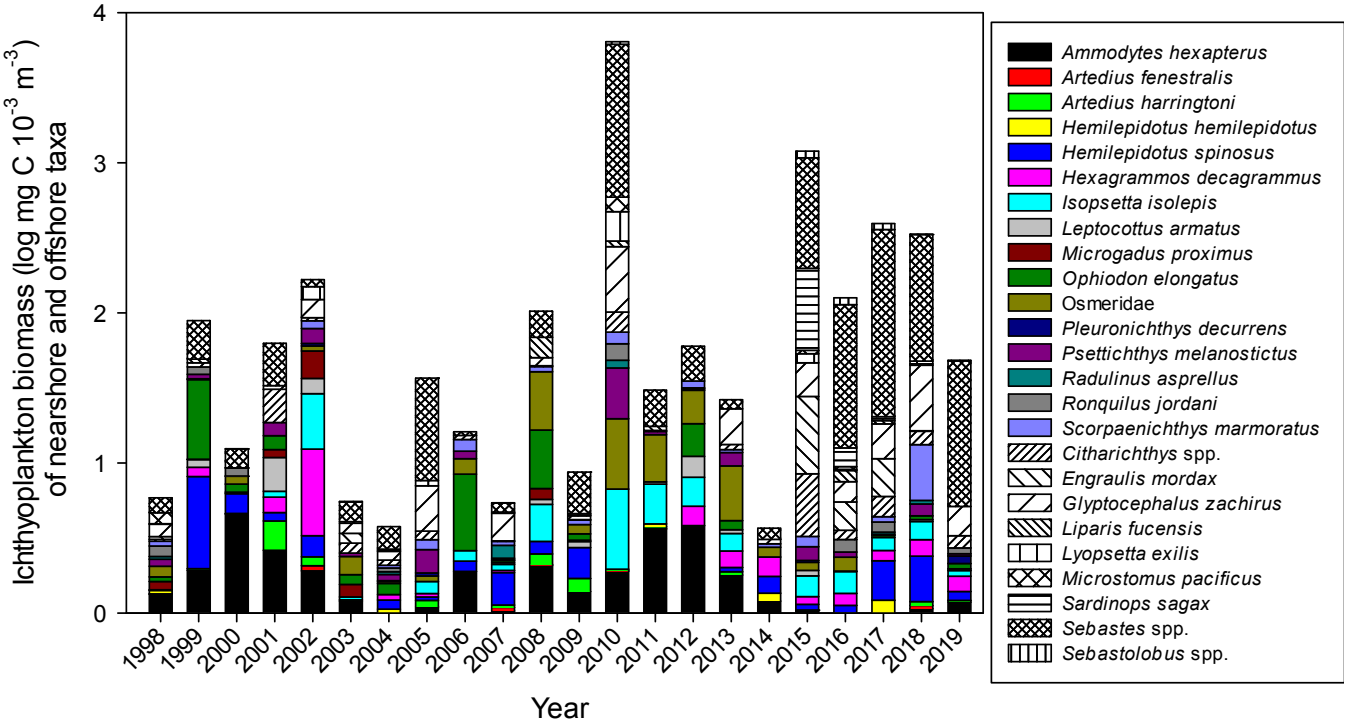

Figure 25. Annual average biomass of ichthyoplankton from winter (January–March) collected along the Newport Hydrographic Line (NH) line stations NH05-25. Taxa listed in color are coastal and make up the index of coastal prey biomass (ICPB). Taxa in black and white patterning reside offshore relative to the coastal taxa.

various sculpins (Cottidae) dominated the winter (January–March) fish communities (Daly et al. 2017). By contrast, when the ocean was relatively warm (coincident with onshore transport) in October–December of 1997 to 2013, overall winter ichthyoplankton biomass was low and dominated by offshore taxa such as rockfishes and winter–spawned northern anchovy (*Engraulis mordax*). Importantly, from 1997 to 2013, juvenile salmon survival was higher during the cold periods and lower during the warm periods.

The marine heat wave and El Niño of 2014–16 coincided with dramatic increases in SST temperatures throughout much of the northeast Pacific Ocean (+2.5°C; Bond et al. 2015), and this warming contributed to changes in the winter ichthyoplankton biomass and community not previously observed in the now 22-year time series (Auth et al. 2018). Specifically, there was a substantial increase in the observed cross-shelf differences in ichthyoplankton biomass (Daly et al. under review). Since 2015, the biomasses of offshore ichthyoplankton taxa increased significantly along the Newport Hydrographic Line (44.65°N, fig. 1), and juvenile salmon increasingly consumed these taxa (Daly et al. 2017). Moreover, the juvenile salmon that out-migrated in 2015–17, when there was a high biomass of offshore ichthyoplankton taxa, returned as adults to the Columbia River one to two years later in much reduced numbers compared to previous years[23].

In light of these changes, the winter ichthyoplankton biomass index based on winter ichthyoplankton samples from the Newport Hydrological Line[24] was modified from last year's State of the California Current report (fig. 31 in Thompson et al. 2018) to include only taxa with cold-water affinity/coastal adult habitats (see fig. 25 for detailed list of the coastal [colored bars] and offshore [black and white bars] taxa). In addition, the number of taxa included in the new Index of Coastal Prey Biomass (ICPB) was expanded to include the coastal and offshore taxa beyond the top five fish prey of juvenile salmon that were analyzed previously (Thompson et al. 2018). Since 2014, the ICPB was below average with the exception of 2018 (which was more of an average year) and the coastal biomass index in 2019 was the third lowest in the 22-year time series (fig. 25). The community composition of ichthyoplankton in 2019 was once again dominated by offshore taxa, with the community indicator suggesting poor food conditions for piscivorous juvenile salmon that out-

[23]Columbia River Data Access in Real Time [DART]; www.cbr.washington.edu/dart/query/adult_daily/; last accessed July 30, 2019.

[24]Ichthyoplankton samples were collected from 5 stations spaced ~9 km apart along the Newport Hydrographic Line with a bongo net lowered to 100 m (or within 5 m of the bottom at shallow stations) and towed obliquely to the surface. Sampling was conducted approximately every 2 wk between January and March. Only samples from January–March were used, assuming that larvae collected during these months would have had sufficient time to grow to the average size of prey eaten by juvenile salmon in late spring and early summer (complete methods in Daly et al. 2017).

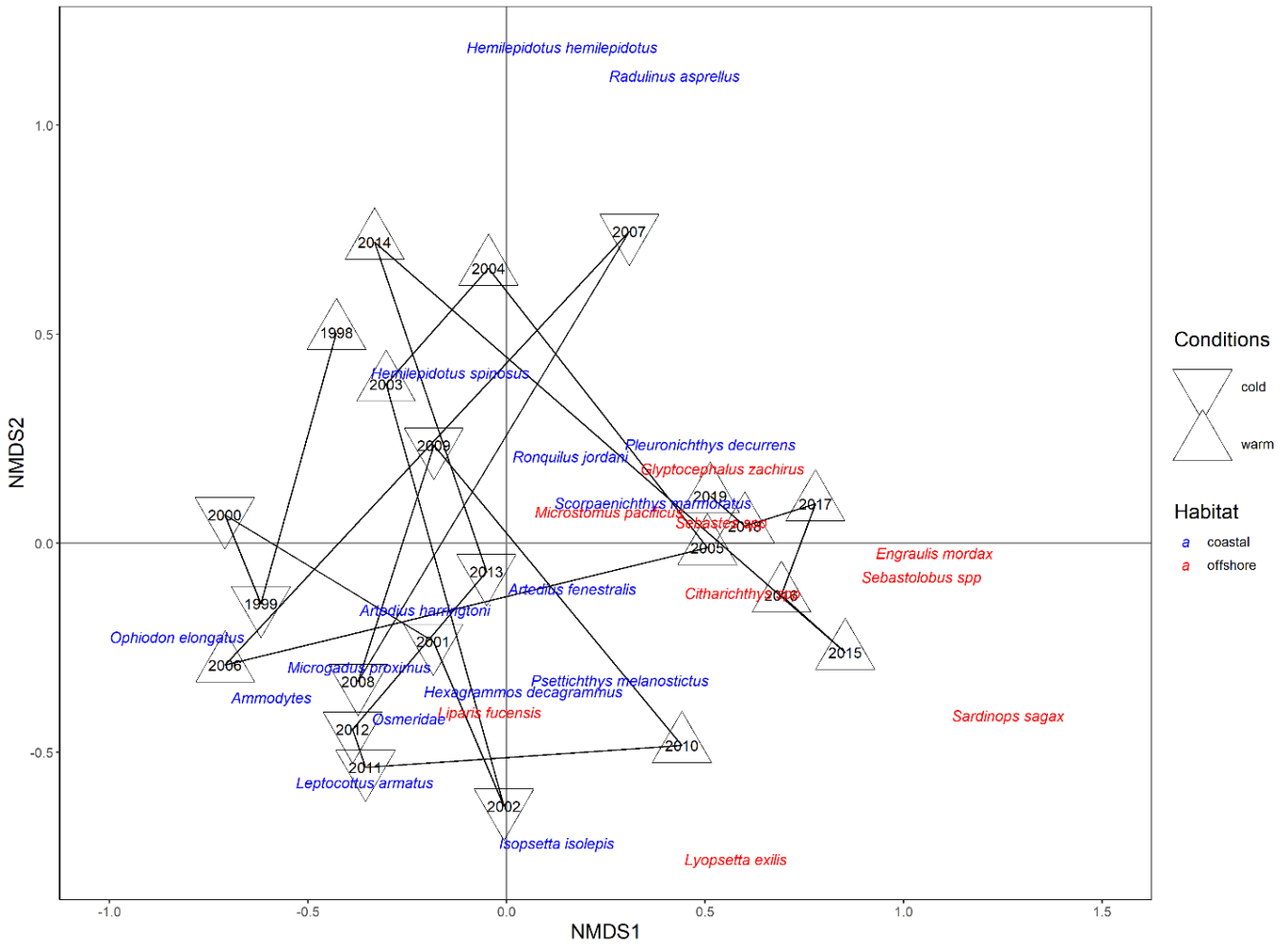

Figure 26. NMDS analysis of winter ichthyoplankton collected off the Newport Hydrographic line stations NH05-25. Taxa colored blue reside in coastal habitats as adults and those colored red live in offshore habitats as adults. Upward-facing triangles delineate warm years and downward-facing triangles cold years.

migrate into the ocean in 2019 (figs. 25, 26). Warm ocean conditions influence both the biomass and the community composition of winter ichthyoplankton in the NCC. Survival has uniformly been poor for juvenile salmon that out-migrated into the ocean since the marine heat wave of 2014–16. Ichthyoplankton biomass and species composition in 2019 were similar to those observed during 2015–18 (fig. 26), suggesting a continuation of the poor salmon returns for at least the next several years. Winter ichthyoplankton, especially the coastal taxa represented in the ICPB, are an important indicator of future food conditions for piscivorous juvenile salmon during a vulnerable and critical time in their life cycle.

Summer Pre-Recruit ichthyoplankton assemblage and micronekton assemblage In contrast to the *winter* findings described above, the composition and concentration of the *summer* ichthyoplankton assemblage along the central-northern coast of Oregon[25] in June 2019 was close to average relative to the previous 12 years (with the exception of the unusually high concentrations of northern anchovy in 2014 and 2016; fig. 27). Total mean larval concentration was the fourth highest in the 13-year time series. Larval myctophids in 2019 had the highest concentration of the time series, flatfish and "other" the second highest (although the "other" group still accounted for only 2% of the total mean larval concentration), and northern anchovy the fourth highest concentration. These observations are an indication that the larval fish community in the northern California Current was returning to a more "normal" or average state in the summer of 2019.

[25]Ichthyoplankton samples were collected from 3-4 stations representing coastal (<100 m in depth), shelf (100-1000 m), and offshore (>1000 m) regions along both the Newport Hydrographic Line (44.65°N, 124.35-125.12°W) and Columbia River Line (46.16°N, 124.22-125.18°W) lines off the coast of Oregon during May-July in 2007–19. A bongo net lowered to 100 m (or within 5 m of the bottom for stations <100 m deep) and towed obliquely to the surface collected samples (complete methods in Auth (2011).

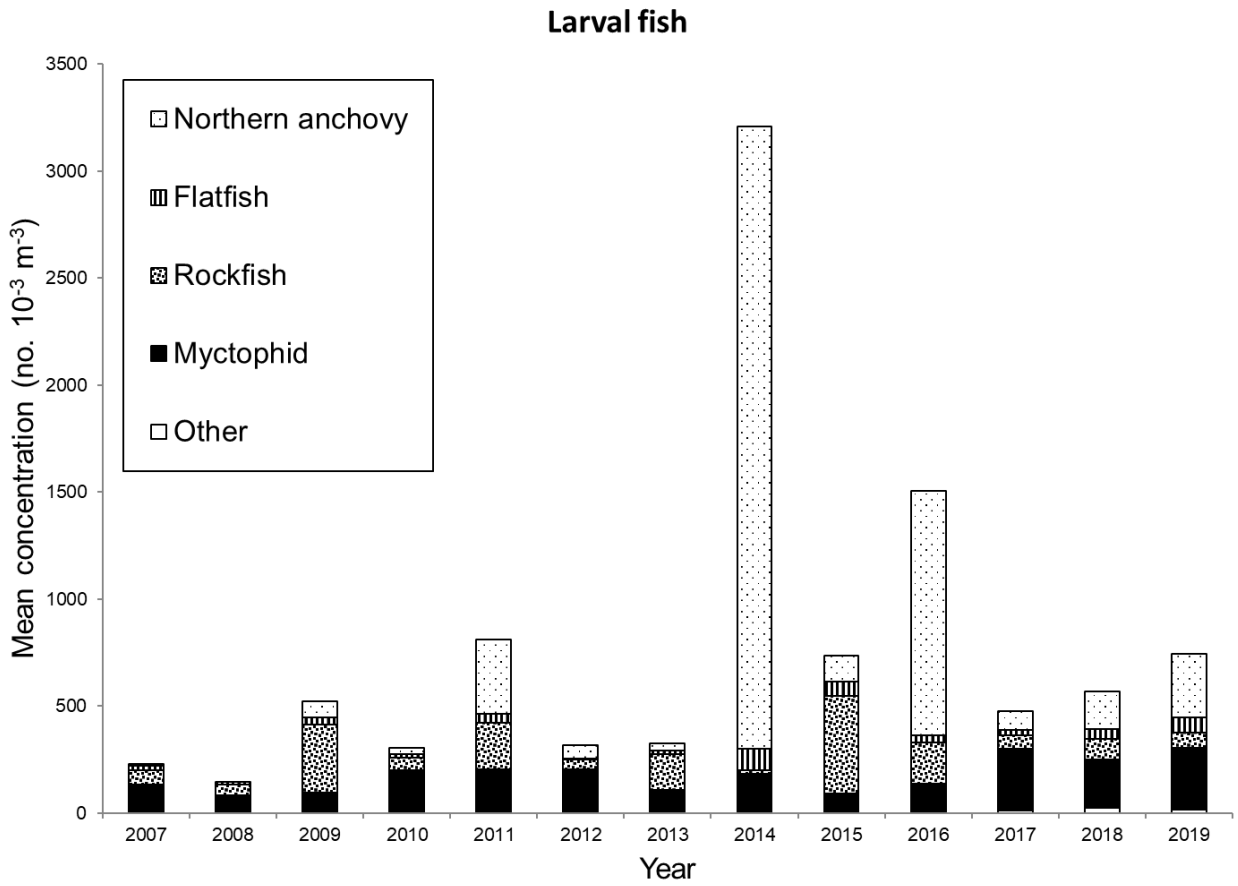

Figure 27. Mean concentrations (no. 10^{-3} m^{-3}) of the dominant larval fish taxa collected during May–July in 2007–19 along the Newport Hydrographic (NH; 44.65°N, 124.35–125.12°W) and Columbia River (CR; 46.16°N, 124.22–125.18°W) lines off the coast of Oregon.

The summer micronekton assemblage[26], which consists of post-larval fish (i.e., juvenile and adult pelagic fish), in the NCC in June 2019 had average abundance for the eight-year time series, reversing the precipitous decline from 2016 to 2018 (fig. 28). The abundance of Clupeiformes and "other" taxa was the second lowest in the time series, while flatfish abundance was the highest. Rockfish abundance in 2019 was by far the highest for the time series (35 times the average rockfish abundance in 2011–18). High rockfish catch was primarily due to one large haul at the shelf-break station along the Columbia River line (46.0°N), where 7,474 juvenile rockfish were collected—mostly shortbelly rockfish (*Sebastes jordani*; n = 7343). Fourteen different taxa of rockfish were collected in 2019, with the dominant species consisting of shortbelly (97% of total rockfish), widow (*S. entomelas*; 1.5%), and canary (*S. pinniger*; 0.7%). In addition, only one small pyrosome was collected in 2019, which was in sharp contrast to the extraordinarily high numbers throughout the sampling area in the previous three years (Brodeur et al. 2018). These observations are an indication that the pelagic juvenile/adult fish and tunicate communities in the northern California Current were returning to a more "normal" or average state in the summer of 2019.

In summary, the epipelagic ichthyoplankton and micronekton assemblages in the northern California current in 2019 exhibited different ecosystem states and spawning assemblages depending on the time of year the sampling occurred. In the NCC, the warm fall/winter SST conditions of 2018–19 induced low biomass of coastal ichthyoplankton taxa available in winter, as well as a predominance of fish taxa associated with warm water and offshore distributions. In contrast, by summer both the summer ichthyoplankton assemblage and the micronekton assemblages showed a return in both abundance and community composition to resemble an average ocean year. In addition to the seasonal difference

[26]Post-larval (i.e., juvenile and some adult) fish were collected using a modified-Cobb midwater trawl (MWT) with a 26 m headrope and a 9.5 mm codend liner fished for 15 min at a headrope depth of 30 m and ship speed of ~2 kt. MWT collections were made at 3-6 evenly spaced, cross-shelf stations representing coastal, shelf, and offshore regions along nine half-degree latitudinal transects between 42.0 and 46.0°N latitude in the northern California Current region during May-July in 2011–19 (although no sampling was conducted in 2012). Sampled volume was assumed to be uniform for all hauls. All fish collected were counted and identified to the lowest taxonomic level often onboard, although pre-recruit rockfish were frozen and taken back to the lab for identification using precise meristic and pigmentation metrics.

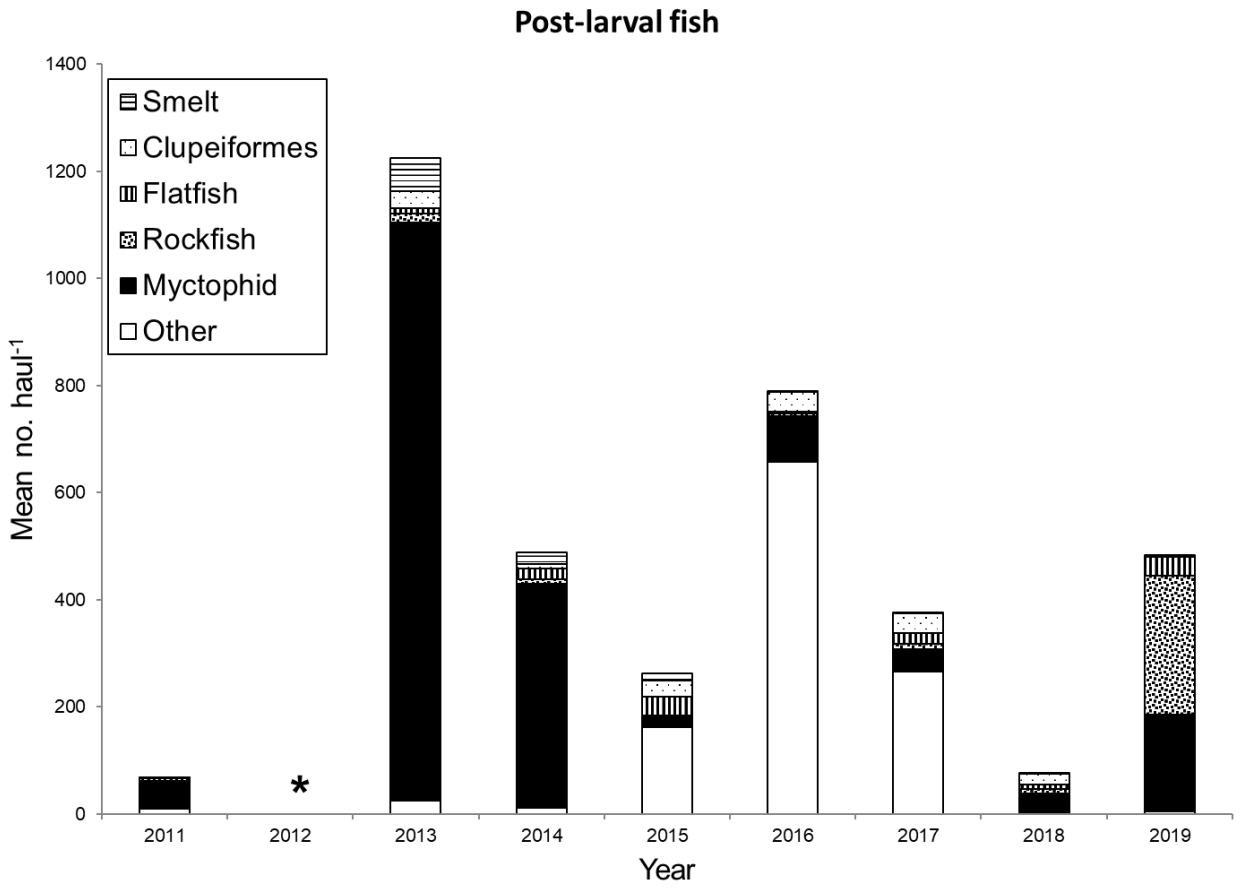

Figure 28. Mean catches (no. haul^{-1}) of the dominant post-larval fish taxa collected during May–July in 2011–19 along nine half-degree latitudinal transects between 42.0 and 46.0°N latitude in the northern California Current region. * = no samples were collected in 2012.

in when these ichthyoplankton data sets were collected, there were also differences in the spatial extend of sampling, suggesting that the differences between the two metrics could be either ecological change over time or simply representations of different ecosystems.

Juvenile Salmon and Ocean Ecosystem Survey (JSOES)

The fish and invertebrate assemblage from trawls in the upper 20 m off Oregon and Washington[27] in June 2018 and 2019 was less anomalous than during the preceding three years (fig. 29). During 2015–17, the NCC was dominated by taxa such as pyrosomes, Pacific mackerel (*Scomber pacificus*), and jack mackerel (*Trachurus symmetricus*) that typically reside in warmer waters to the south of the study area. An NMS ordination clearly showed that the 2015–17 assemblages were outliers, distinct not only from the 1999 La Niña assemblages, but also from the assemblage sampled during the 2005 warm event (Brodeur et al. 2006) in the NCC (fig. 29).

In 2018 and 2019, taxa such as Pacific pompano (*Peprilus simillimus*), which are typically only caught during warm years, were still present. Additionally, more California market squid (*Doryteuthis opalescens*) were captured in 2019 than any other year in the 22-year time series. Other common taxa in 2018 and 2019 included gelatinous species, yearling Chinook (*Oncorhynchus tshawytscha*), coho (*O. kisutch*), and juvenile chum (*O. keta*) salmon, and Pacific herring (*Clupea pallasii*). Pyrosomes, that were first captured in 2017 and still present in 2018, were absent in 2019.

Beginning in 2015, the jellyfish community off Washington and Oregon was quite different from previous years (fig. 30). Prior to 2015, the large, cool-water scyphozoan species, sea nettle (*Chrysaora fuscescens*), was numerically dominant. However, during the warm ocean years of 2015–16 and 2018, the more offshore-oriented

[27]The JSOES has been conducted by the Northwest Fisheries Science Center (NWFSC) in late June every year between 1998 and 2019. Sampling occurred along 11 east–west transect lines off Washington and Oregon (fig. 1), ranging from approximately 45° to 48°N. Trawls were conducted at 6 to 8 stations on each transect from the shallowest bottom depth possible (~30 m) out to ~50 km from shore, often extending beyond the continental shelf (Brodeur et al. 2005; Barcelo et al. 2018). Sampling was conducted during daytime in the upper 20 m of the water column at every station using a pelagic rope trawl with the headrope at about 1 m, that had a 336 m^2 mouth opening with variable mesh sizes (162.6 cm at mouth to 8.9 cm at cod end). To retain catches of small nekton, a 6.1 m long, 0.8 cm mesh knotless liner was sewn into the cod end. The rope trawl was towed for 30 minutes at a speed over ground of approximately 6 km h^{-1}.

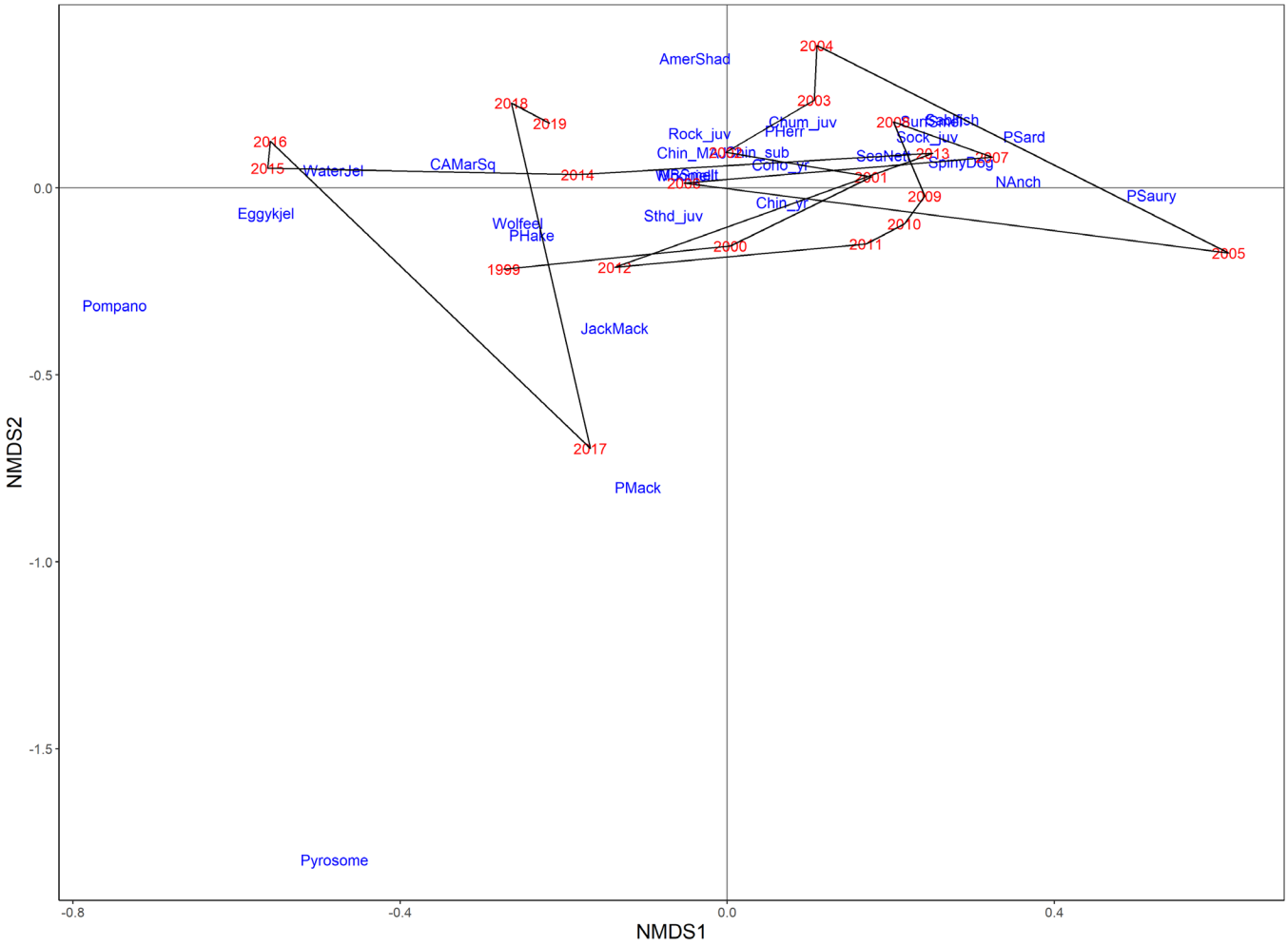

Figure 29. NMDS plot for taxa collected by the Juvenile Salmon and Ocean Ecosystem Survey off Oregon and Washington. Taxa are in blue and years in red font. Consecutive years are connected by black lines

water jellyfish (*Aequorea* spp.) was much more abundant, while densities of sea nettles were low. In 2019, both sea nettle and water jellyfish were at average densities.

Yearling Chinook salmon abundance during June surveys correlate positively with returning spring Chinook jack and adult salmon counts at the Bonneville Dam (with 1 and 2 year lags, respectively), as did the abundance of yearling coho salmon to subsequent coho salmon smolt to adult survival (Morgan et al. 2019). Catch-per-unit effort of both yearling Chinook and coho salmon during the June 2019 survey was near average (fig. 31). Based solely on the correlations observed in previous years, this suggests that adult returns of spring Chinook in 2021 and coho salmon returns in 2020 will be close to average, though other ecological factors will influence this relationship.

Taken as a whole, the nekton community in the summer of 2019 off Washington and Oregon indicated that the ecosystem was in a mixed state. On the one hand, the 2014 surface warming and the 2015–16 El Niño still had a noticeable impact on the nekton in this region, as taxa such as Pacific pompano were still present and California market squid were very abundant. On the other hand, average catches of water jellyfish, sea nettles, and juvenile salmonids suggest that the ecosystem may be returning to a close to average state. However, the last sampling event was in June, before the emergence of a new marine heat wave.

Central and southern California

Rockfish Recruitment and Ecosystem Assessment Survey (RREAS) Catches of juvenile groundfishes and epipelagic micronekton from the RREAS[28] (32.3°N to 41.56°N) in late spring 2019 indicated continued declines for pelagic young-of-the-year (YOY) rockfishes

[28]Epipelagic micronekton samples were collected during May and June by the Southwest Fisheries Science Center Rockfish Recruitment and Ecosystem Assessment Survey. A modified midwater Cobb trawl towed at a depth of 30 m (10 m at sites shallower than 50 m) sampled pelagic species along the CCE in the mixed layer where juvenile rockfishes are typically found. Methods are fully described by Sakuma et al. (2016).

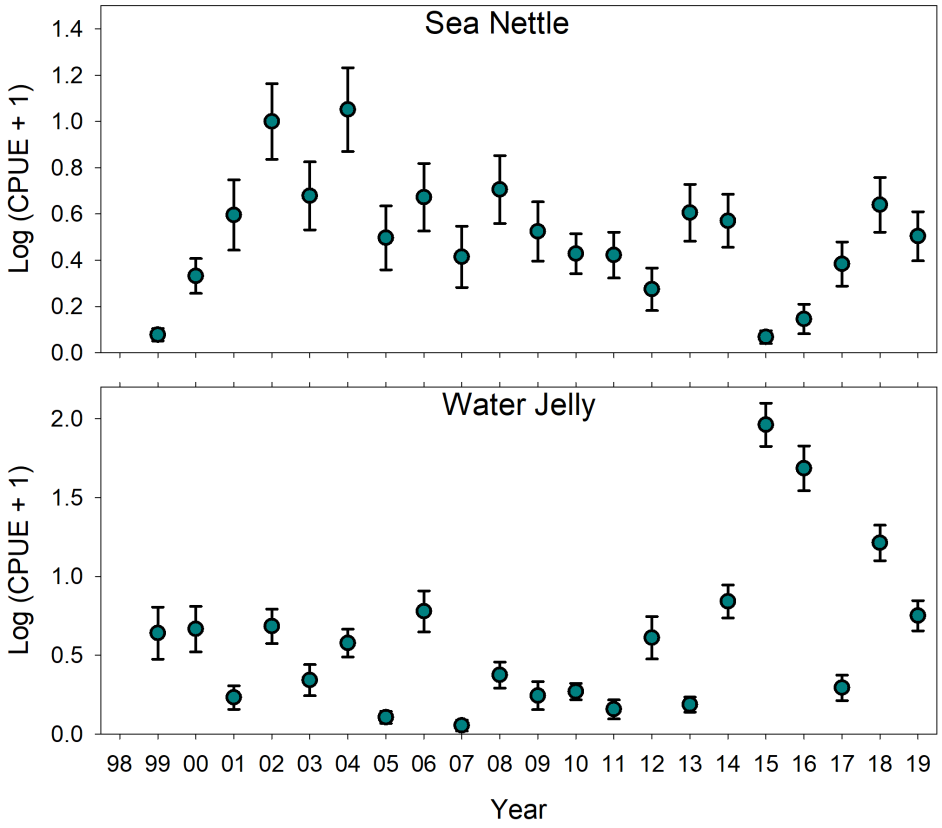

Figure 30. Catch per unit effort for common jellyfish by the Juvenile Salmon and Ocean Ecosystem Survey off Oregon and Washington.

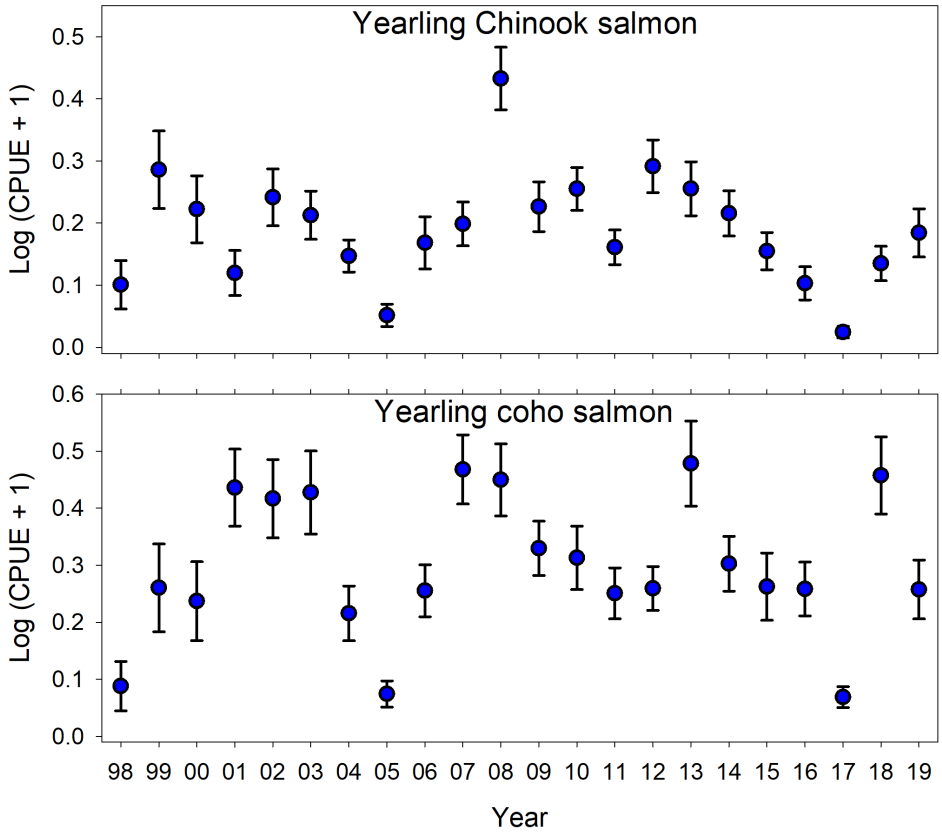

Figure 31. Catch per unit effort for yearling coho and Chinook salmon by the Juvenile Salmon and Ocean Ecosystem Survey off Oregon and Washington.

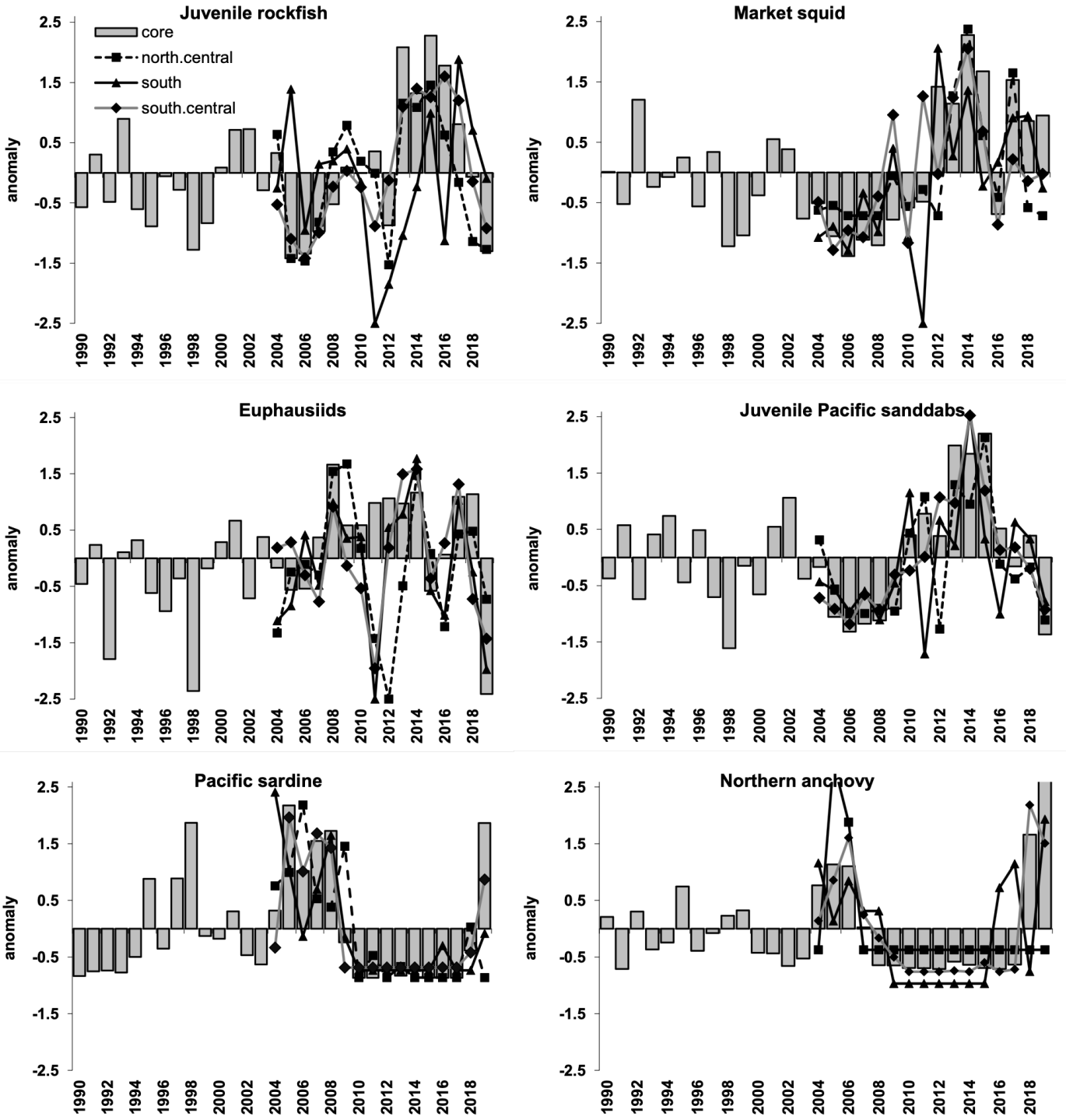

Figure 32. Standardized anomalies (of average (ln(catch+1)) catches) for key forage taxa sampled by the Rockfish Recruitment and Ecosystem Assessment Survey.

and sanddabs (*Citharichthys* spp.), with strongly negative anomalies following near-average levels in 2018 and very high abundances from 2013–17 (fig. 32). Abundance of YOY rockfishes was greatest again in the Southern California Bight, where catches were close to the long-term average. YOY Pacific hake (*Merluccius productus*, not shown) were at low abundance in central California, although this species was fairly abundant in the Southern California Bight. No YOY lingcod (*Ophiodon elongates*) were captured in 2019.

The high abundance of adult northern anchovy in the core and south central regions continued in 2019

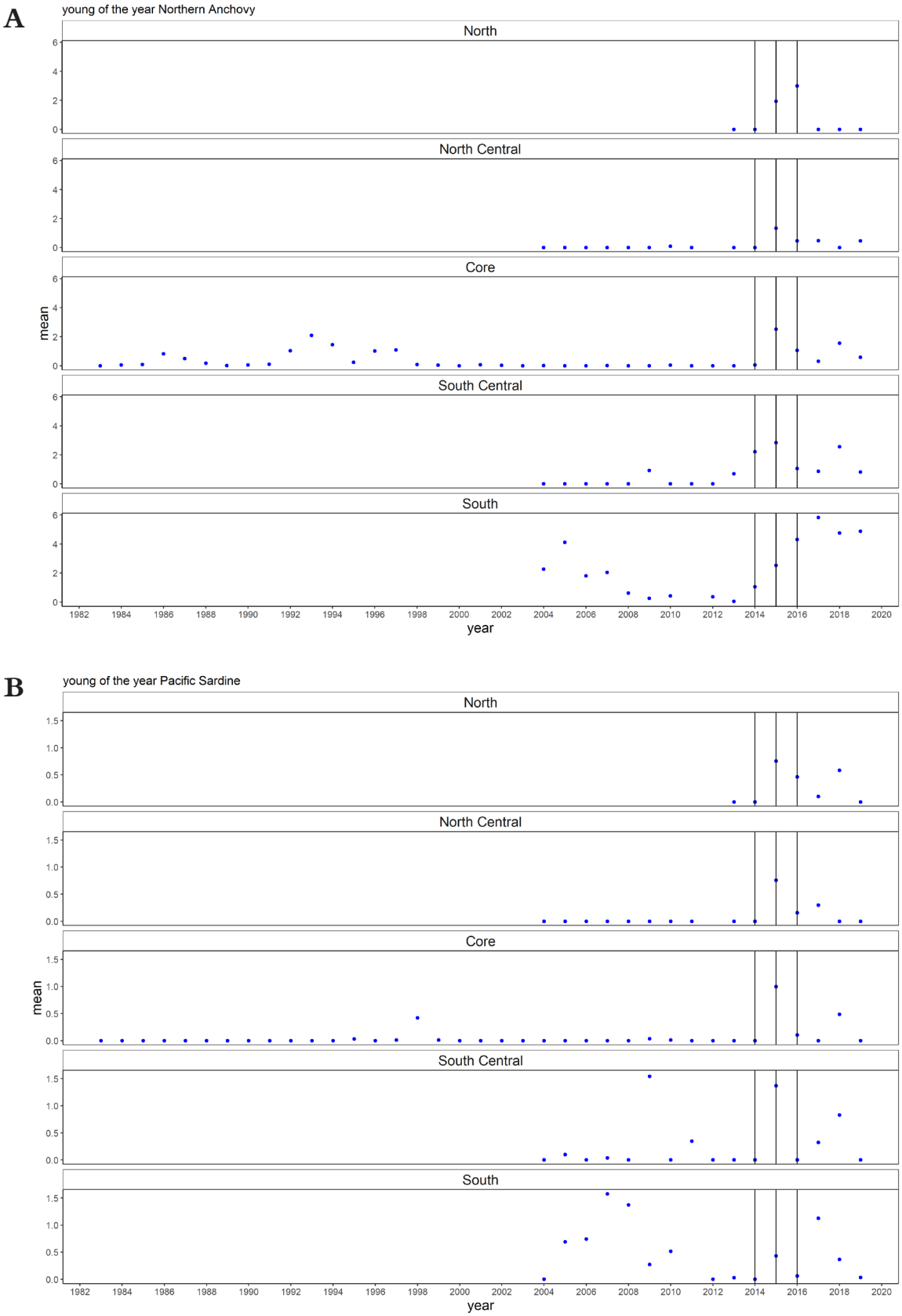

Figure 33. Ln(catch+1) average catch for (A) young-of-the-year northern anchovy and (B) young of the year Pacific sardine from the RREAS in 5 regions off California.

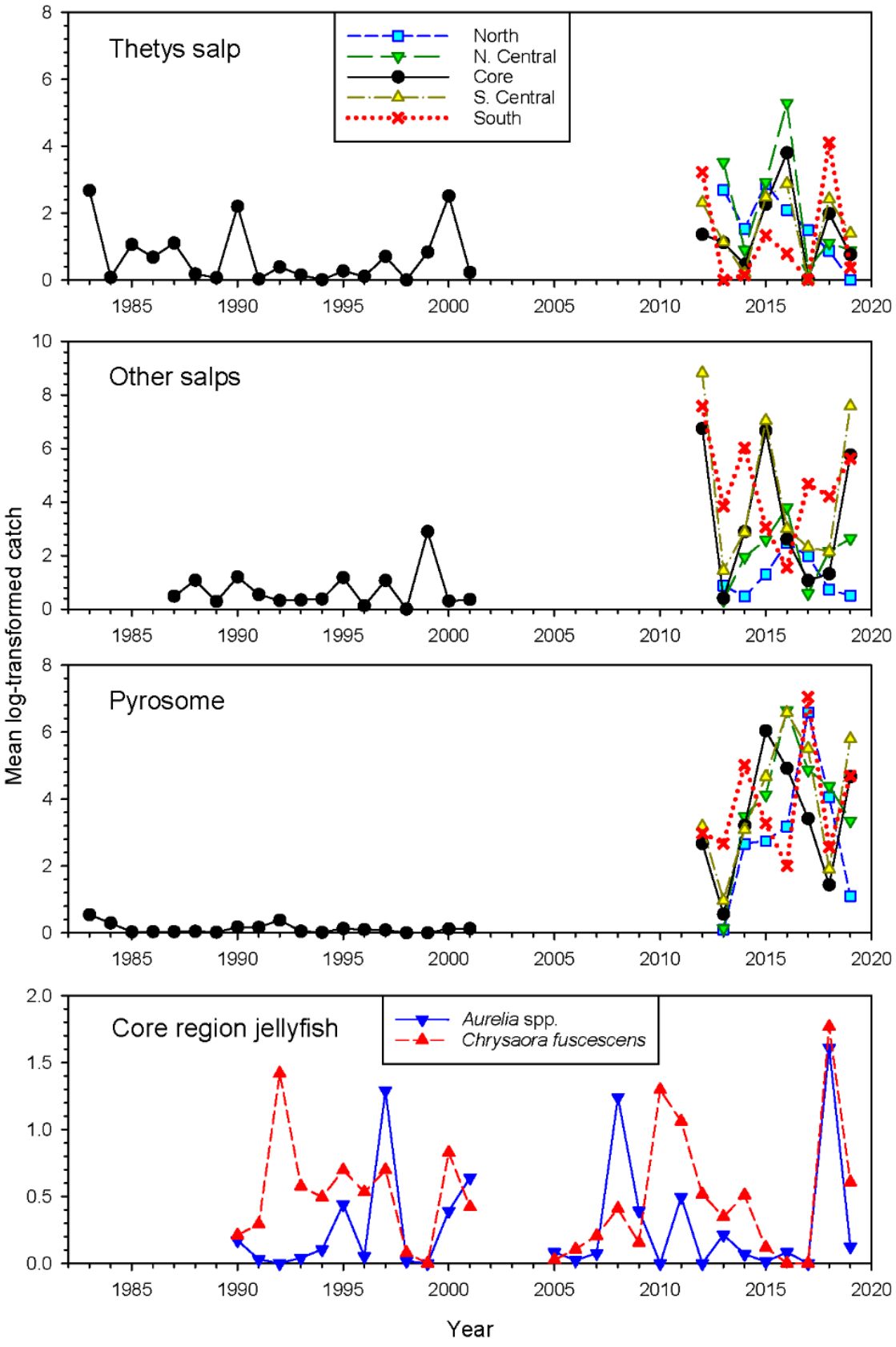

Figure 34. Standardized catches of and pelagic tunicates (*Thetys* salps, other salps, and pyrosomes) and jellyfish (*Aurelia* spp. and *Chrysaora fuscescens*) in the core and expanded survey regions.

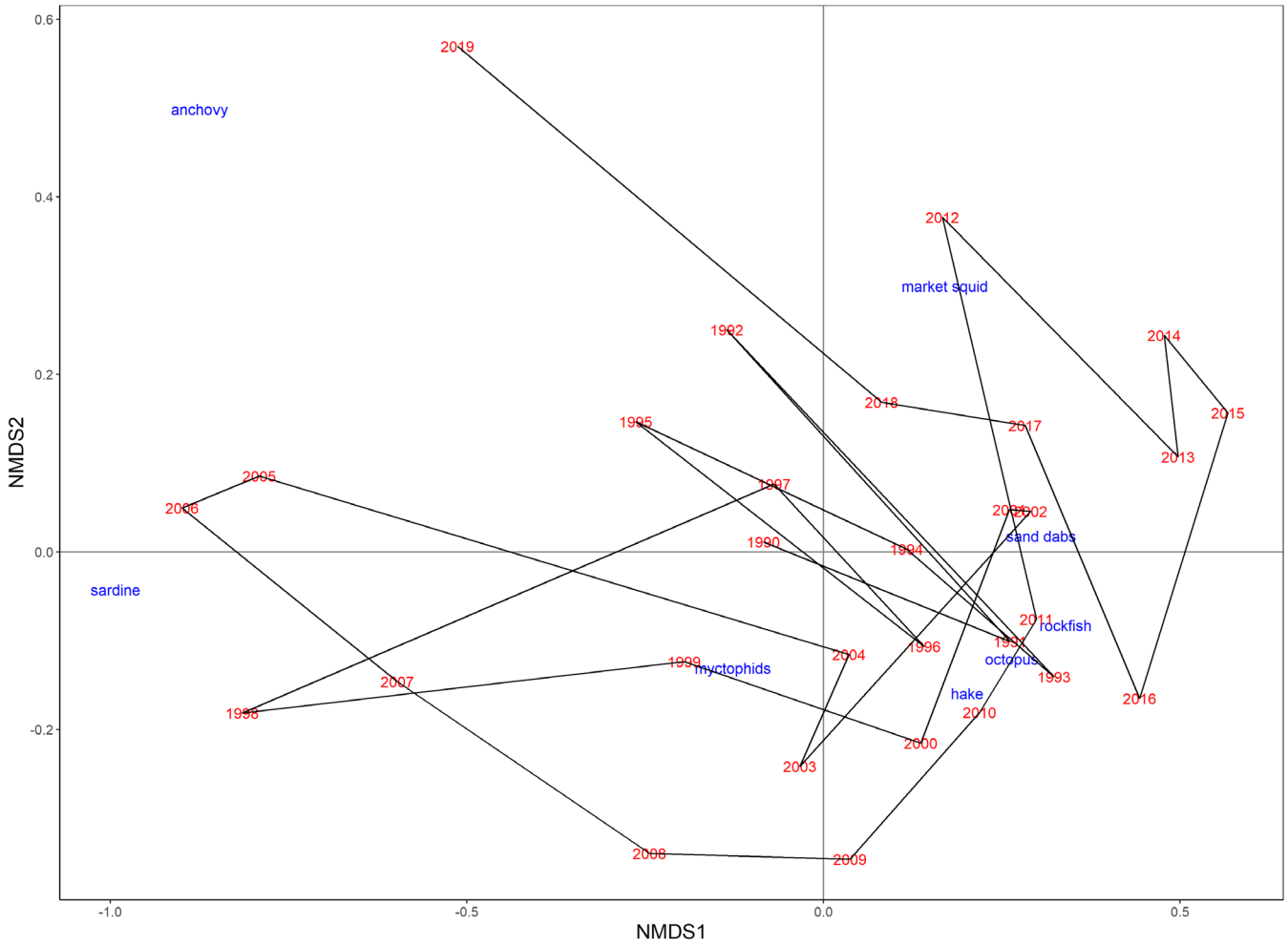

Figure 35. NMDS graph for the nine key taxonomic groups of forage species sampled in the central California core region in the 1990–2019 period.

(fig. 32). In fact, the relative abundance of adult anchovy in the core area was higher in 2019 than any previous year in the survey (extending back to 1983). Adult Pacific sardine were more abundant than in roughly the last ten years but still at low abundance relative to the late 1990s and early 2000s.

In 2015, YOY northern anchovy were at the highest level on record in each region with the exception of the south where abundance was second-highest only to 2005 (fig. 33). YOY northern anchovy remained high in 2016 in the north, south central and core regions in 2016. In 2019, YOY northern anchovy (fig. 33a) were at low levels throughout the survey area in, with the exception of the Southern California Bight, where abundances have been very high since 2015 (fig. 33a). YOY Pacific sardine abundance was also high in 2015 relative to prior years (fig. 33b). Subsequent to 2015, YOY Pacific sardine abundance was high in select regions and years (2018 in the north, core and south central; 2017 in the south), but was uniformly low in 2019. Overall, YOY northern anchovy were much more abundant than YOY Pacific sardine (note that scales differ between panels in fig. 33a and b).

There were substantial declines in krill, particularly in the core region where abundance was comparable to 1998 (the lowest value in the 1990–2019 time series), a pattern which extended throughout most California waters (fig. 32). However, market squid were at fairly high abundance levels in the core region, and closer to average or just below average levels in other regions. Pelagic red crab (*Pleuroncodes planipes*, not shown) also continued to be encountered in the southern California Bight, albeit with a slow decline since the 2015 peak.

Shifts in the abundance of various gelatinous organisms showed reversals for 2019 relative to recent years (fig. 34). Catches of salps in the genus *Thetys* were low in 2019 relative to recent years; however, catches of other salps and pyrosomes were higher in 2019 than 2018, reflecting sustained high abundance of pelagic Thalacians in California waters (despite the tremendous drop in pyrosome abundance off Oregon and Washington). There

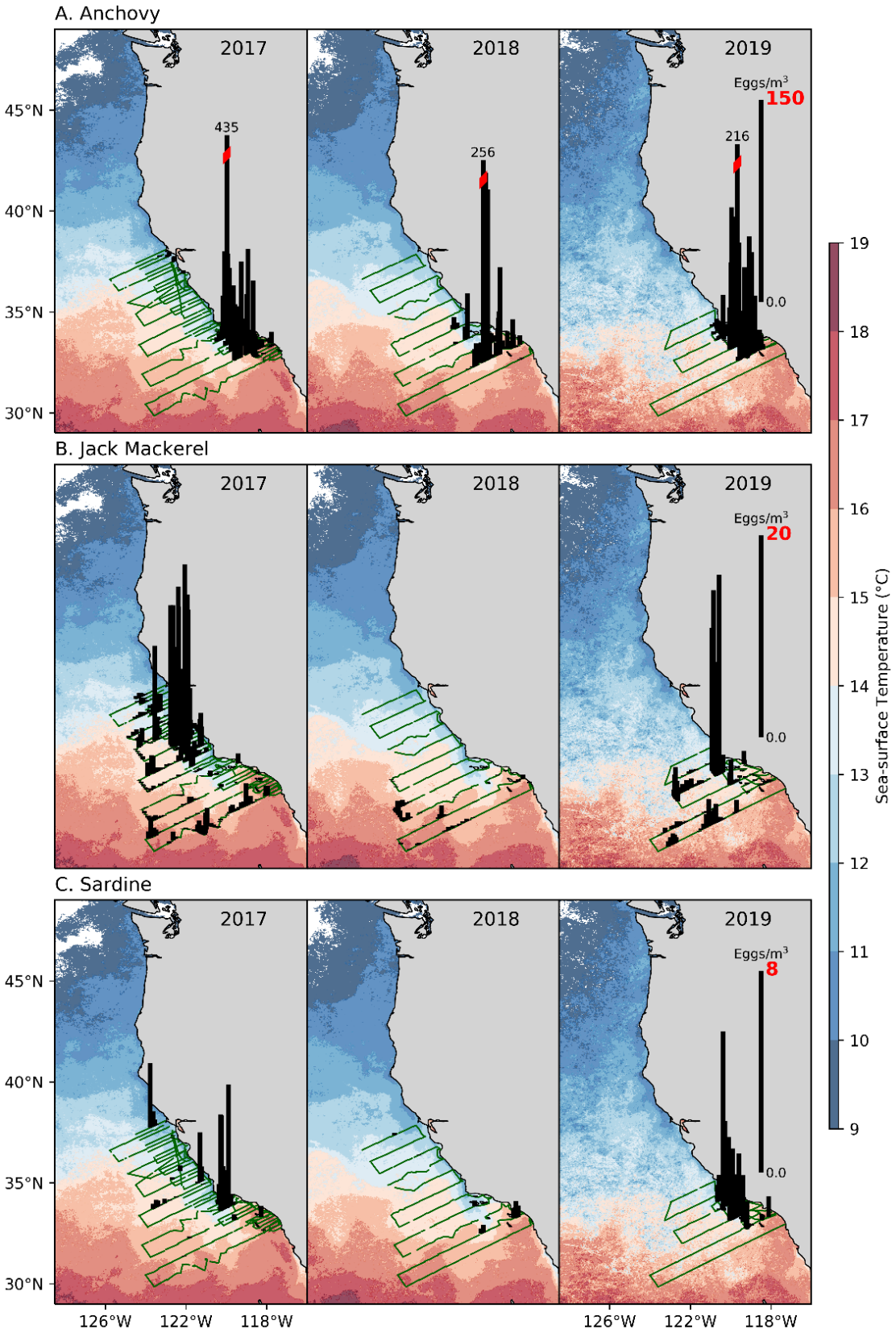

Figure 36. Density of eggs of anchovy (A), jack mackerel (B), and sardine (C) collected with the continuous underway fish egg sampler (CUFES) during the spring 2016–18 CalCOFI cruises. Data were overlaid on satellite-derived sea surface temperatures (AVHRR 1.4-km resolution; ˚C). Note that scales differ among species.

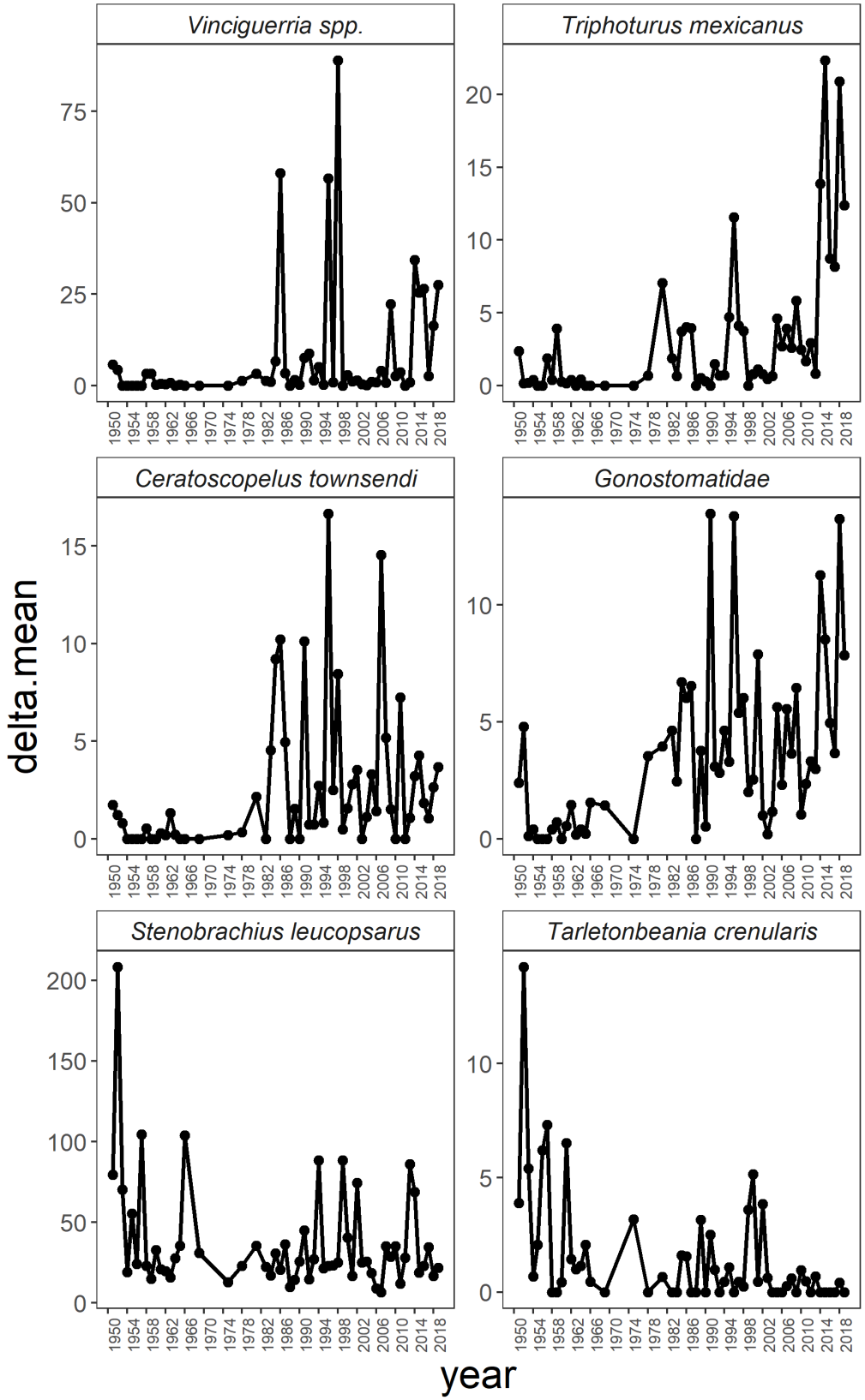

Figure 37. Mean abundances (calculated using the delta method of Nelson (2016), which accounts for zero inflation) of ichthyoplankton of mesopelagic taxa with warm (*Vinciguerria* spp., *Triphoturus mexicanus*, *Ceratoscopelus townsendi* and Gonostomatidae) and cool (*Steonobrachius leucopsarus*, *Tarletonbeania crenularis*) water affinities collected in spring on CalCOFI lines 80 and 90.

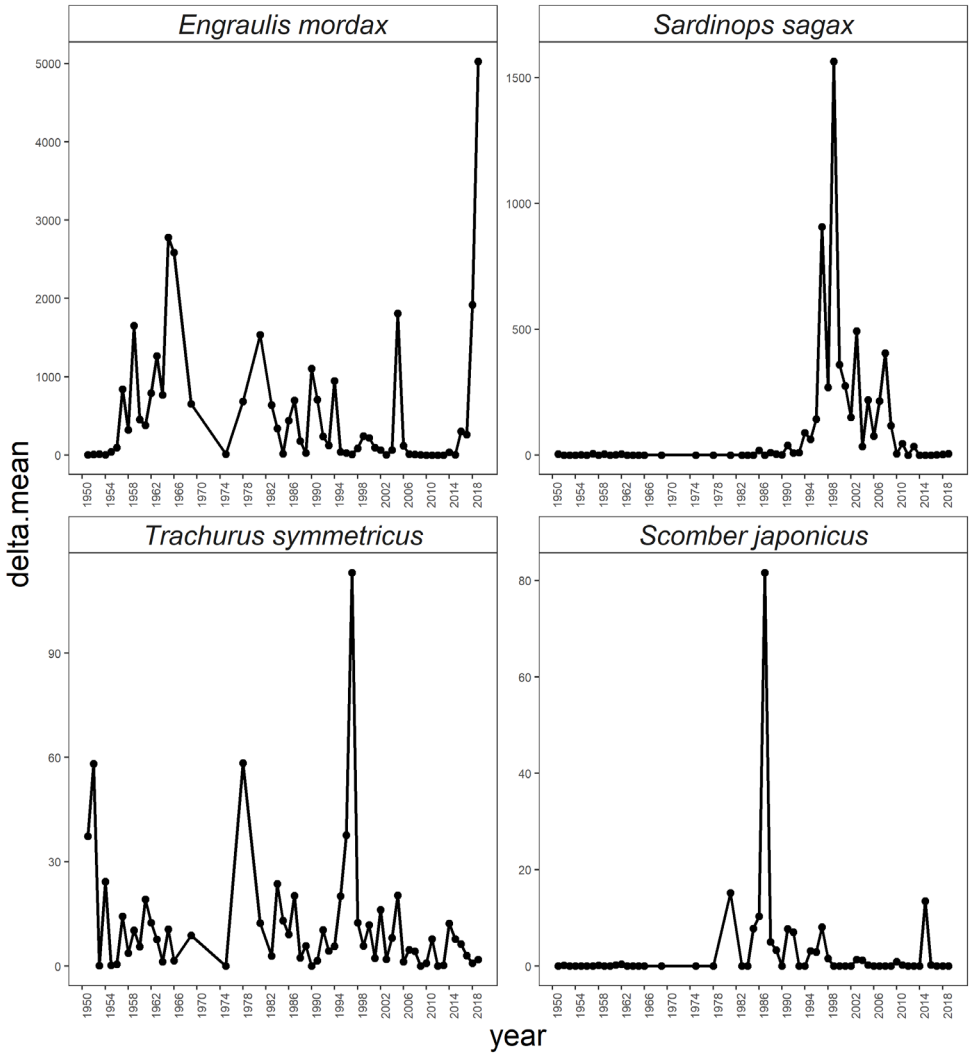

Figure 38. Mean delta abundances of ichthyoplankton from coastal pelagic species collected in spring on CalCOFI lines 80 and 90.

was a sharp reversal of the very high catches of scyphozoan jellyfish (primarily *Aurelia* spp. and *Chrysaora fuscescens*) from 2018, when both species were encountered at high abundance levels, although catches of *C. fuscescens* was close to long-term average levels.

NMDS analysis based on mean log catch of the fish and cephalopod community from the core RREAS region between 1990 and 2019 reflected the unprecedented dominance of adult northern anchovy the increase in Pacific sardine, and the scarcity of rockfishes and sanddabs (fig. 35). NMDS axis 2 correlated positively with anchovy and market squid abundance, and negatively with YOY Pacific hake and myctophids; the 2019 NMDS 2 value was the highest in the time-series. NMDS axis 1 correlated negatively with both northern anchovy and Pacific sardine abundance and positively with YOY rockfishes and sanddabs, and the 2019 NMDS axis 1 value was also relatively low, reflecting a reversal of the positive values observed over the preceding decade.

CalCOFI Continuous Underway Fish Egg Sampling (CUFES) Egg abundance of northern anchovy, jack mackerel, and Pacific sardine in spring 2019[29] was greatest in the northwest portion of the Southern California Bight and off Point Conception in waters with sea-surface temperatures of about 13.5–15°C (fig. 36). Although the spring CalCOFI survey often extends north to San Francisco, the spatial coverage of 2019 sampling was limited to the core CalCOFI area (fig. 1).

Northern anchovy was the most abundant species sampled in 2019. Northern anchovy egg abundances

[29]Water was continuously pumped onto the ship from a depth of 3 m while the ship was underway. Water samples were filtered on the ship and collected sequentially at regular (5–30 minutes) intervals. Detailed methods in Checkley et al. (1997).

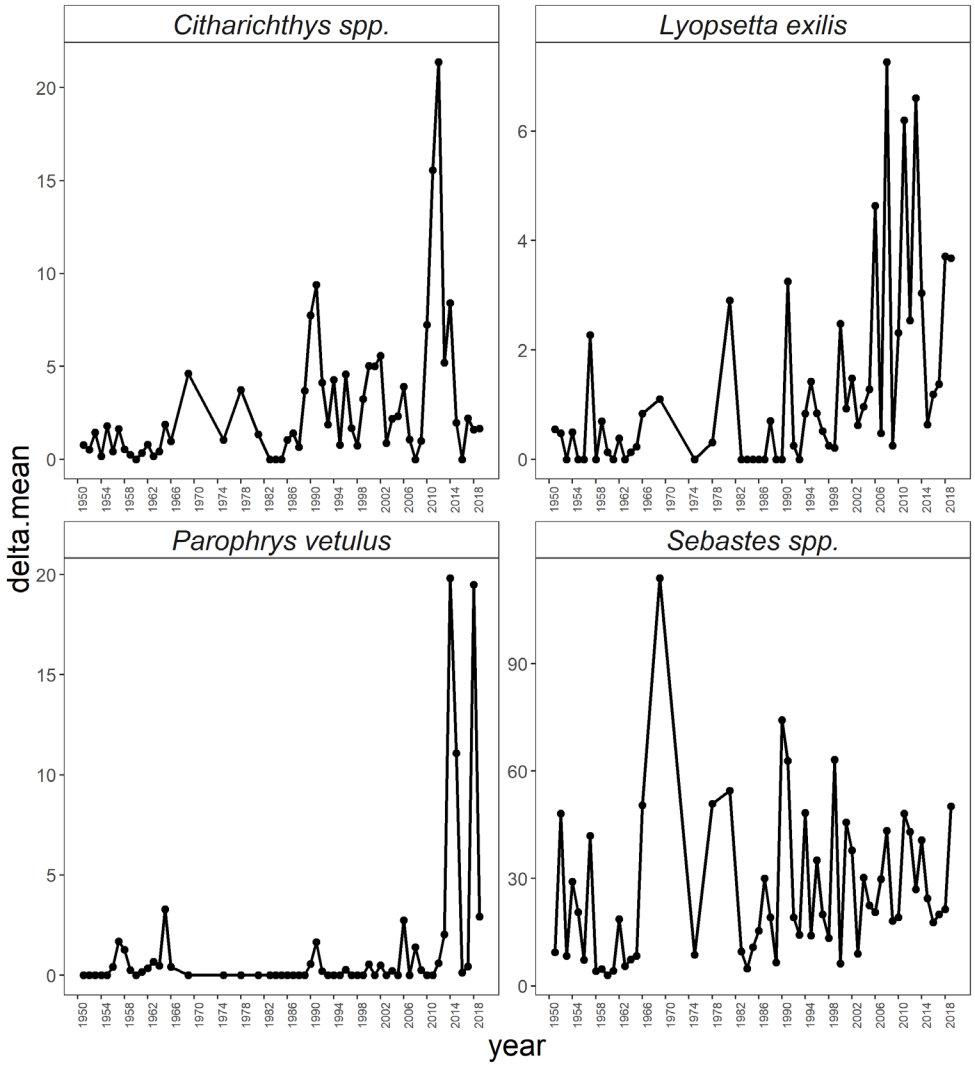

Figure 39. Mean delta abundances of ichthyoplankton from groundfishes collected in spring on CalCOFI lines 80 and 90.

have been some of the greatest in the CUFES time series (1996–present) for the three-year period 2017–19, following a period of very low abundance from 2009–16. The distribution pattern of anchovy eggs was similar in 2019 to that of the previous 2 years (fig. 36a).

Jack mackerel egg abundance was greater in 2019 than the extremely low-abundance year of 2018 (fig. 36b; note that scales differ by species). Overall, jack mackerel egg abundance was high relatively to the last decade but generally less than that of the early and mid-2000s. Relatively large catches of jack mackerel eggs occurred near Point Conception but eggs were captured as well throughout the core CalCOFI sampling area.

Pacific sardine egg abundance also increased somewhat in 2019 following the lowest abundances recorded in the CUFES data set in 2018 (fig. 36c). However, Pacific sardine egg densities remained very low relative to the 2000s, as they have been since 2014.

CalCOFI Ichthyoplankton The larval fish assemblage[30] from CalCOFI lines 80 (~34°N, fig. 1) and 90 (~32.5°N, fig. 1) in spring 2019 revealed the continued high abundance of mesopelagic species with warm-water, southern affinities such as Panama lightfish (*Vinciguerria lucetia*), Mexican lampfish (*Triphoturus mexicanus*), dogtooth lampfish (*Ceratoscopelus townsendi*) and bristlemouths (Gonostomatidae—mostly *Cyclothone signata*) (fig. 37). Although the abundance of these taxa was lower than the peak years subsequent to 2013, abundances were still very high relative to pre-MHW years. By contrast, mesopelagic species with cool-water affini-

[30]Bongo nets lowered to 210 m (or 10 m from the bottom in shallow sites) and towed obliquely to the surface collected ichthyoplankton. See Thompson et al. (2019) for detailed methods.

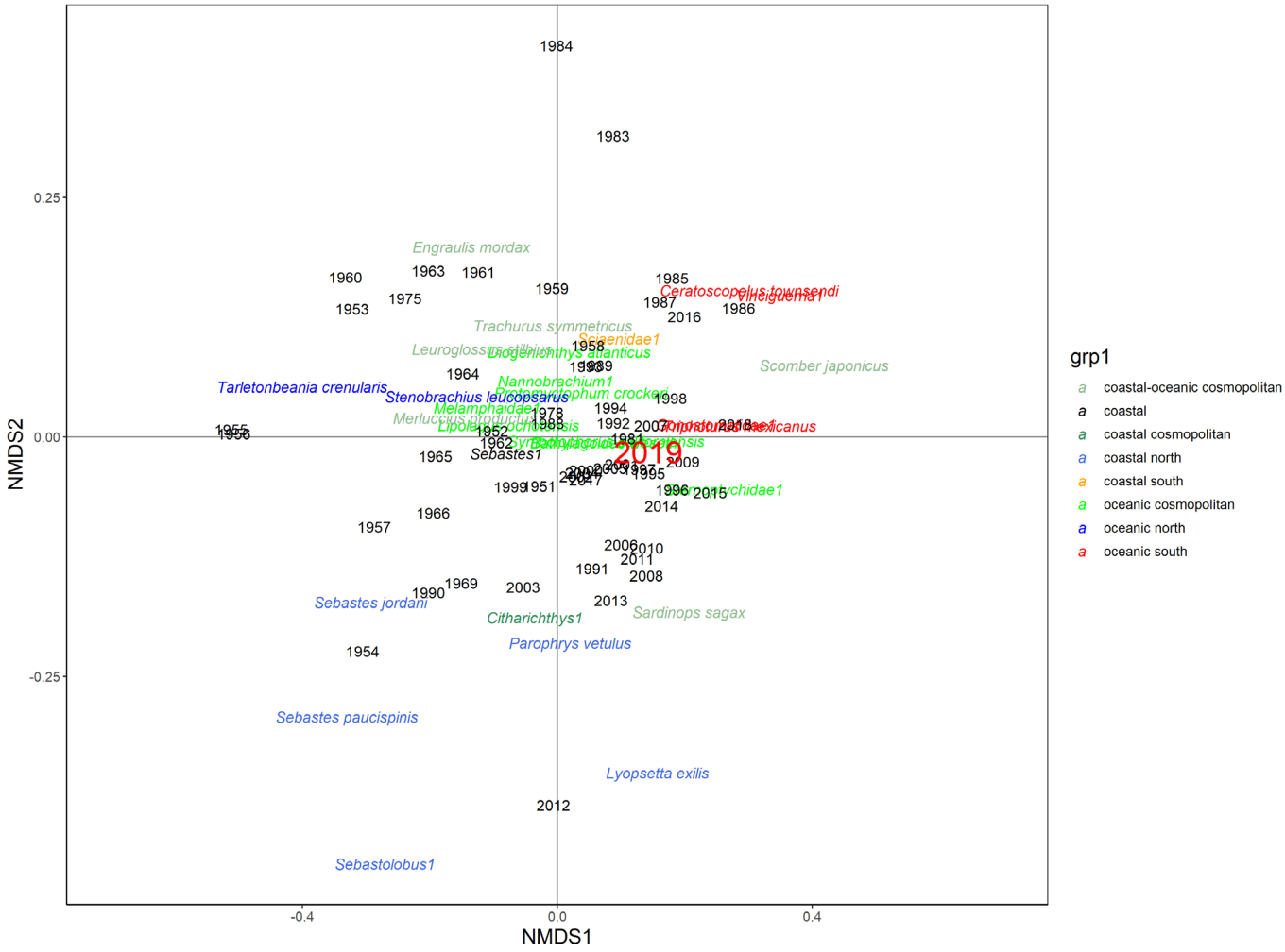

Figure 40. NMDS plot of the ichthyoplankton assemblage from CalCOFI lines 80 and 90 in spring. Adult habitat affinity defines taxa colors. 2019 is demarcated by the yellow circle to the right of the plot center.

ties (northern lampfish [*Stenobrachius leucopsarus*)] and blue lampfish [*Tarletonbeania crenularis*] remained near historically low abundances in 2019 (fig. 37).

Coastal pelagic species provided the most anomalous finding in the larval fish assemblage in 2019 (fig. 38). Whereas Pacific sardine, jack mackerel and Pacific mackerel remained at low levels, northern anchovy larvae were the most abundant in the history of CalCOFI. Indeed, 2019 northern anchovy values were nearly double the prior record high from the 1960s.

Among groundfishes, sanddabs abundances were low relative to prior years (fig. 39). Slender sole (*Lyopsetta exilis*), English sole (*Parophrys vetulus*) and rockfishes were close to long-term averages.

From a multivariate perspective, NMDS axis 1 separated assemblages dominated by warm water versus cool water taxa (fig. 40), and NMDS axis 2 mainly separated northern anchovy from rockfishes, slender sole, Pacific sardine, and English sole. The larval fish assemblage from 2014–18 loaded heavily and positively on NMDS axis 1, reflecting high abundances of warm mesopelagics. In 2019, these warm water mesopelagics were still abundant, but northern anchovy were by far the most abundant species over all. In fact, 2018 and 2019 were the only years when both northern anchovy and the mesopelagics were all top 5 in yearly abundance. The 2019 NMDS value likely reflected the competing influence of northern anchovy and warm water mesopelagic taxa. Whereas the 2019 value still aligned with the warm water mesopelagics, it was closer to the center than 2018, likely reflecting the influence of northern anchovy.

REGIONAL PATTERNS IN BIRDS

Northern California Current: Yaquina Head, Oregon

Common murre (*Uria aalge*) at Yaquina Head (44.4°N, fig. 1) experienced moderate reproductive success in

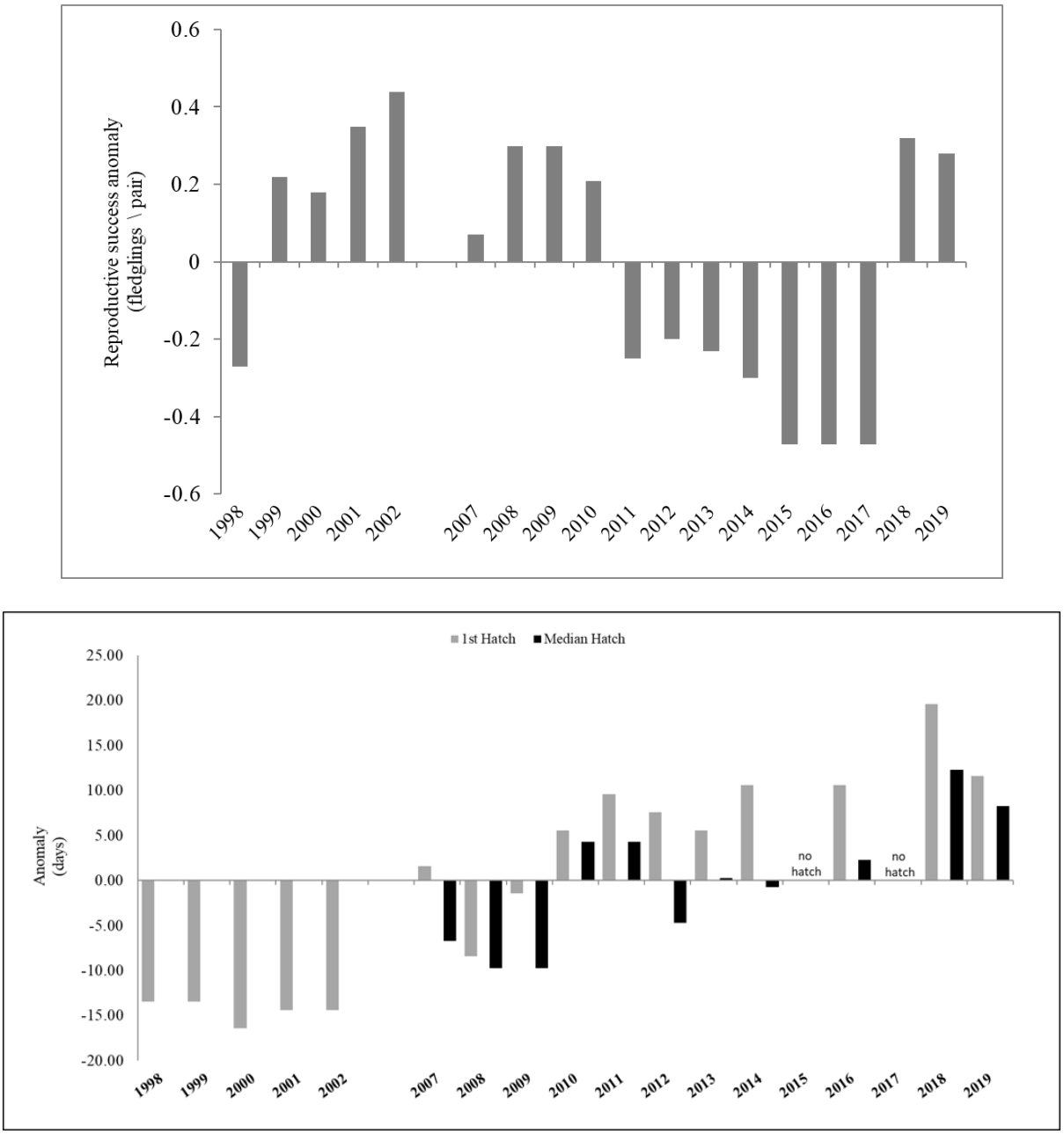

Figure 41. Anomalies of reproductive success (top), and first and median chick hatch dates (bottom) for common murres nesting at Yaquina Head, Oregon, 1998–2019. 2019 was the second year of reproductive success following consecutive years of near or total failure (2014–17).

both 2018 and 2019 following a sustained period of near or total failure from 2014–17 (fig. 41 top). Median hatch dates were later than the mean from 1998 to 2017 in both years: July 15 (2018), and July 9 (2019; fig 41 bottom). In 2018, overall hatching success was 51% and 79% of these chicks successfully fledged. In 2019, there was higher hatching success (69.7%), and 79% of these chicks successfully fledged. These were the most successful years for common murre since productivity at Yaquina Head began a steady decline in 2010.

As in previous years, both top-down predation and bottom-up prey availability affected common murre reproductive success at Yaquina Head. Bald eagles (*Haliaeetus leucocephalus*) prey on adult common murre, often leading to colony disturbances that allow secondary predators access to eggs and chicks (Horton 2014). Notably, in 2018, egg (0.78 eggs/hr) and chick (0.04 chicks/hr) depredation was the lowest since 2009 despite average rates of disturbance (0.39 disturbances/hour; long-term mean: 0.38 disturbances/hour). Ninety

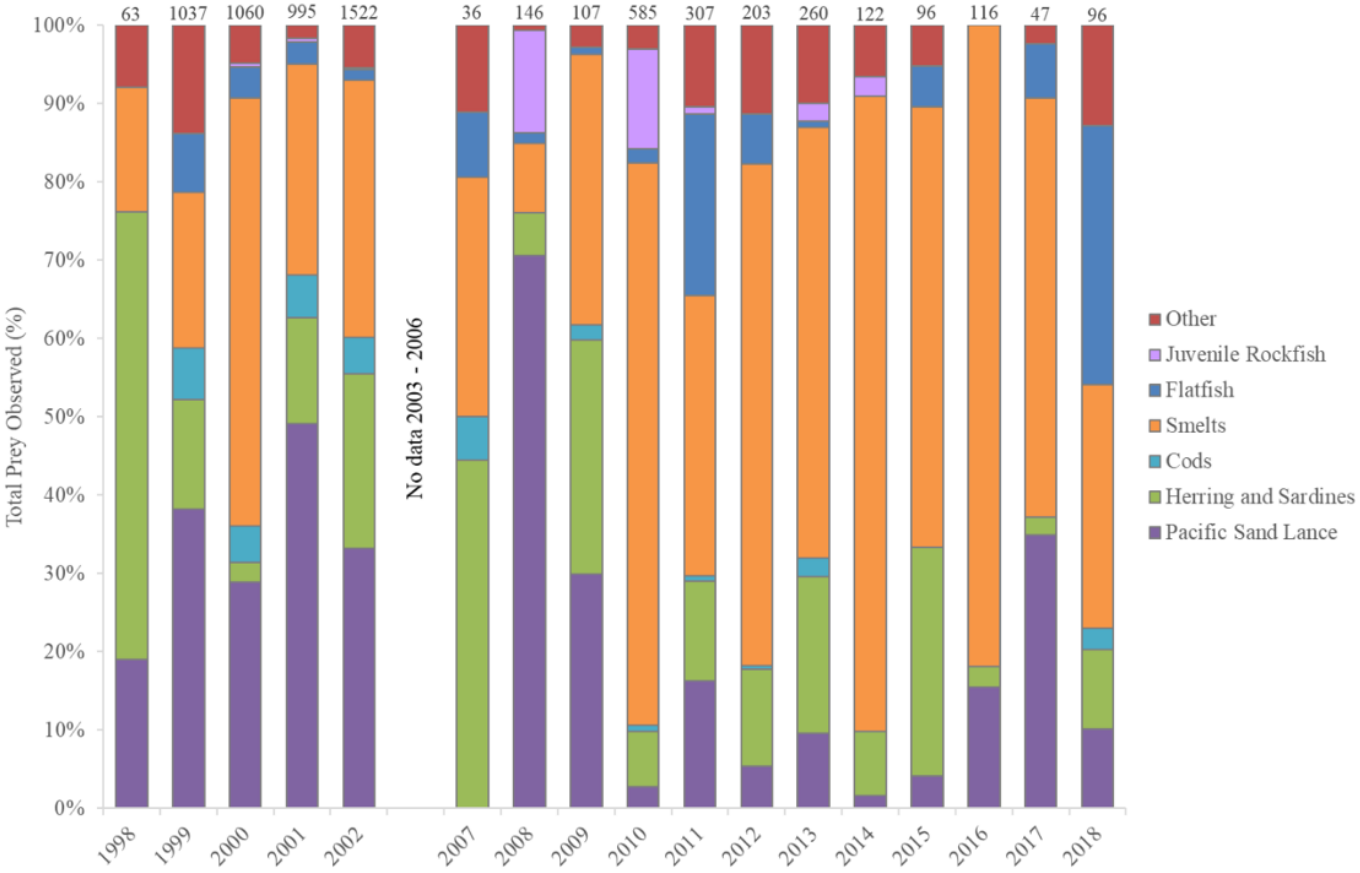

Figure 42. Prey composition of common murre diets at Yaquina Head 1998–2018 with annual sample size of identified prey items indicated above each bar. Proportions were highly variable year to year, and smelts typically appeared as the majority of diet composition (particularly 2010–17).

percent of all observed disturbances in 2018 occurred prior to the first observed chick hatch (July 7). Common murre appeared less likely to flush and abandon eggs than in years of reproductive failure (2015–17). In 2019, the frequency of predator disturbance events was the lowest of the past 10 years (0.15 disturbances/hr). From 2013–19, the "Flat Top" subcolony experienced near or complete failure, while the largest subcolony, Colony Rock, appeared to be more resilient (experienced failure 2015–17). Consistent with this, Colony Rock had medium-to-high rates of productivity in both 2018 (68% of nests hatched chicks, 47% of chicks successfully fledged) and in 2019 (91% of hatched chicks, 86% successfully fledged).

Common murre[31] diets at Yaquina Head were highly dynamic between 1998 and 2018 (fig. 42). In 2018, the rate of flat fish provisions was the highest in the data set. Although smelts typically represented a large portion of the diet there appears to be a negative correlation between the proportion of smelt in common murre diet and reproductive success (figs. 41, 42). Diet observations were collected in 2019, but prey identification is forthcoming.

In 2018, overall reproductive success increased for Brandt's cormorant (*Phalacrocorax penicillatus*) and pelagic cormorant (*Phalacrocorax pelagicus*) (fig. 43). Both species were similarly successful in rearing and fledging chicks in 2019. Brandt's reproductive success in 2018 was high (1.69 fledglings/nest), and in 2019 was the highest (1.89 fledglings/nest) in the time series (2008–19; fig. 43). Median hatch date for Brandt's cormorants was later in 2018 (July 10) than in 2019 (July 5, fig. 44).

Northern California Current: JSOES Cape Flattery, Washington to Newport, Oregon

The JSOES (44.4°N to 48.3°N, fig. 1) has sampled at-sea seabird distribution and density patterns for the northern domain of the California Current during June from 2003–19. Data from 2019 indicated this region returned to more typical (near-median) summer seabird densities and distributions compared to the extremely low densities observed in 2017 (fig. 45). Mean total bird density in the 2019 survey was the 9th highest reported

[31]Diet data were collected 2-5 days per week during the chick-rearing period. Single prey items carried in the bill of adult murres were digitally photographed for identification.

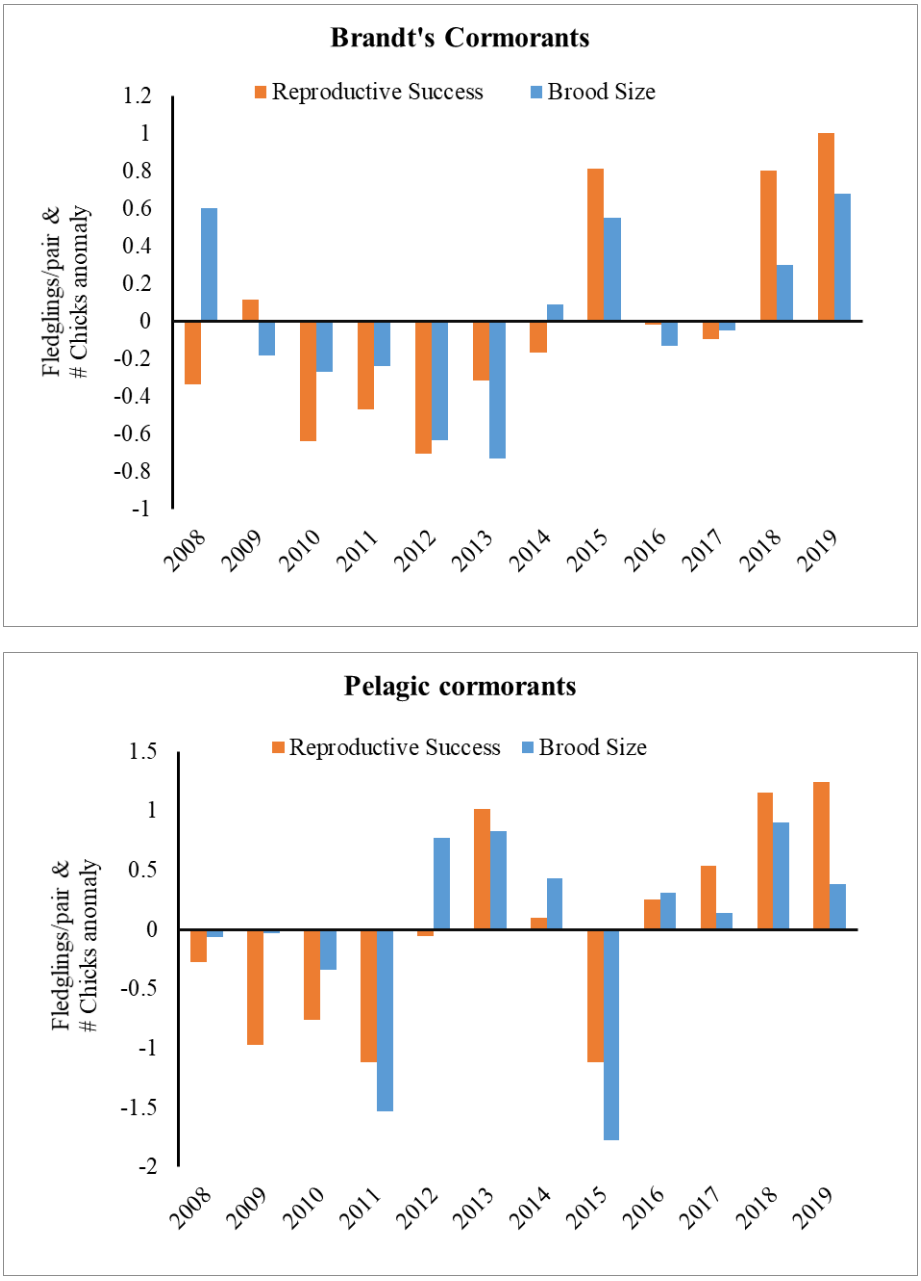

Figure 43. Anomalies of reproductive success and brood size for cormorants nesting at Yaquina Head, Oregon, 2008–19. In both 2018 and 2019, cormorants had above average reproductive success and brood size. Over the time series, average reproductive success and brood size for Brandt's is 0.89, and 1.78 respectively; for pelagic cormorants average reproductive success is 1.12 and brood size is 1.86.

in the 15-year JSOES data set (41.1 birds per km^2 compared to a median value of 42.9 birds per km^2). The majority of birds observed in 2019 were either sooty shearwater (*Ardenna grisea*, 55%) or common murre (34%). Sooty shearwater abundance was the 7th highest (22.4 birds per km^2, compared to the time-series median of 20.3 birds per km^2) (fig. 45). This species was aggregated on the Grays Harbor, WA, transect (47°N) where 70% of all individuals observed during in 2019. This distribution pattern was consistent with previous findings showing that during May and June, sooty shearwaters were observed in large numbers near the northern boundary of ocean waters affected by freshwater discharge from the Columbia River (Zamon et al. 2014; Phillips et al. 2017; Phillips et al. 2018). This region overlaps with distribution centers of dominant forage fish species such as northern anchovy, Pacific herring, Pacific sardine, and smelts (Phillips et al. 2017).

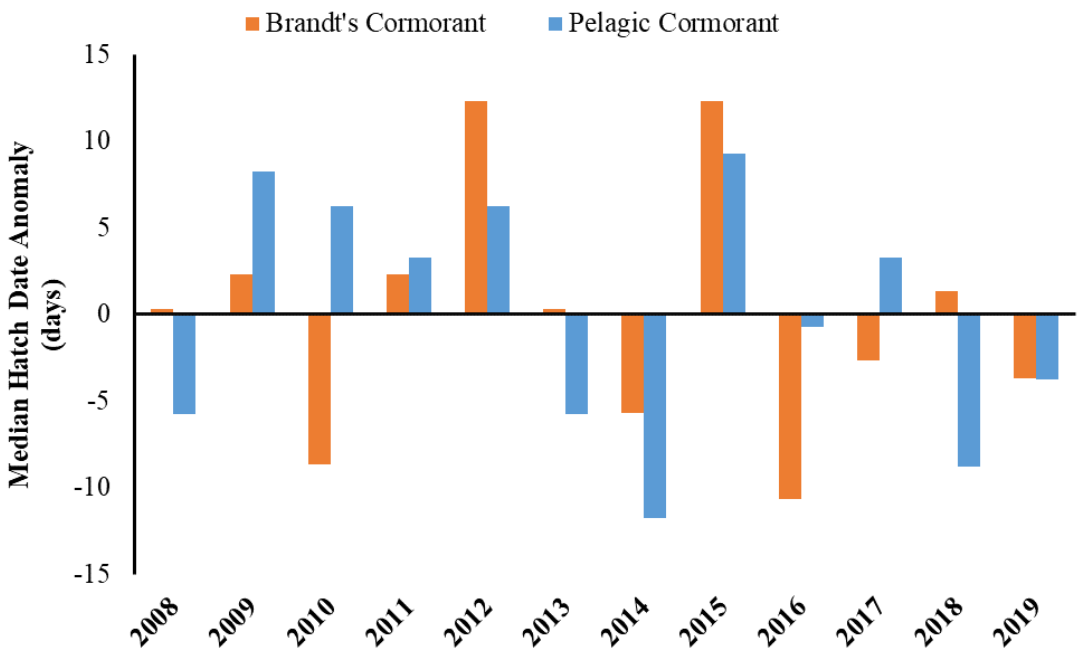

Figure 44. Anomalies of median hatch dates for Brandt's and pelagic cormorants at Yaquina Head, Oregon 2007–19. Over the time series, median hatch date is July 9 for Brandt's and July 15 for pelagic cormorants.

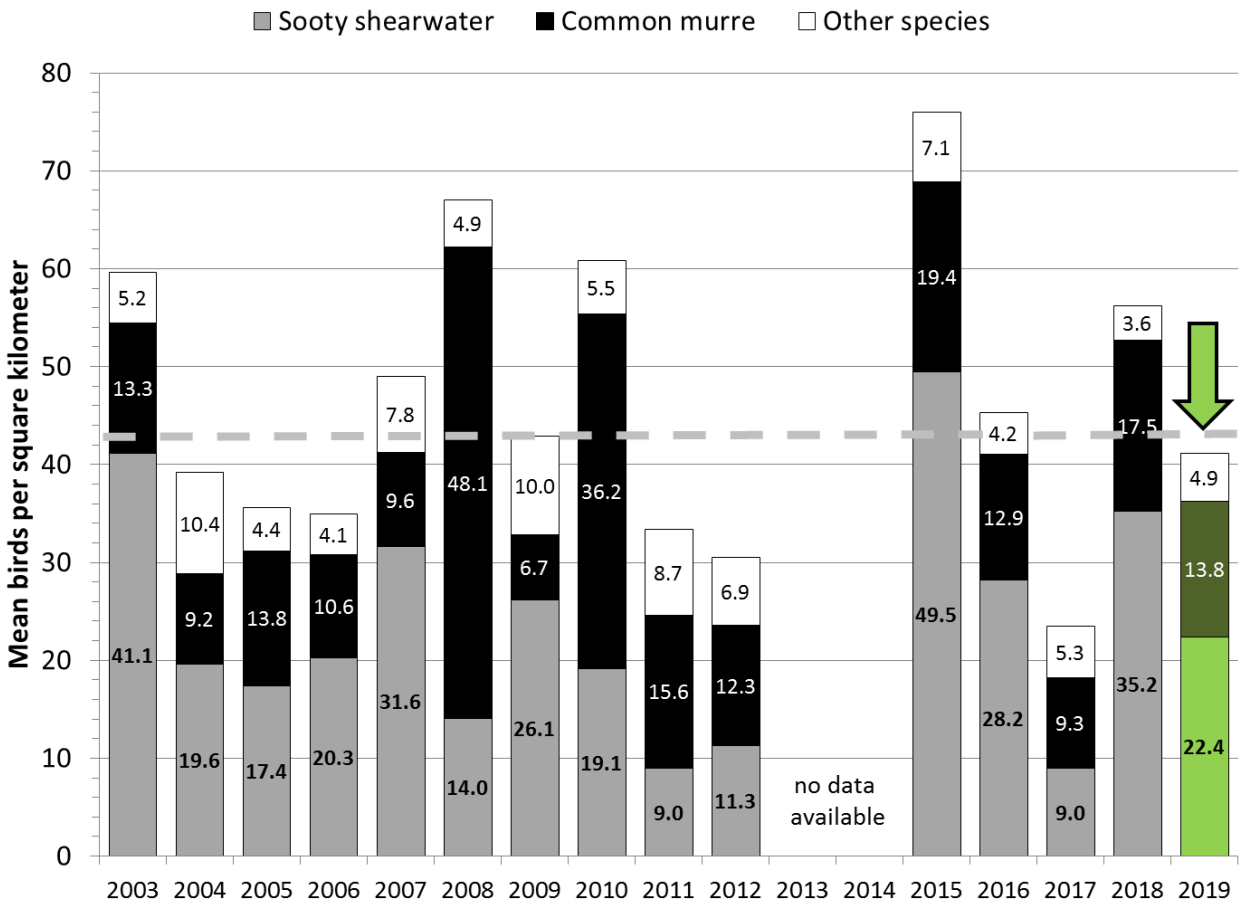

Figure 45. Mean seabird density observed on the continental shelf between Cape Flattery, WA (48.23°N) and Newport, OR (44.67°N) during annual JSOES surveys during late June. Data for 2019 are indicated with green; overall median seabird density for the survey time series (42.9 birds per km^2) is shown with the gray dashed line.

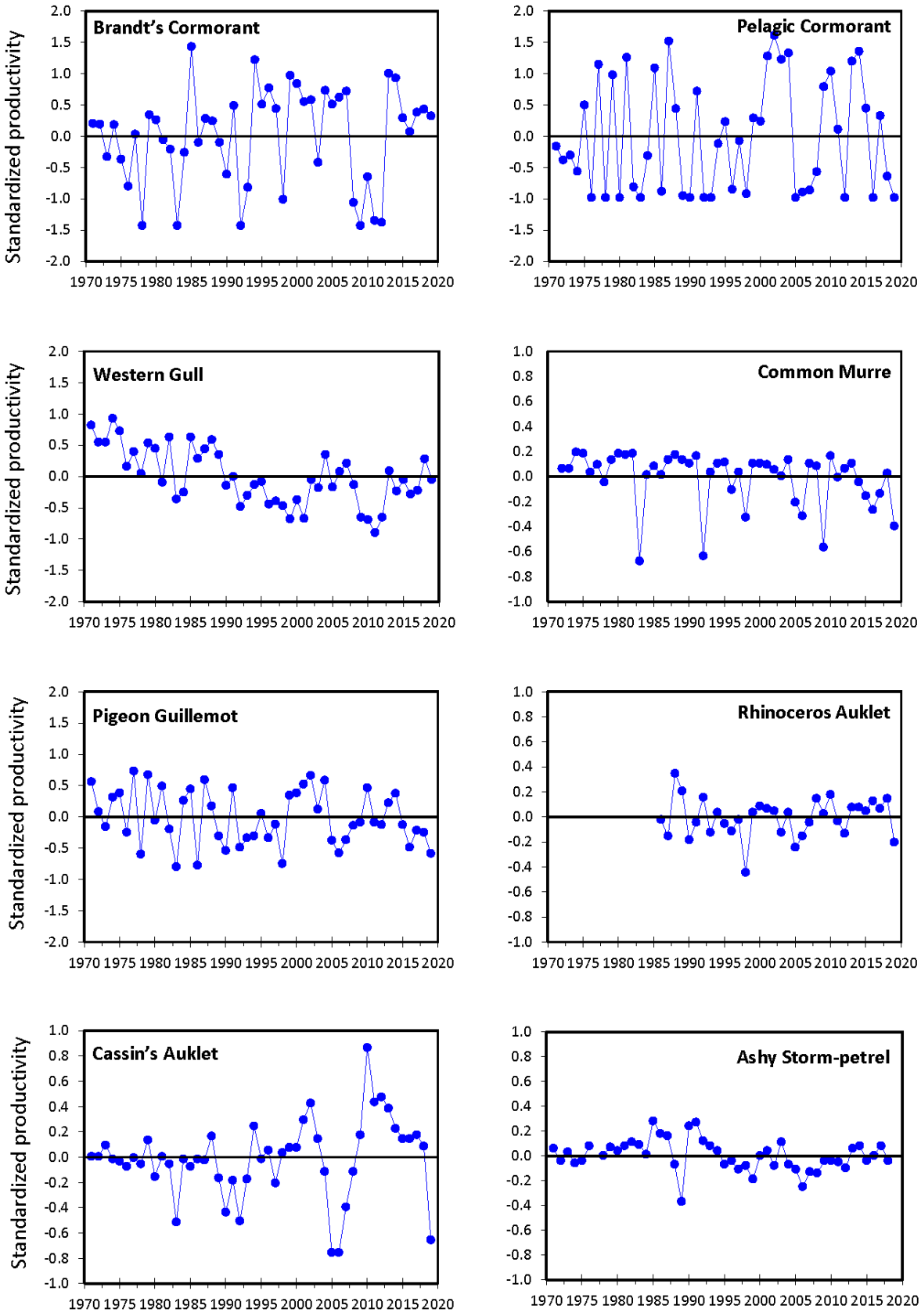

Figure 46. Standardized productivity anomalies for sea birds from Southeast Farallon Island.

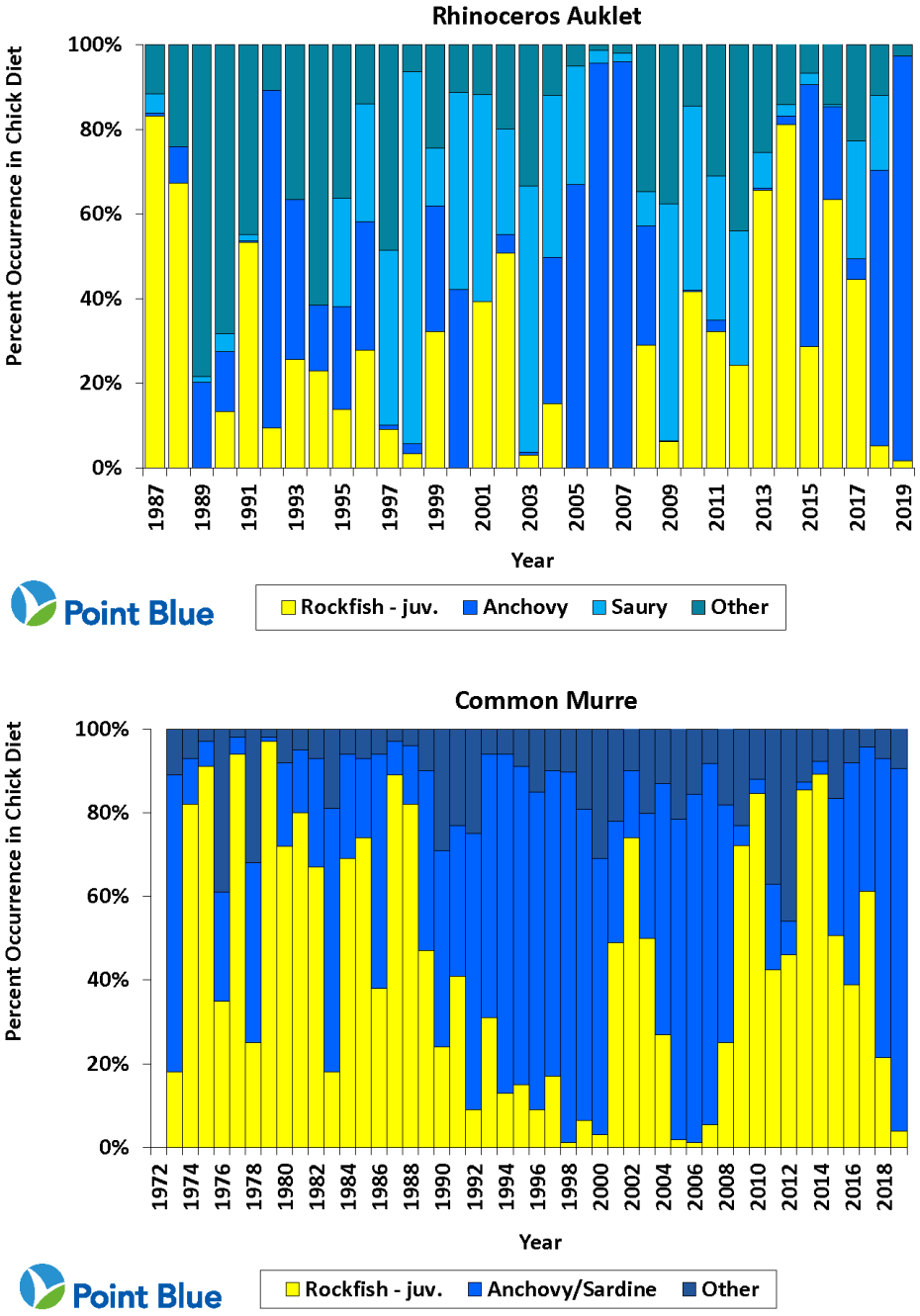

Figure 47. Percent of rhinoceros aucklet (top) and common murre (bottom) chick diet comprised of juvenile rockfishes, anchovy/sardine or other fishes at Southeast Farallon Island.

Similar to sooty shearwater, common murre abundance was the sixth highest on record (13.8 birds per km^2, compared to the median of 13.4 birds per km^2). Common murre was most abundant in the area directly affected by freshwater discharge from the Columbia River, with 66.8% of all individuals observed on the three transects closest to the Columbia River (from Cape Meares, OR 45.48°N to Willapa Bay, WA 46.67°N). Common Murre were also abundant near the Newport, OR, colony (44.67°N; 23.7% of observations). This pattern of June common murre abundance being high near colonies and in areas affected by the Columbia River plume was consistent with past findings in the northern domain of the California Current (Zamon et al. 2014; Phillips et al. 2017; Phillips et al. 2018; Loredo et al. 2019; Phillips et al. 2019).

JSOES surface trawls in 2019 sampling nekton on the same transects where seabird density was surveyed

(fig. 25) indicated that prey species potentially available to fish-eating seabirds in the northern domain of the California Current included a mix of cool water (e.g., Pacific herring) and warmer water taxa (e.g., Pacific pompano and market squid). It is worth noting that market squid were more abundant than in any previous survey, continuing a recent upward trend in the occurrence of this species in daytime surface trawls. Whether this represented a short vs. longer-term shift in nekton community composition was not clear. It was also unclear if changes in squid abundance correlated with changes in squid consumption by seabird predators. The few studies on sooty shearwaters and common murre diets in the northern domain of the California Current indicated that these birds do not typically consume squid (Varoujean and Matthews 1983; Thompson et al. 2018). Regardless of diet information, distribution and density data from June 2019 continued to support the hypothesis that the Columbia River plume impacts trophic interactions between seabirds and fish in this region of the California Current (Adams et al. 2012; Zamon et al. 2014; Phillips et al. 2017; Phillips et al. 2018; Loredo et al. 2019; Phillips et al. 2019).

Central California: Southeast Farallon Island

In contrast with Yaquina Head, common murre production at Southeast Farallon Island (37.4°N, fig. 1) was low in 2019 and the fourth lowest since 1970 (fig. 46). In addition, pelagic cormorant, pigeon guillemot (*Cepphus columba*), rhinoceros auklet (*Cerorhinca monocerata*) and Cassin's auklet (*Ptychoramphus aleuticus*) reproduction was quite low in 2019. Brandt's cormorant production was slightly above the long-term mean, while western gull (*Larus occidentalis*) and ashy storm petrel (*Oceanodroma homochroa*) were close to average. The northern anchovy surge was reflected in the diets of rhinoceros auklet and common murre as northern anchovy constituted >90% of the diet of both species (fig. 47).

Central and Southern California: RREAS and CalCOFI

Seabird distribution and abundance anomalies from the RREAS core region in spring 2019 covered the region from Point Sur to Bodega Bay (36.18°N to 38.2°N, fig. 1). Observation efforts yielded a total of 15 survey days, resulting in 1,356 km (area surveyed 402 km^2) of trackline sampled, and detection of 35 seabird species with an overall density of 74.6 seabirds per km^2. The RREAS typically encounters higher concentrations of resident breeding species within the Gulf of the Farallones, as well as the influx of trans-hemisphere migratory species and migrants from Hawaii. During 2019, resident breeders such as common murre and Brandt's cormorant displayed positive density anomalies, while Cassin's auklet had negative density anomalies (fig. 48). Furthermore, the trans-hemisphere migrants, pink-footed shearwater (*Puffinus creatopus*) and sooty shearwater, also showed large positive anomalies (first time for pink-footed shearwater since 2009), with the anomaly for sooty shearwater being the highest ever recorded in the time series. The positive density anomalies for common murre, Brandt's cormorant and shearwaters may in part reflect the observed increased aggregation intensity of these species, attributed to the very high positive anomaly of adult northern anchovy observed by the RREAS in 2019 (fig. 32). The negative anomaly for Cassin's auklet may reflect the low numbers of euphausiids reported by the RREAS, although the anomalies for this species have been low since 2013. The migrant black-footed albatross (*Phoebastria nigripes*) densities continued to show negative anomalies since 2015.

A total of 15 days of survey effort covering 1,602 km (area surveyed 481 km^2) of ocean habitat was recorded on the spring CalCOFI survey off southern California between lines 76.7 and 93.3, resulting in the detection of 36 seabird species and an overall total density of 4.2 seabirds per km^2. Spring CalCOFI seabird density anomalies may be correlated with water temperature variability as well as other factors such as prey availability (Sydeman et al. 2015) or population trends or range shifts in breeding or wintering distributions (Velarde et al. 2015). Anomalies of seabird density within southern California indicated mixed responses within warm and cool-water affinity species in 2019. For cool-water species, Sabine's gull (*Xema sabini*) was well above average while sooty shearwater and common murre were slightly below average (fig. 49). The upswing in Sabine's gull may indicate that this species' migration or conditions in the sub-Arctic (where this species breeds) was impacted by the spring ocean-climate conditions. The continued negative anomaly of common murre in southern California is likely a continued repercussion of the 2014–16 marine heat wave. Comparison of sooty shearwater between central and southern California indicate that sooty shearwater aggregations were less concentrated in southern California compared to central California (fig. 48, 49).

Among the warm-water species off southern California, Cook's petrel (*Pterodroma cookie*) and pink-footed shearwater were above average, Elegant Tern (*Thalasseus elegans*) was close to average, and black-footed albatross and Leach's storm petrel (*Oceanodroma leucorhoa*) were below average (figs. 49, 50; (Hyrenbach and Veit 2003; Santora and Sydeman 2015)).

A positive density anomaly of pink-footed shearwater was linked previously to the onset of warm-water conditions and this pattern held in 2019 (Hyrenbach and Veit 2003). The 2019 positive anomalies in pink-footed

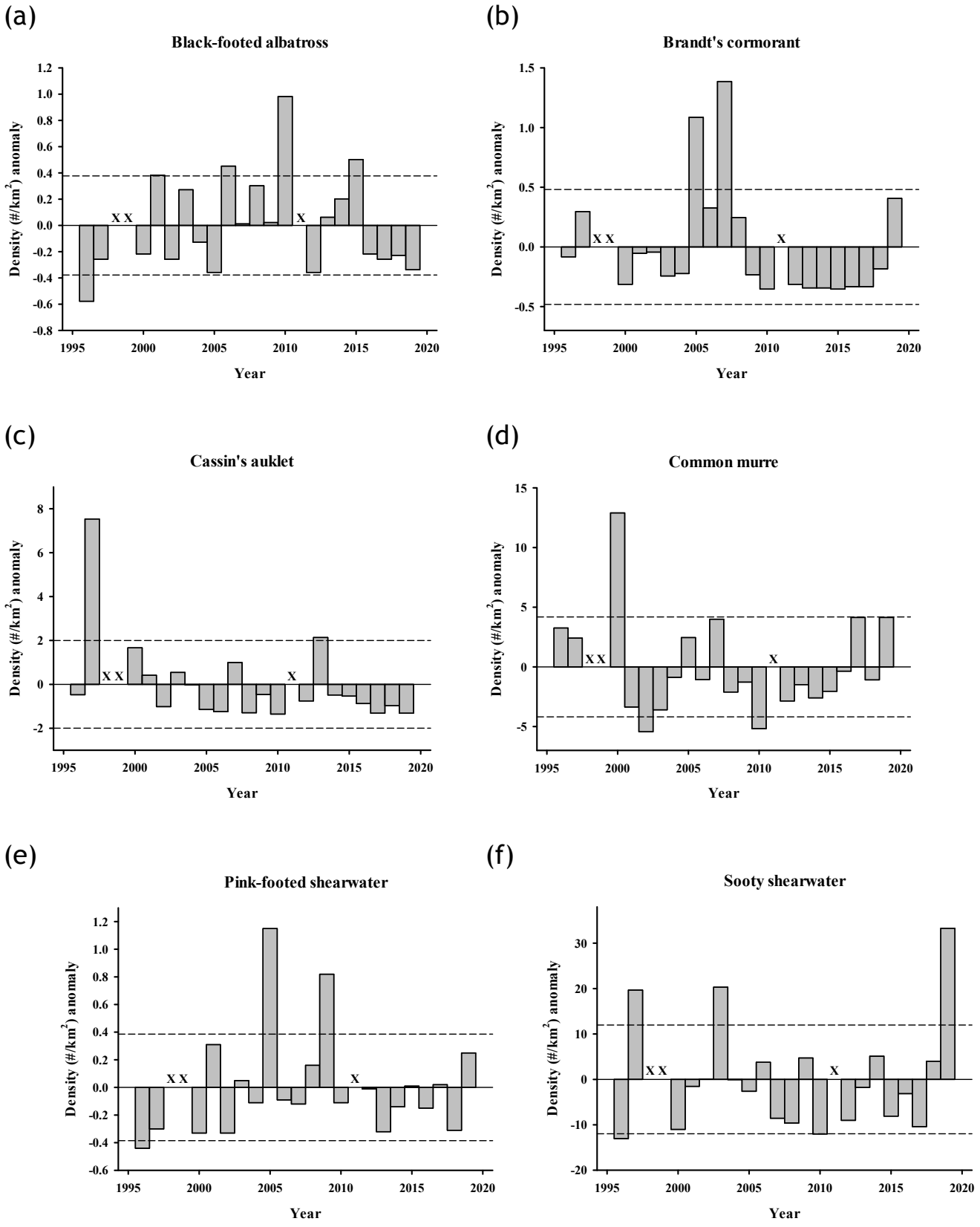

Figure 48. Density (number/km²; expressed as anomalies) over time from RREAS central California core area surveys, 1996–2019: (a) black-footed albatross, (b) Brandt's cormorant, (c) Cassin's auklet, (d) common murre, (e) pink-footed shearwater, (f) sooty shearwater; dashed lines indicate ± 1 s.d. of the long-term mean, and "x" indicates years when no survey was conducted.

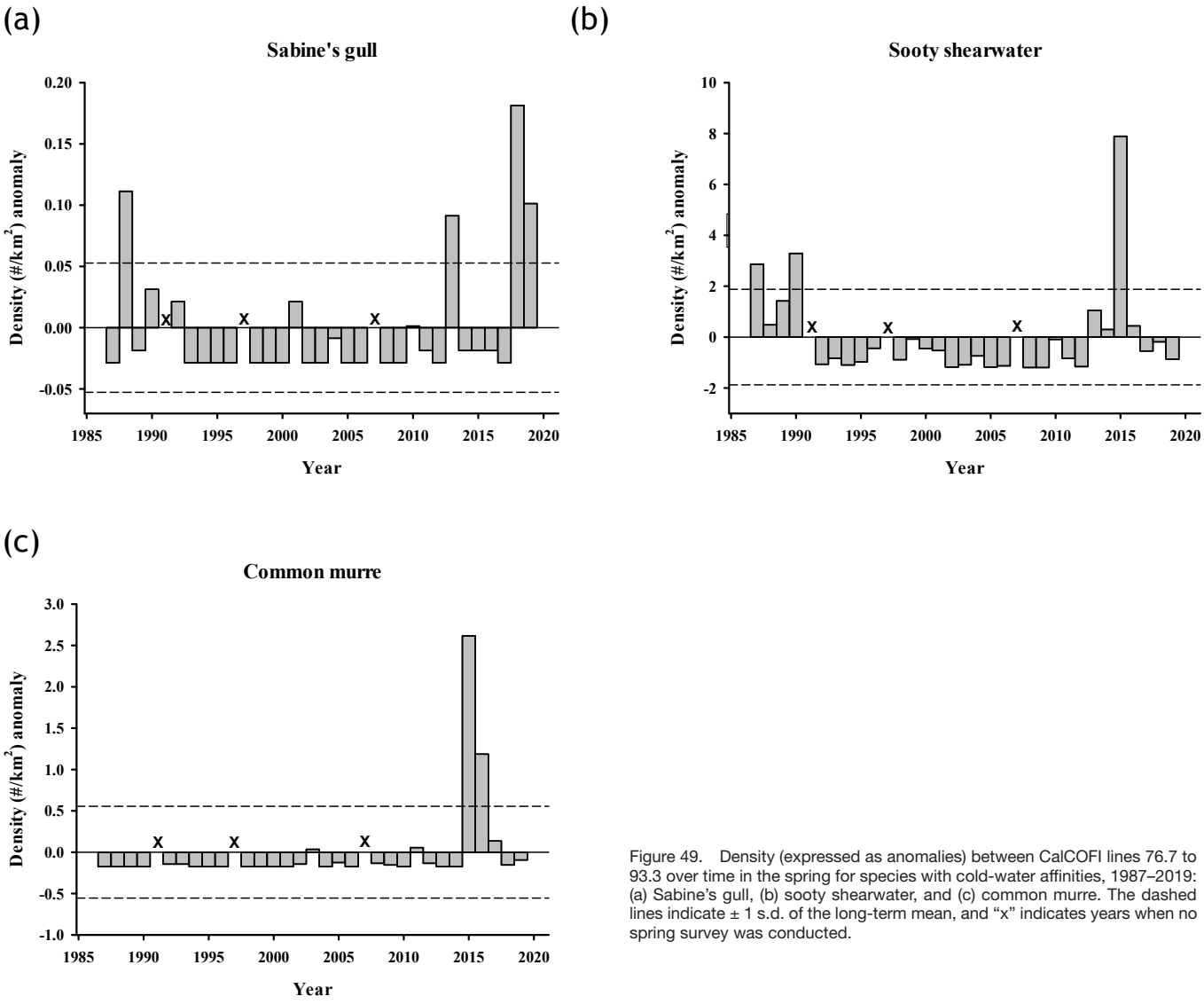

Figure 49. Density (expressed as anomalies) between CalCOFI lines 76.7 to 93.3 over time in the spring for species with cold-water affinities, 1987–2019: (a) Sabine's gull, (b) sooty shearwater, and (c) common murre. The dashed lines indicate ± 1 s.d. of the long-term mean, and "x" indicates years when no spring survey was conducted.

shearwater and Cook's petrel were similar to their sustained strong positive anomalies during 2014–16 (fig. 50). The decline in black-footed albatross may be related to the overall decline of their populations in Hawaii and elsewhere in the North Pacific (fig. 50).

MARINE MAMMALS

Central CA: Humpback Whales

Marine mammal surveys from the RREAS within central California continue to report increasing encounter rates for humpback whales (*Megaptera novaeangliae*) encounter rate continued to increase over the past decade (fig. 51). In 2019, humpback whale were regularly observed in high concentrations on the shelf feeding on northern anchovy (Jarrod Santora, personal observation). These observations continued to indicate that humpback whale populations are likely increasing and that foraging conditions (e.g., availability of krill and northern anchovy aggregations) have been favorable for concentrating whales off central California in spring.

Southern CA: California Sea Lions at San Miguel Island, California

California sea lions (*Zalophus californianus*) are an indicator species to quantify the status of upper trophic level species in the CCE because they live, feed and breed in the CCE year round (Melin et al. 2012). The population breeding at San Miguel Island (34°N) is one of the largest in the world (about 45% of the US breeding population) and has been monitored for decades. Since 1997, four indices were used to measure trends in the population: 1) live pup census, 2) pup condition at 4 months of age, 3) pup growth rates during

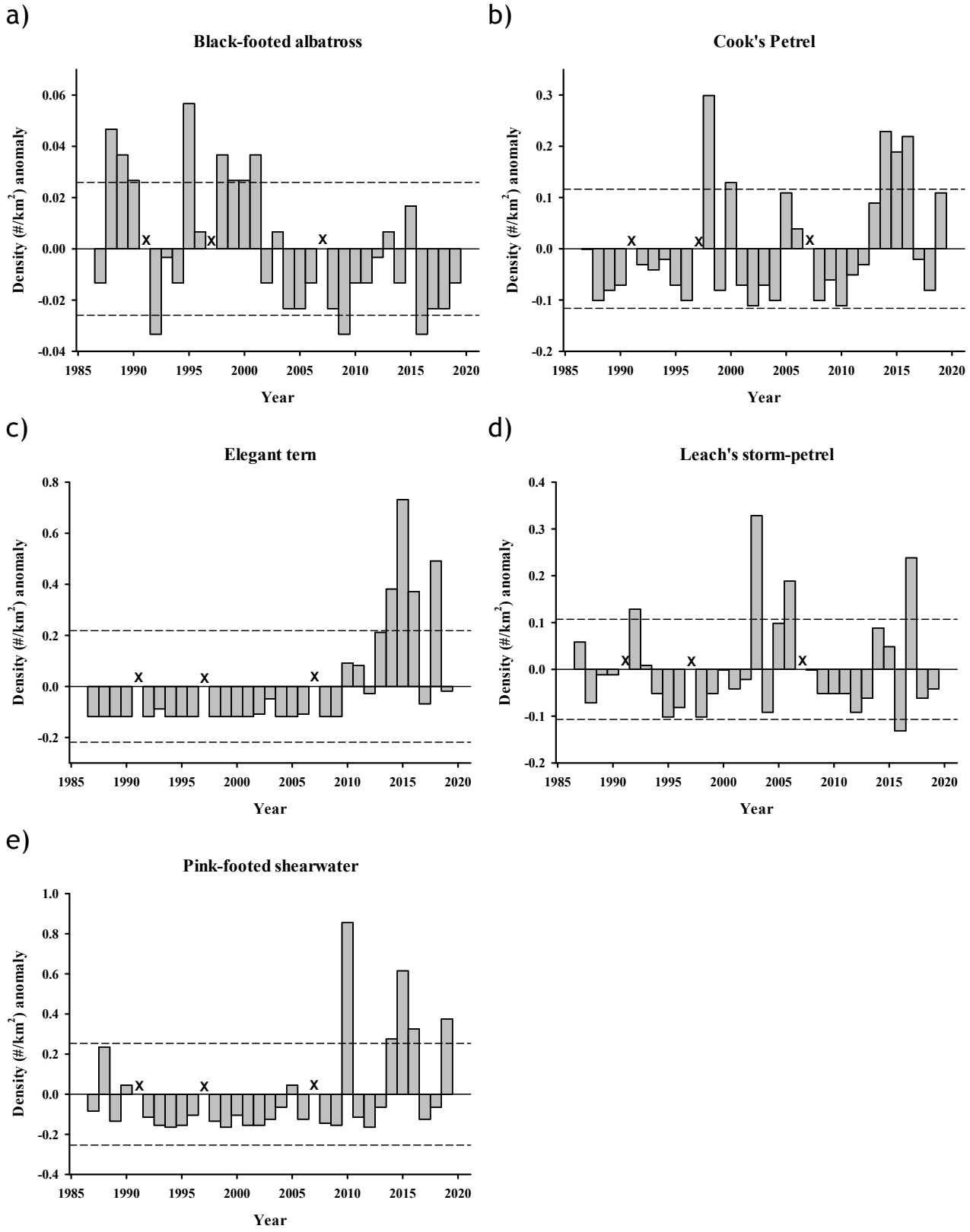

Figure 50. Density (expressed as anomalies) between CalCOFI lines 76.7 to 93.3 over time in the spring for species with warm-water affinities, 1987–2019: (a) black-footed albatross, (b) Cook's petrel, (c) elegant tern, (d) Leach's storm petrel, and (e) pink-footed shearwater. The dashed lines indicate ± 1 s.d. of the long-term mean, and "x" indicates years when no spring survey was conducted.

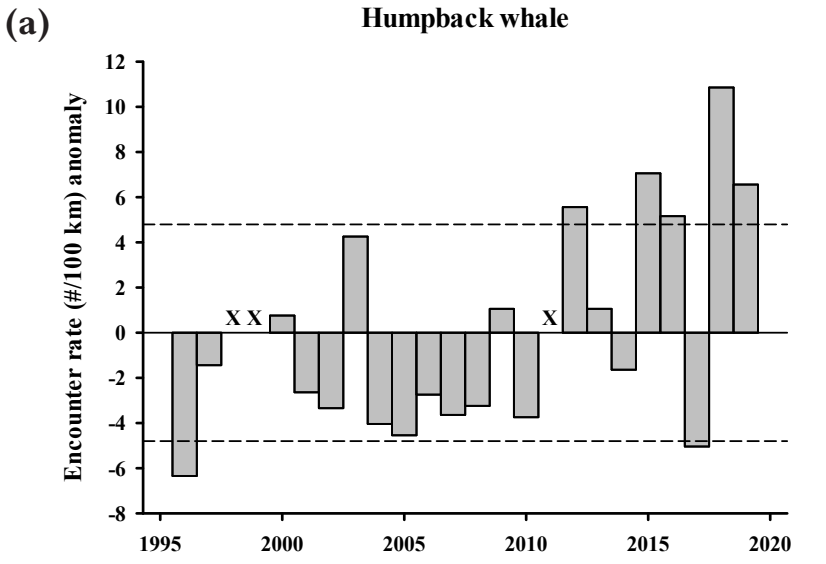

Figure 51. Encounter rate (number/100 km; expressed as anomalies) over time from RREAS central California core area surveys, 1996–2019, of (a) humpback whale; dashed lines indicate ± 1 SD of the long-term mean, and 'x' indicates years when no survey was conducted.

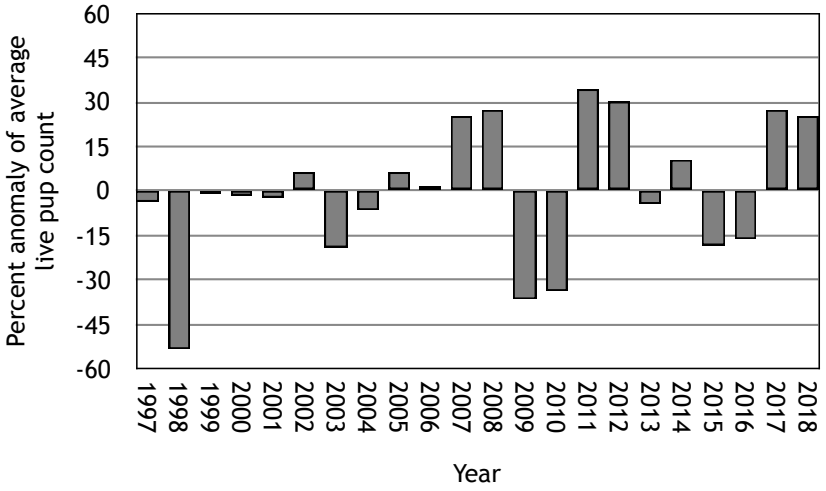

Figure 52. The percent anomaly of live California sea lion pup counts at San Miguel Island, California, based on a long-term average of live pup counts between 1997 and 2018 in late July when surviving pups were about 6 weeks old.

the period of maternal nutritional dependence, and 4) nursing female diet during the maternal care period[32]. The live pup census is a measure of successful births and is an indicator of prey availability to and nutritional status of nursing females from October to the following June. Pup condition and growth rates during the period of nutritional dependence measure the transfer of energy from the mother to the pup through lactation between June and the following February that is dependent on prey available to nursing females during that time. The frequency of occurrence of prey in the diet of nursing females provides a relative measure of the available forage community during the period of pup nutritional dependence.

Three indices of California sea lion population showed improvement in 2018, representing the third consecutive year of average or above average values following 2015, the worst year in the 1997–2018 time series. In 2018, pup births declined 2% from 2017 but were still 24% above the long-term average (fig. 52). Pup weights at 3 months of age were similar to 2017 (fig. 53). Although pup growth rates at 7 months of age were lower than 2017 they were still above the long-term average (fig. 54). Continued improvement in the population indices coincides with a shift in the frequency of occurrence

[32]The number of pups alive were counted in late July and the average weights of pups at 4 months and 7 months of age. The number of live pups in late July represents the number of pups that survived from birth to about 6 weeks of age. Live pups were counted after all pups were born (between 20 and 30 July). A mean of the number of live pups was calculated from the total number of live pups counted by each observer. A long-term average live pup count was used to create annual anomaly percentages. Between 200 and 500 pups were weighed per year when about 4 months old. Pups were sexed, weighed, tagged, branded, and released. Up to 60 pups were captured in February and weighed and measured at 7 months of age. Of the 60 pups captured in February, up to 30 pups were branded which provided a longitudinal data set for estimating a daily growth rate between 4 months and 7 months old.

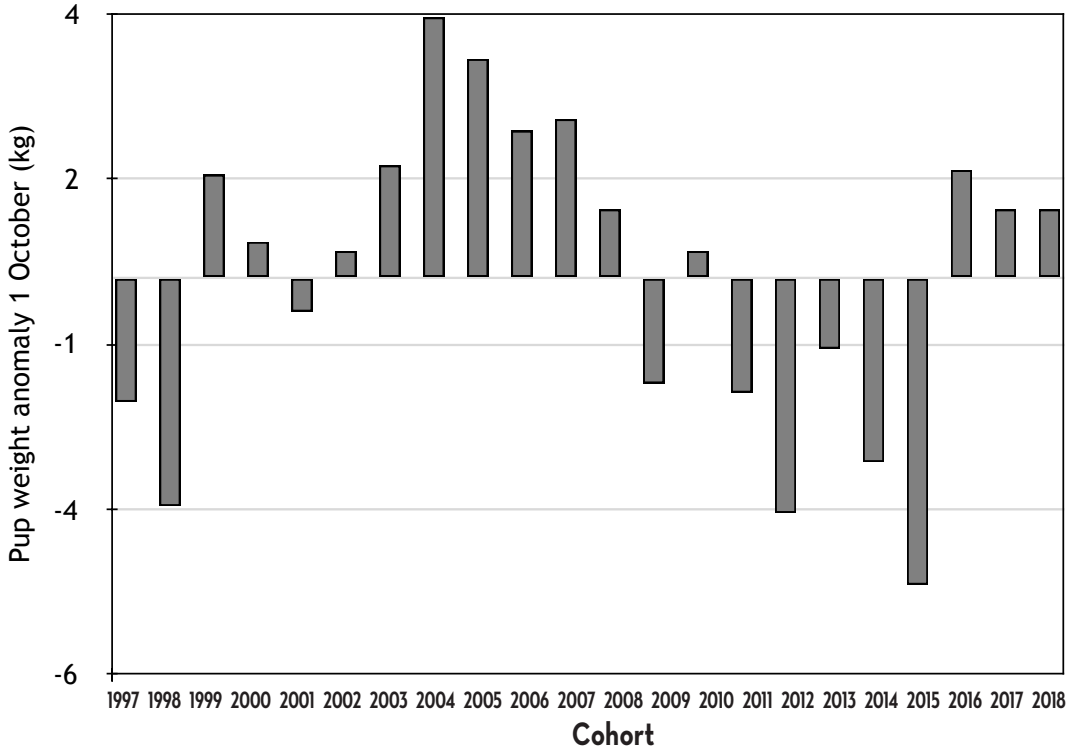

Figure 53. Average pup weight anomaly (kg) from predicted average weights of 4-month-old female California sea lion pups at San Miguel Island, California, from the long-term average between 1997 and 2018.

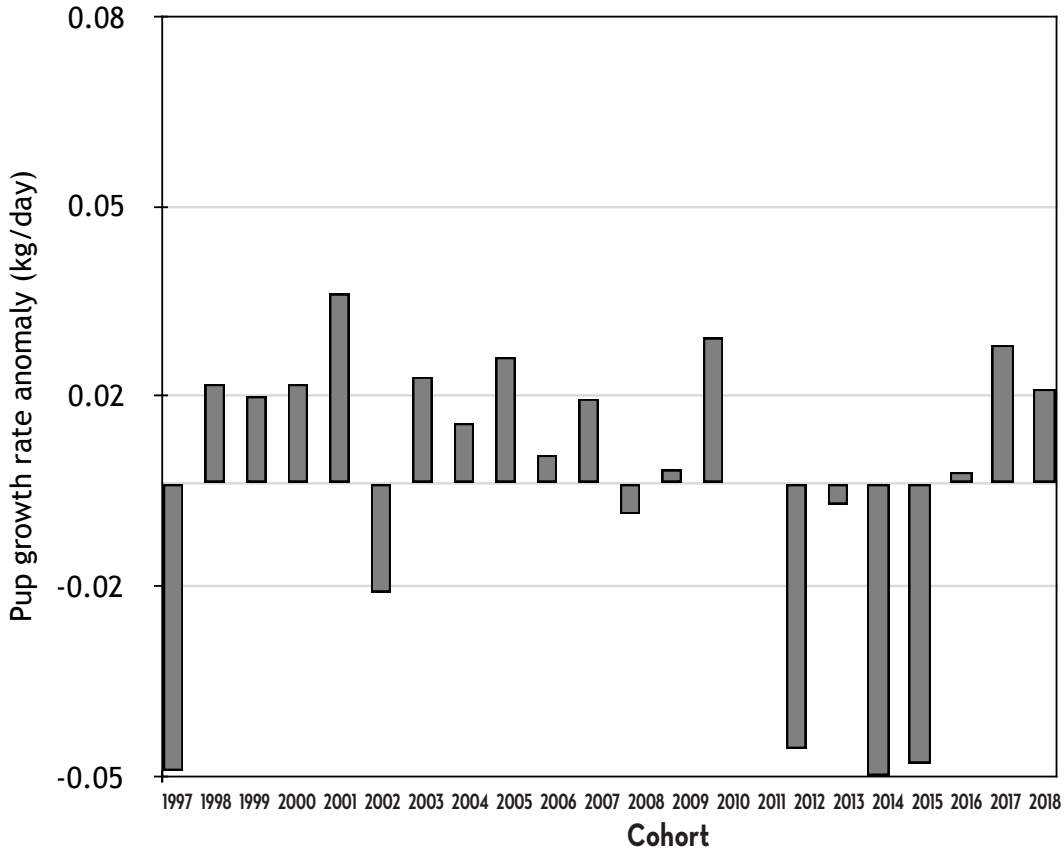

Figure 54. Average daily growth rate anomaly of female California sea lion pups from 4 and 7 months old at San Miguel Island, California, from the long-term average between 1997 and 2018.

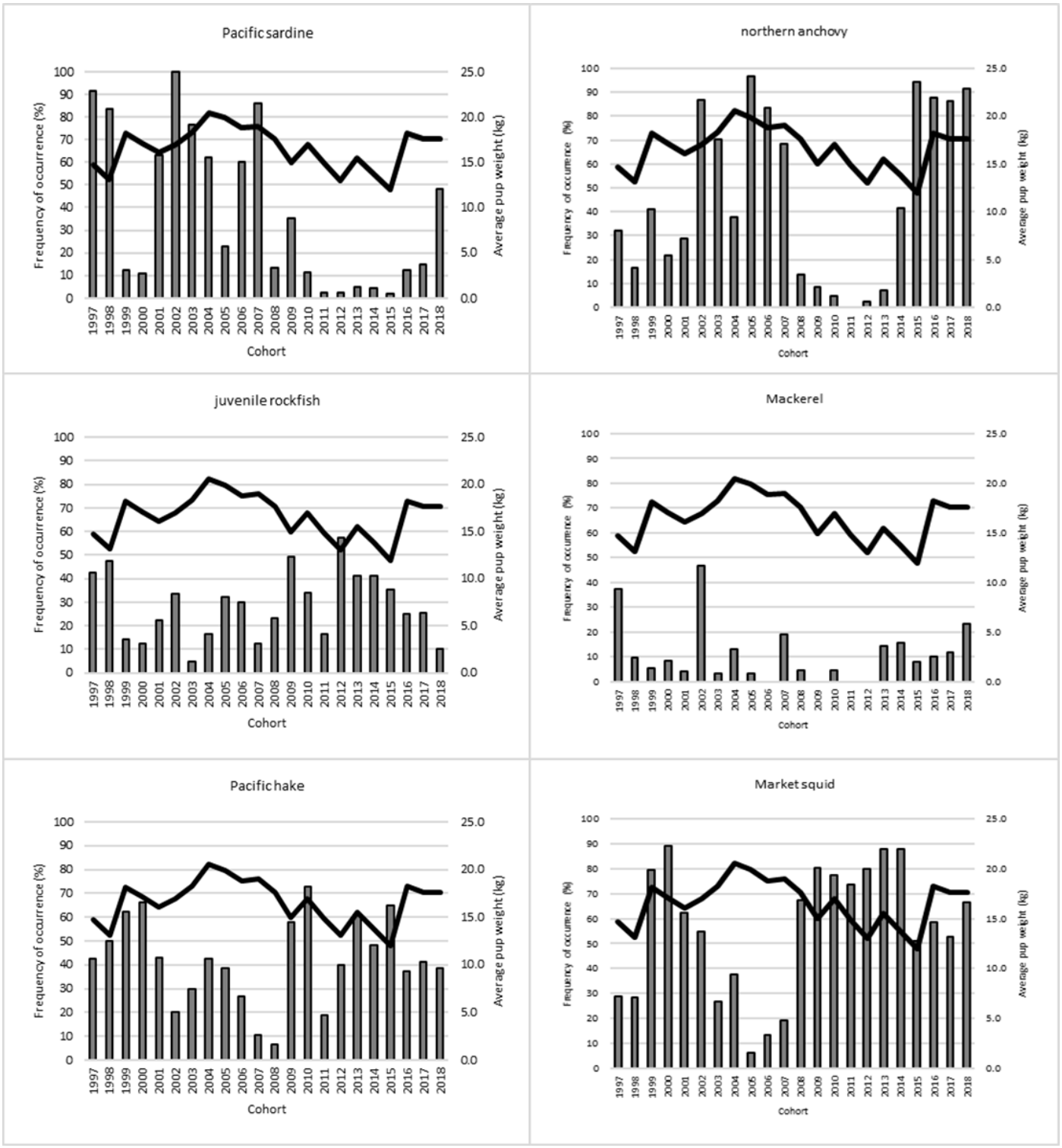

Figure 55. Frequency of occurrence of prey taxa (bars) identified from nursing female fecal samples collected at San Miguel Island during the first 4 months of lactation and average California sea lion female pup weight at 4 months old (line), 1997–2018.

(FO) of the primary prey in the nursing female diet[33]. More favorable ocean conditions for northern anchovy and Pacific sardine resulted in the return of northern anchovy as the most frequently occurring prey (>85%) in the past four years, and the resurgence of Pacific sardine in the diet in 2018 (48%; fig. 55). Pacific hake, market squid and mackerel (Pacific and jack) also had high FO in 2018 resulting in a diverse diet of high quality prey for nursing females that likely contributed to the positive trends in the population indices.

DISCUSSION

A novel anchovy regime?

Northern anchovy larval abundances were the highest in the 70-year history of CalCOFI and adult northern anchovy catches the greatest in the 36-year history of the RREAS in 2019. Taken together, this provides strong evidence that the overall northern anchovy population size is as high as it has been since the onset of quantitative marine monitoring in the CCE. The surge in northern anchovy appears to be the product of an extremely high recruitment class in 2016 fueled by high survival of larvae or juveniles spawned in 2015 (Zwolinski et al. 2017; Stierhoff et al. 2019; Zwolinski et al. 2019).

The high recruitment of 2016 and subsequent rapid increase in population size qualifies as an ecological surprise (Lindenmayer et al. 2010). Indeed, analysis of northern anchovy stock size from 1951–2011 suggested that the population was near an all-time low from 2009–11 (MacCall et al. 2016), and subsequent analysis showed that the population remained depressed through 2015 (Thayer et al. 2017). Although some relatively small but dense aggregations remained in patches that were missed by CalCOFI and other marine sampling programs (McClatchie et al. 2018), analyses examining data sources outside of the core CalCOFI region failed to turn up significant numbers of northern anchovy (Davison et al. 2017). By every indication, overall northern anchovy population size was quite low in the CCE entering 2015.

The resurgence of northern anchovy in 2015 points out that there is not a complete mechanistic understanding of the forces that drive northern anchovy population dynamics in the CCE. Indeed, the picture is not as clear as suggested by previous correlative time-series analysis showing that northern anchovy thrive in cold regimes and Pacific sardine in warm regimes (Chavez et al. 2003; McClatchie 2012). A critical question that thus emerged from observation of the CCE since 2014 is: What went right for northern anchovy in 2015–16?

Wild fluctuations in populations sizes is a hallmark of coastal pelagic species worldwide (Dickey-Collas et al. 2014; Peck et al. 2014), and understanding the causes of these fluctuations has often been elusive (Houde 1987, 2008). In the CCE, Reuben Lasker and colleagues conducted years of research on the causes of northern anchovy population fluctuation in the 1970s and 1980s (Lasker et al. 1970; Lasker 1975; Scura and Jerde 1977; Lasker 1978, 1981, 1985). Lasker's premise, based on seminal work by Hjort (Hjort 1914, 1926), was that recruitment classes are set during a "critical period" that occurs after the yolk sack is absorbed in a larval fish. Once the yolk sack runs out, a fish must rapidly begin to feed or starve to death. Based on lab and field experiments and CalCOFI observations, Lasker's stable ocean hypothesis essentially concluded that to induce high recruitment the right species of larval prey must be available, the prey must be dense, and the ocean must be non-turbulent such that young, poor swimming larvae can catch the prey (Lasker 1985).

The stable ocean hypothesis may help explain the very successful recruitment class of 2016. There was an unusual mixture of high production coupled with high stratification in 2015, potentially creating the type of conditions conducive for larval survival identified by Lasker. Analysis of ocean conditions in areas where northern anchovy larvae were found in 2015 using Regional Ocean Modeling System (Schroeder et al. 2019) should determine if ocean conditions were stable enough to foster larval feeding. Aside from lacking turbulence, the stable ocean hypothesis states that the right type of prey at high density has to be present to feed larvae. Indeed, laboratory experiments evaluating larval northern anchovy growth demonstrated that a high proportion of larvae fed the dinoflagellate *Gymnodinium splendens* survived after 10 days while there was no survival when fed a different dinoflagellate, *Gonyaulax polyedra* (Scura and Jerde 1977). Despite the major effect of prey type on northern anchovy survival, northern anchovy did not discriminate among the two dinoflagellate species when exposed to both (Scura and Jerde 1977). Quantifying the prey available to larvae is therefore likely an important factor for mechanistically understanding drivers of larval survival and recruitment. Environmental DNA (eDNA) (Goodwin et al. 2017) holds the potential to quantify the larval prey field. eDNA analysis involves sequencing DNA from multiple species using primers that target various trophic levels. For water collected in the CCE, primers exist to enumerate the amount of DNA in bacterial, phytoplankton, zooplankton, and fish communities. Whereas the DNA from higher trophic level species such as fish

[33]Fecal samples were collected from haulout areas on San Miguel Island, California where California sea lions nursed their pups. Samples were collected between late May and September each year 1997-2018. Prey taxa were identified from hard parts recovered from the samples, and frequency of occurrence (FO) was calculated using methods described in Lance et al. (2001) and Orr et al. (2003).

probably comes from sloughed cells, DNA from bacteria and phytoplankton is more likely to come directly from the entire species. Hence, eDNA has the potential to accurately characterize the amount of different phytoplankton species available to larval fishes. eDNA has been collected regularly on CalCOFI cruises since 2014, and comparison of phytoplankton assemblages between 2015 and other years could lend insight as to the type of prey that fosters larval northern anchovy survival.

In addition to living past first feeding, fish must survive later stages to recruit into the adult population, and it is possible that conditions experienced at later stages also affect year class strength (Houde 2008). For example prey for late larvae and juveniles can significantly influence survival. As northern anchovy larvae grow, zooplankton prey becomes important (Scura and Jerde 1977). eDNA can be a useful tool for assessing the prey field of older larvae and juveniles as universal primers exist to characterize the zooplankton assemblage in the California Current (Goodwin et al. 2017). Comparison of the zooplankton assemblage between 2014, when there were relatively few young-of-the-year northern anchovy in southern California, and 2015–19 when abundances were very high, could deduce if optimal prey for older larvae and juveniles became more abundant during and subsequent to the MHW.

Given the hyper-abundance of adult northern anchovy in 2018 (Thompson et al. 2018) and 2019, another question that arises is whether the CCE is currently in a new "anchovy regime." Northern anchovy were scarce when CalCOFI began in 1949 but increased beginning in the 1960s and stayed abundant through the late 1980s (MacCall et al. 2016). Because most northern anchovy do not live past 6 years, the most recent ~30-year northern anchovy regime included multiple strong recruitment classes. Results from Southwest Fisheries Science Center coast-wide acoustic-trawl survey detected very large numbers of young northern anchovy in 2016, indicating that a high proportion of larvae spawned in 2015 survived into 2016 (Stierhoff et al. 2019). Ocean conditions in 2015 had surface water warming that originated in late 2013 in the Gulf of Alaska, impinged the coast of California by late 2014, and persisted into 2015 during the peak northern anchovy spawning period. A relatively strong El Niño during late 2015 and most of 2016 also affected the CCE (Jacox et al. 2016). Given that a strong MHW developed during summer 2019, reflecting ocean conditions that are similar and second in magnitude only to the event in to 2014–15, and that young-of-the-year northern anchovy abundance was high in southern California in 2019, it is possible that conditions will be primed for high northern anchovy recruitment in 2020. Ultimately, getting a mechanistic understanding of what controls recruitment variation in northern anchovy is the only way to predict whether this novel "regime" will last.

A new blob?

During summer 2019, another large MHW reminiscent of "the blob" of 2014–15 (Leising et al. 2015) developed in the Gulf of Alaska. This event reached its peak area in late August, but then showed a slight decline through September. The magnitude of this event is rivaled only by the 2014–15 event, with most other events over the past 38 years coming in a distant third (fig. 14). Beyond the potential impacts on small pelagics such as northern anchovy (discussed above), this new MHW is likely to impact other portions of the CCE. This new MHW reached the Washington coast in July, and then much of the Oregon coast in August. Continued upwelling in patches along the California coast, however, kept the 2019 MHW mostly offshore in much of the California region. Unlike the 2014–15 event, the early phases of the 2019 MHW did not penetrate as deeply into the water column, nor did it include secondary, strongly anomalous warm area in the further offshore regions of southern California. These are two important differences between the 2019 MHW and the "blob" of 2014–15, and thus the impacts may be different than noted before.

Even with its noted physical differences, the MHW of 2019 is still a highly unusual event in terms of its size and magnitude, and is thus likely to have many effects. The impacts of the 2014–15 event included coast-wide harmful algal blooms, shifts in species distributions, changes in planktonic community structure, increased large marine mammal entanglements, decreased salmon survival, and seabird and marine mammal die-offs and strandings (Leising et al. 2015; Cavole et al. 2016; Daly et al. 2017). Given that the 2019 MHW was present from May–September 2019 in the Pacific Northwest, it is likely that salmon returns will be low in subsequent years. Fortunately for marine mammals, the lack of the southern California offshore warming, and offshore position of this MHW for much of the rest of California, is likely to have less impact on this group than the previous event if these conditions persist. It is still too early to tell exactly how the 2019 MHW will evolve; if this event does end up proceeding more similarly to the 2014–15 event, then its impact will be apparent in 2020.

Implications for predators: winners and losers

Although the California Current broadly defines much of the marine ecosystem from Baja California, Mexico, to Washington State, USA, regional differences in population dynamics are often found within the CCE (Thompson et al. 2014; Thompson et al. 2019).

In 2018–19, south of approximately San Francisco, predators that thrive on northern anchovy were highly productive while those that require prey items other than northern anchovy tended to have low productivity. Sea lions benefited from the abundance of northern anchovy. Female sea lions give birth to a pup in May or June and undergo foraging trips ranging between the Channel Islands in the south and Monterey Bay in the north (Melin et al. 2008). In years when adequate prey is available, females produce enough milk to nourish pups, but when females are malnourished milk supply is limited and pups can starve (Melin et al. 2010). Pup condition was very poor in 2014–15, leading to the declaration of an "unusual mortality event" (McClatchie et al. 2016b). In 2016, the number of pups born was low, but pup condition improved greatly relative to 2015. The augmented pup condition of 2016 likely resulted from the female sea lions beginning to exploit the strong 2016 northern anchovy year class (adult northern anchovy abundance was positively anomalous in southern California in late spring, 2016, fig. 33). All measures of pup condition were positively anomalous in 2017 and 2018, again probably due to the high abundance of northern anchovy. Whereas many long-standing ecological patterns need to be reconsidered in light of the 2014–16 MHW (Daly et al. 2017; Koslow et al. 2019), the strong, positive correlation between summed northern anchovy/Pacific sardine abundance and sea lion pup condition (McClatchie et al. 2016a) appears to be holding strong.

Whereas sea lions overwhelmingly responded positively to the northern anchovy surge, the story varied for sea birds in California. On Southeast Farallon Island, Cassin's auklet, common murre, pelagic cormorant, pigeon guillemot, and rhinoceros auklet exhibited historically low productivity, suggesting that prey other than northern anchovy are needed for these species to thrive. This pattern mostly fits well with Santora et al. (2014) who found positive correlations between availability of krill and production of common murre, rhinoceros auklet, and Brandt's cormorant; juvenile rockfish availability to Cassin's auklet and pelagic cormorant production and sanddab to pigeon guillemot production. Life history traits of these birds explains their inability to thrive on northern anchovy. Common murre and rhinoceros auklet feed chicks whole prey items and because the northern anchovy population was comprised almost exclusively of adults, the available northern anchovy were simply too large to feed the chicks. Indeed, adult northern anchovy lying next to nests, but untouched by chicks, were common in 2019 (Peter Warzybok, personal observation). Pelagic cormorants and pigeon guillemots, by contrast, forage very close to shore where northern anchovy are typically unavailable and rely on benthic fishes such as juvenile rockfishes and sanddabs. Finally, Cassin's auklet rely on krill (Jones et al. 2018), which, in addition to juvenile rockfishes and sanddabs, were historically scarce off central California in 2019 (fig. 33). Brandt's cormorant, which feed their chicks partially digested regurgitation, was the only species that had above average productivity at Southeast Farallon Island. Hence, adult Brandt's cormorant adults directly consumed adult northern anchovy and were able to translate this prey into nourishment for the chicks. Overall, 2019 was unusual given that northern anchovy were hyperabundant but many other common prey species were scarce. This dynamic had direct and predictable effects on sea bird productivity.

North of the Farallon Islands in Yaquina Head, Oregon, common murre reproductive success was positively anomalous in 2018 and 2019 following seven consecutive years of very low production. The uptick in common murre productivity was also likely affected by different prey availability in recent years. In 2018, there was a large increase in the percent of flatfish, and a decrease in the percent of smelts, in common murre chick diets. In addition to common murre, both Brandt's cormorants and pelagic cormorants exhibited record production in 2018 and/or 2019. This enhanced production was probably also a result of the availability of abundant and appropriate prey species as well as lower predation on eggs and chicks by avian predators such as bald eagles.

Distribution shifts

The 2014–16 MHW induced northward shifts to many marine species. Prior to 1977, mesopelagic fishes such as Panama lightfish were uncommon in southern California in winter and spring, but following the 1977 regime shift, taxa inhabiting similar habitats as Panama lightfish were frequently encountered in southern California ichthyoplankton samples throughout the year (Peabody et al. 2018). Subsequent to 2014, however, these fishes became some of the most common in the ichthyoplankton assemblage. Mexican lampfish, for example, had higher springtime abundances in 2014, 2015, 2018, and 2019 than any year prior to 2014 (fig. 37). Most of these warm-water mesopelagic species vertically migrate to the epipelagic or surface at night and therefore would be available as prey to higher trophic level species such as sea lions. Indeed, Mexican lampfish otoliths were identified in sea lion scat in 2015 (Mark Lowry, personal communication). Understanding the energetic contributions of these taxa, therefore, is likely important for elucidating drivers in ecosystem dynamics.

To the north, taxa associated with warm-water conditions continued to be prevalent, and those with cool-water conditions were relatively uncommon, near shore off Oregon and Washington in 2019. Reduced survival

of yearling salmon is one ecosystem implication of the elevated abundance of warm-water prey species (Daly and Brodeur 2015; Daly et al. 2017). Shortbelly rockfish, a semi-pelagic, diminutive rockfish with a biogeographic center of distribution off central California, was also hyper-abundant near the shelf break in Oregon and Washington. Although there is not a directed fishery for shortbelly rockfish, this species sometimes is caught as bycatch by the commercial hake fishery. Hence, the Pacific Fisheries Management Council (PFMC) set an annual catch limit (AC) for shortbelly rockfish off Oregon and Washington. Because shortbelly rockfish historically did not occur in large numbers in the Pacific Northwest, the ACL was set low and the surge in abundance resulted in the hake fishery exceeding the ACL very early in the fishing season in both 2018 and 2019 (PFMC 2019b). To avoid shutting down the hake fishery the PFMC increased sixfold the shortbelly rockfish ACL (PFMC 2019a). The northern movement of species, therefore, has the potential to affect both ecosystem dynamics and ecosystem-based management.

SUMMARY

Warm conditions largely persisted into 2019 in the CCE (table 1). Whereas temperatures were close to the long-term average in early 2019, a new MHW formed in the Gulf of Alaska in May and impinged on most of the coast by September 2019. Despite the warm conditions, productivity was above average in most of the CCE. In the Pacific Northwest, fish and invertebrate assemblages included taxa associated with both warm and cool conditions. In California, northern anchovy abundance from both larval and midwater surveys was the highest in recorded history while many common forage fish (e.g., juvenile rockfishes, sanddabs) and krill were very low. This unique forage base had clear and predictable effects on predators. In Oregon, seabird productivity was the highest in years, as juvenile flatfish comprised a large portion of chick diet. In central California, production of seabirds such as Cassin's auklet, common murre, and pelagic cormorant was very low as these species could not feed chicks adult northern anchovy and smaller, more appropriate prey was mostly unavailable. Sea lions, by contrast, preyed copiously on northern anchovy and translated this energy source into successfully rearing pups. The main questions going into 2020 are: 1) Will the 2019 MHW will persist into 2020 in a manner similar to the 2014 MHW or dissipate? and 2) Are we in a novel anchovy regime that will last for years to come?

ACKNOWLEDGEMENTS

We thank with all sincerity the crews of ships that helped collect samples and the researchers that conducted land-based surveys of sea birds and marine mammals. The manuscript benefitted greatly from reviews by Greg Williams and Noelle Bowlin.

LITERATURE CITED

Adams, J., C. MacLeod, R. M. Suryan, K. D. Hyrenbach, and J. T. Harvey. 2012. Summer-time use of west coast US National Marine Sanctuaries by migrating sooty shearwaters (*Puffinus griseus*). Biological Conservation 156:105–116.

Auth, T. D. 2011. Analysis of the spring–fall epipelagic ichthyoplankton community in the northern California Current in 2004–09 and its relation to environmental factors. California Cooperative Oceanic Fisheries Investigations Reports 52:148–167.

Bakun, A. 1973. Coastal upwelling indices, west coast of North America, 1946–71. US Department of Commerce NOAA Technical Report NMFS-SSRF 671:1–103.

Barcelo, C., L. Ciannelli, and R. D. Brodeur. 2018. Pelagic marine refugia and climatically sensitive areas in an eastern boundary current upwelling system. Global Change Biology 24:668–680.

Behrenfeld, M. J., and P. G. Falkowski. 1997. Photosynthetic rates derived from satellite-based chlorophyll concentration. Limnology and Oceanography 42:1–20.

Bjorkstedt, E. P., R. Goericke, S. McClatchie, E. Weber, W. Watson, N. Lo, W. T. Peterson, R. D. Brodeur, T. Auth, J. Fisher, C. Morgan, J. Peterson, J. Largier, S. J. Bograd, R. Durazo, G. Gaxiola-Castro, B. Lavaniegos, F. P. Chavez, C. A. Collins, B. Hannah, J. Field, K. Sakuma, W. Satterthwaite, M. O'Farrell, S. Hayes, J. Harding, W. J. Sydeman, S. A. Thompson, P. Warzybok, R. Bradley, J. Jahncke, R. T. Golightly, S. R. Schneider, R. M. Suryan, A. J. Gladics, C. A. Horton, S. Y. Kim, S. R. Melin, R. L. DeLong, and J. Abell. 2012. State of the California Current 2011–12: ecosystems respond to local forcing as La Niña wavers and wanes. California Cooperative Oceanic Fisheries Investigations Reports 53:41–76.

Black, B. A., I. D. Schroeder, W. J. Sydeman, S. J. Bograd, and P. W. Lawson. 2010. Wintertime ocean conditions synchronize rockfish growth and seabird reproduction in the central California Current ecosystem. Canadian Journal of Fisheries and Aquatic Sciences 67:1149–1158.

Bograd, S. J., I. D. Schroeder, N. Sarkar, X. M. Qiu, W. J. Sydeman, and F. B. Schwing. 2009. Phenology of coastal upwelling in the California Current. Geophysical Research Letters 36.

Bond, N. A., M. F. Cronin, H. Freeland, and N. Mantua. 2015. Causes and impacts of the 2014 warm anomaly in the NE Pacific. Geophysical Research Letters 42:3414–3420.

Brodeur, R. D., E. A. Daly, C. A. Benkwitt, C. A. Morgan, and R. L. Emmett. 2011. Catching the prey: Sampling juvenile fish and invertebrate prey fields of juvenile coho and Chinook salmon during their early marine residence. Fisheries Research 108:65–73.

Brodeur, R. D., J. P. Fisher, R. L. Emmett, C. A. Morgan, and E. Casillas. 2005. Species composition and community structure of pelagic nekton off Oregon and Washington under variable oceanographic conditions. Marine Ecology Progress Series 298:41–57.

Brodeur, R. D., I. Perry, J. Boldt, L. Flostrand, M. Galbraith, J. King, J. Murphy, K. M. Sakuma, and A. R. Thompson. 2018. An unusual gelatinous plankton event in the NE Pacific: The Great Pyrosome Bloom of 2017. PICES Press 26:22–27.

Brodeur, R. D., W. T. Peterson, T. D. Auth, H. L. Soulen, M. M. Parnel, and A. A. Emerson. 2008. Abundance and diversity of coastal fish larvae as indicators of recent changes in ocean and climate conditions in the Oregon upwelling zone. Marine Ecology Progress Series 366:187–202.

Cavole, L. M., A. M. Demko, R. E. Diner, A. Giddings, I. Koester, C. M. S. Pagniello, M. L. Paulsen, A. Ramirez-Valdez, S. M. Schwenck, N. K. Yen, M. E. Zill, and P. J. S. Franks. 2016. Biological impacts of the 2013–2015 warm-water anomaly in the northeast Pacific: winners, losers, and the future. Oceanography 29:273–285.

Chavez, F. P., J. Ryan, S. E. Lluch-Cota, and M. Niquen. 2003. From anchovies to sardines and back: Multidecadal change in the Pacific Ocean. Science 299:217–221.

Checkley, D. M., and M. Lindegren. 2014. Sea Surface Temperature Variability at the Scripps Institution of Oceanography Pier. Journal of Physical Oceanography 44:2877–2892.

Checkley, D. M., P. B. Ortner, L. R. Settle, and S. R. Cummings. 1997. A continuous, underway fish egg sampler. Fisheries Oceanography 6:58–73.

Chhak, K., and E. Di Lorenzo. 2007. Decadal variations in the California Current upwelling cells. Geophysical Research Letters 34:L14604.

Daly, E. A., T. D. Auth, R. D. Brodeur, and K. C. Jacobson. 2019. Changes in juvenile salmon prey fields associated with a recent marine heat wave in the northern California Current. NPAFC Technical Report 15:in press.

Daly, E. A., T. D. Auth, R. D. Brodeur, and W. T. Peterson. 2013. Winter ichthyoplankton biomass as a predictor of early summer prey fields and survival of juvenile salmon in the northern California Current. Marine Ecology Progress Series 484:203–217.

Daly, E. A., and R. D. Brodeur. 2015. Warming Ocean Conditions Relate to Increased Trophic Requirements of Threatened and Endangered Salmon. PLoS One 10:e0144066.

Daly, E. A., R. D. Brodeur, and T. D. Auth. 2017. Anomalous ocean conditions in 2015: impacts on spring Chinook salmon and their prey field. Marine Ecology Progress Series 566:169–182.

Davison, P., W. J. Sydeman, and J. A. Thayer. 2017. Are there temporal or spatial gaps in recent estimates of anchovy off California? California Cooperative Oceanic Fisheries Investigations Reports 58:1–13.

Di Lorenzo, E., J. Fiechter, N. Schneider, A. Bracco, A. J. Miller, P. J. S. Franks, S. J. Bograd, A. M. Moore, A. C. Thomas, W. Crawford, A. Pena, and A. J. Hermann. 2009. Nutrient and salinity decadal variations in the central and eastern North Pacific. Geophysical Research Letters 36:L14601.

Di Lorenzo, E., N. Schneider, K. M. Cobb, P. J. S. Franks, K. Chhak, A. J. Miller, J. C. McWilliams, S. J. Bograd, H. Arango, E. Curchister, T. M. Powell, and P. Riviere. 2008. North Pacific Gyre Oscillation links ocean climate and ecosystem change. Geophysical Research Letters 35:L08607.

Dickey-Collas, M., G. H. Engelhard, A. Rindorf, K. Raab, S. Smout, G. Aarts, M. van Deurs, T. Brunel, A. Hoff, R. A. M. Lauerburg, S. Garthe, K. H. Anderson, F. Scott, T. van Kooten, D. Beare, and M. A. Peck. 2014. Ecosystem-based management objectives for the North Sea: riding the forage fish rollercoaster. ICES Journal of Marine Science 71:128–142.

Durazo, R., and T. R. Baumgartner. 2002. Evolution of oceanographic conditions off Baja California: 1997–1999. Progress in Oceanography 54:7–31.

Feinberg, L. R., and W. T. Peterson. 2003. Variability in duration and intensity of euphausiid spawning off central Oregon, 1996–2001. Progress in Oceanography 57:363–379.

Feinberg, L. R., W. T. Peterson, and C. Tracy Shaw. 2010. The timing and location of spawning for the Euphausiid Thysanoessa spinifera off the Oregon coast, USA. Deep Sea Research Part II: Topical Studies in Oceanography 57:572–583.

Fiedler, P. C., and N. J. Mantua. 2017. How are warm and cool years in the California Current related to ENSO? Journal Geophysical Research Oceans 122:5936–5951.

Frölicher, T. L., E. M. Fischer, and N. Gruber. 2018. Marine heat waves under global warming. Nature 560:360–364.

Goodwin, K. D., L. R. Thompson, B. Duarte, T. Kahlke, A. R. Thompson, J. C. Marques, and I. Caçador. 2017. DNA Sequencing as a Tool to Monitor Marine Ecological Status. Frontiers in Marine Science 4:107.

Gruber, N., and J. L. Sarmiento. 1997. Global patterns of marine nitrogen fixation and denitrification. Global Biogeochemical Cycles 11:235–266.

Hjort, J. 1914. Fluctuations in the great fisheries of Northern Europe viewed in the light of biological research. Rapports et Procès-Verbaux des Réunions 20:1–228.

Hjort, J. 1926. Fluctuations in the year classes of important food fishes. Journal du Conseil / Conseil Permanent International pour l'Exploration de la Mer 1:5–38.

Hobday, A. J., L. V. Alexander, S. E. Perkins, D. A. Smale, S. C. Straub, E. C. J. Oliver, J. A. Benthuysen, M. T. Burrows, M. G. Donat, M. Feng, N. J. Holbrook, P. J. Moore, H. A. Scannell, A. Sen Gupta, and T. Wernberg. 2016. A hierarchical approach to defining marine heat waves. Progress in Oceanography 141:227–238.

Horton, C. A. 2014. Top-down influences of Bald Eagles on Common Murre populations in Oregon. MS. Thesis. Oregon State University.

Houde, E. 2008. Emerging from Hjort's shadow. Journal of the Northwest Atlantic Fisheries Science 41:53–70.

Houde, E. D. 1987. Fish early life dynamics and recruitment variability. Transactions of the American Fisheries Society 2:17–29.

Hyrenbach, D. K., and R. R. Veit. 2003. Ocean warming and seabird communities of the Southern California Current System (1987–98): response at multiple temporal scales. Deep Sea Research II 50:2537–2565.

Jacox, M. G., M. A. Alexander, N. J. Mantua, J. D. Scott, G. Hervieux, R. S. Webb, and F. E. Werner. 2018a. Forcing of multiyear extreme ocean temperatures that impacted california current living marine resources in 2016. Bulletin of the American Meteorological Society 99:S27–S33.

Jacox, M. G., C. A. Edwards, E. L. Hazen, and S. J. Bograd. 2018b. Coastal upwelling revisited: Ekman, Bakun, and improved upwelling indices for the U.S. west coast. Geophysical Research Letters 123:7332–7350.

Jacox, M. G., J. Fiechter, A. M. Moore, and C. A. Edwards. 2015. ENSO and the California Current coastal upwelling response. Journal Geophysical Research Oceans 120:1691–1702.

Jacox, M. G., E. L. Hazen, K. D. Zaba, D. L. Rudnick, C. A. Edwards, A. M. Moore, and S. J. Bograd. 2016. Impacts of the 2015–2016 El Niño on the California Current System: Early assessment and comparison to past events. Geophysical Research Letters 43:7072–7080.

Jones, T., J. K. Parrish, W. T. Peterson, E. P. Bjorkstedt, N. A. Bond, L. T. Ballance, V. Bowes, J. M. Hipfner, H. K. Burgess, J. E. Dolliver, K. Lindquist, J. Lindsey, H. M. Nevins, R. R. Robertson, J. Roletto, L. Wilson, T. Joyce, and J. Harvey. 2018. Massive Mortality of a Planktivorous Seabird in Response to a Marine Heat wave. Geophysical Research Letters 45:3193–3202.

Kahru, M., M. G. Jacox, and M. D. Ohman. 2018. CCE1: Decrease in the frequency of oceanic fronts and surface chlorophyll concentration in the California Current System during the 2014–2016 northeast Pacific warm anomalies. Deep Sea Research Part I: Oceanographic Research Papers 140:4–13.

Kahru, M., R. M. Kudela, C. R. Anderson, and B. G. Mitchell. 2015a. Optimized merger of ocean chlorophyll algorithms of MODIS-Aqua and VIIRS. IEEE Geoscience and Remote Sensing Letters 12:11.

Kahru, M., R. M. Kudela, M. Manzano-Sarabia, and B. G. Mitchell. 2012. Trends in the surface chlorophyll of the California Current: Merging data from multiple ocean color satellites. Deep Sea Research II 77-80:89–98.

Kahru, M., Z. Lee, R. M. Kudela, M. Manzano-Sarabia, and B. G. Mitchell. 2015b. Multi-satellite time series of inherent optical properties in the California Current. Deep Sea Research II 112:91–106.

Koslow, J. A., P. Davison, E. Ferrer, S. Rosenberg, G. Aceves-Medina, and W. Watson. 2019. The evolving response of mesopelagic fishes to declining midwater oxygen concentrations in the southern and central California Current. ICES Journal of Marine Science 76:626–638.

Lance, M. M., A. J. Orr, S. D. Riemer, M. J. Weise, and J. L. Laake. 2001. Pinniped food habits and prey identification techniques protocol. Alaska Fisheries Science Center Processed Report 2001–04.

Lasker, R. 1975. Field criteria for survival of anchovy larvae: The relation between inshore chlorophyll maximum layers and successful first feeding. Fishery Bulletin 73:453–462.

Lasker, R. 1978. The relation between oceanographic conditions and larval anchovy food in the California Current: Identification of factors contributing to recruitment failure. Rapports et Proces-verbaux des Réunions. Conseil International pour l'Éxploration de la Mer 173:212–230.

Lasker, R. 1981. Factors contributing to variable recruitment of the northern anchovy (*Engraulis mordax*) in the California Current: Contrasting years 1975 through 1978. Rapports et Proces-verbaux des Réunions. Conseil International pour l'Éxploration de la Mer 178:375–388.

Lasker, R. 1985. What limits clupeoid production. Canadian Journal of Fisheries and Aquatic Sciences 42:31–38.

Lasker, R., H. M. Feder, G. H. Theilacker, and R. C. May. 1970. Feeding, growth, and survival of *Engraulis mordax* larvae reared in the laboratory. Marine Biology 5:345–353.

Leising, A. W., I. D. Schroeder, S. J. Bograd, J. Abell, R. Duranzo, G. Gaxiola-Castro, E. P. Bjorkstedt, J. C. Field, K. M. Sakuma, R. R. Robertson, R. Goericke, W. T. Peterson, R. D. Brodeur, C. Barcelo, T. D. Auth, E. A. Daly, R. M. Suryan, A. J. Gladics, J. M. Porquez, S. McClatchie, E. D. Weber, W. Watson, J. A. Santora, W. J. Sydeman, S. R. Melin, F. C. Chavez, R. T. Golightly, S. R. Schneider, J. Fisher, C. A. Morgan, R. Bradley, and P. Warybok. 2015. State of the California Current 2014–15: Impacts of the warm-water "Blob". California Cooperative Oceanic Fisheries Investigations Reports 56:31–68.

Lindenmayer, D. B., G. E. Likens, C. J. Krebs, and R. J. Hobbs. 2010. Improved probability of detection of ecological "surprises." Proceedings of the National Academy of Sciences 107:21957–21962.

Long, M. C., C. Deutsch, and T. Ito. 2016. Finding forced trends in oceanic oxygen. Global Biogeochemical Cycles 30:381–397.

Loredo, S. A., R. A. Orben, R. M. Suryan, D. E. Lyons, J. Adams, and S. W. Stephensen. 2019. Spatial and temporal diving behavior of non-breeding common murres during two summers of contrasting ocean conditions. Journal of Experimental Marine Biology and Ecology 517:13–24.

Lynn, R. J., and J. J. Simpson. 1987. The California Current System: The seasonal variability of its physical characteristics. Journal of Geophysical Research 92:12947–12966.

MacCall, A. D., W. J. Sydeman, P. Davison, and J. A. Thayer. 2016. Recent collapse of northern anchovy biomass off California. Fisheries Research 175:87–94.

Mantua, N., S. R. Hare, Y. Zhang, J. M. Wallace, and R. C. Francis. 1997. A Pacific decadal climate oscillation with impacts on salmon. Bulletin of the American Meteorological Society 78:1069–1079.

McClatchie, S. 2012. Sardine biomass is poorly correlated with the Pacific Decadal Oscillation off California. Geophysical Research Letters 39.

McClatchie, S. 2014. Regional fisheries oceanography of the California Current System and the CalCOFI program. Springer.

McClatchie, S., J. C. Field, A. R. Thompson, T. Gerrodette, M. Lowry, P. C. Fiedler, W. Watson, K. M. Nieto, and R. D. Vetter. 2016a. Food limitation of sea lion pups and the decline of forage off central and southern California. Royal Society Open Science 3:150628.

McClatchie, S., R. Goericke, A. Leising, T. D. Auth, E. Bjorkstedt, R. R. Robertson, R. D. Brodeur, X. Du, E. A. Daly, C. A. Morgan, F. P. Chavez, A. J. Debich, J. Hildebrand, J. C. Field, K. M. Sakuma, M. G. Jacox, M. Kahru, R. Kudela, C. Anderson, B. E. Lavaniegos, J. Gomes-Valdes, S. P. A. Jimenez-Rosenberg, R. McCabe, S. R. Melin, M. D. Ohman, L. M. Sala, B. Peterson, J. L. Fisher, I. D. Schroeder, S. J. Bograd, E. L. Hazen, S. R. Schneider, R. T. Golightly, R. M. Suryan, A. J. Gladics, S. Loredo, J. M. Porquez, A. R. Thompson, E. D. Weber, W. Watson, V. Trainer, P. Warzybok, R. Bradley, and J. Jahncke. 2016b. State of the California Current 2015–16: Comparisons with the 1997–98 El Niño. California Cooperative Oceanic Fisheries Investigations Reports 57:5–61.

McClatchie, S., R. D. Vetter, and I. L. Hendy. 2018. Forage fish, small pelagic fisheries and recovering predators: managing expectations. Animal Conservation 21:445–447.

Melin, S. R., R. L. DeLong, and D. B. Sniff. 2008. The effects of El Nino on the foraging behavior of lactating California sea lions (*Zalophus californianus californianus*) during the nonbreeding season. Canadian Journal of Zoology 86:192–206.

Melin, S. R., A. J. Orr, J. D. Harris, J. L. Laake, and R. L. DeLong. 2012. California sea lions: An indicator for integrated ecosystem assessment of the California Current System. California Cooperative Oceanic Fisheries Investigations Reports 53:140–152.

Melin, S. R., A. J. Orr, J. D. Harris, J. L. Laake, R. L. DeLong, F. M. Gulland, and S. Soudt. 2010. Unprecedented mortality of California sea lion pups associated with anomalous oceanographic conditions along the central California coast in 2009. California Cooperative Oceanic Fisheries Investigations Reports 51:182–194.

Morgan, C. A., A. M. Baptista, B. R. Beckman, R. D. Brodeur, B. J. Burke, E. A. Daly, K. C. Jacobson, E. M. Phillips, D. M. Van Doornik, and J. E. Zamon. 2019. Ocean Survival of Salmonids RME, 1/1/2018– 12/31/2018. Annual Report, 1998-014-00. 54pp. Available at: https://www.cbfish.org/Document.mvc/Viewer/P164449.

Neveu, E., A. M. Moore, C. A. Edwards, J. Fiechter, P. Drake, W. J. Crawford, M. G. Jacox, and E. Nuss. 2016. An historical analysis of the California Current circulation using ROMS 4D-Var: System configuration and diagnostics. Ocean Modelling 99:133–151.

Orr, A. J., J. L. Laake, M. I. Dhruv, A. S. Banks, R. L. DeLong, and H. R. Huber. 2003. Comparison of processing pinniped scat samples using a washing machine and nested sieves. Wildlife Society Bulletin 31:253–257.

Pacific Fisheries Management Council. 2019a. Agenda Item H.6 2020 Harvest Specifications for Cowcod and Shortbelly rockfish. https://www.pcouncil.org/wp-content/uploads/2019/09/H6_CouncilAction_SEPTEMBER2019.pdf.

Pacific Fisheries Management Council. 2019b. Groundfish Management Team Report on 2020 Harvest Specifications for Shortbelly Rockfish. Agenda Item H.6.a, Supplemental GMT Report 1, September 2019 https://www.pcouncil.org/wp-content/uploads/2019/09/H6a_Sup_GMT_Rpt1_SEPT2019BB.pdf.

Peabody, C. E., A. R. Thompson, D. F. Sax, R. E. Morse, and C. T. Perretti. 2018. Decadal regime shifts in southern California's ichthyoplankton assemblage. Marine Ecology Progress Series 607:71–83.

Peck, M. A., S. Neuenfeldt, T. E. Essington, V. M. Trenkel, A. Takasuka, H. Gislason, M. Dickey-Collas, K. H. Anderson, L. Ravn-Jonsen, N. Vestergaard, S. F. Kvamsdal, A. Gardmark, J. Link, and J. C. Rice. 2014. Forage fish interactions: a symposium on "Creating tools for ecosystem-based management of marine resources." ICES Journal of Marine Science 71:1–4.

Peláez, J., and J. A. McGowan. 1986. Phytoplankton pigment patterns in the California Current as determined by satellite1. Limnology and Oceanography 31:927–950.

Peterson, W. T., J. L. Fisher, P. T. Strub, X. Du, C. Risien, J. Peterson, and C. T. Shaw. 2017. The pelagic ecosystem in the Northern California Current off Oregon during the 2014–2016 warm anomalies within the context of the past 20 years. Journal of Geophysical Research: Oceans 122:7267–7290.

Phillips, E. M., M. H. Horn, J. Adams, and J. E. Zamon. 2018. Selective occupancy of a persistent yet variable coastal river plume by two seabird species. Marine Ecology Progress Series 594:245–261.

Phillips, E. M., J. K. Horne, and J. E. Zamon. 2017. Predator-prey interactions influenced by a dynamic river plume. Canadian Journal of Fisheries and Aquatic Sciences 74:1375–1390.

Phillips, E. M., J. K. Horne, J. E. Zamon, J. J. Felis, and J. Adams. 2019. Does perspective matter? A case study comparing Eulerian and Lagrangian estimates of common murre (Uriaaalge) distributions. Ecology and Evolution 9:1–15.

Pozo Buil, M., and E. Di Lorenzo. 2017. Decadal dynamics and predictability of oxygen and subsurface tracers in the California Current System. Geophysical Research Letters 44:4204–4213.

Ralston, S., K. Sakuma, and J. Field. 2013. Interannual variation in pelagic juvenile rockfish (*Sebastes* spp.) abundance—going with the flow. Fisheries Oceanography 22:288–308.

Reynolds, R. W., T. M. Smith, C. Liu, D. B. Chelton, K. S. Casey, and M. G. Schlax. 2007. Daily High-resolution Blended Analyses for sea surface temperature. Journal of Climate 20:5473–5496.

Sakuma, K. M., J. C. Field, B. B. Marinovic, C. N. Carrion, N. J. Mantua, and S. Ralston. 2016. Anomalous epipelagic micronekton assemblage patterns in the neritic waters of the California Current in spring 2015 during a period of extreme ocean conditions. California Cooperative Oceanic Fisheries Investigations Reports 57:163–183.

Santora, J. A., I. D. Schroeder, J. C. Field, B. K. Wells, and W. J. Sydeman. 2014. Spatio-temporal dynamics of ocean conditions and forage taxa reveal regional structuring of seabird-prey relationships. Ecological Applications 24:1730–1747.

Santora, J. A., and W. J. Sydeman. 2015. Persistence of hotspots and variability of seabird species richness and abundance in the southern California Current. Ecosphere 6:214.

Schmidtko, S., L. Stramma, and M. Visbeck. 2017. Decline in global oceanic oxygen content during the past five decades. Nature 542:335–339.

Schroeder, I. D., B. A. Black, W. J. Sydeman, S. J. Bograd, E. L. Hazen, J. A. Santora, and B. K. Wells. 2013. The North Pacific High and wintertime preconditioning of California Current productivity. Geophysical Research Letters 40:541–546.

Schroeder, I. D., J. A. Santora, S. J. Bograd, E. L. Hazen, K. M. Sakuma, A. M. Moore, C. A. Edwards, B. K. Wells, and J. C. Field. 2019. Source water variability as a driver of rockfish recruitment in the California Current Ecosystem: implications for climate change and fisheries management. Canadian Journal of Fisheries and Aquatic Sciences 76:950–960.

Schroeder, I. D., W. J. Sydeman, N. Sarkar, S. A. Thompson, S. J. Bograd, and F. B. Schwing. 2009. Winter pre-conditioning of seabird phenology in the California Current. Marine Ecology Progress Series 393:211–233.

Schwartzlose, R. A., J. Alheit, A. Bakun, T. R. Baumgartner, R. Cloete, R. J. M. Crawford, W. J. Fletcher, Y. Green-Ruiz, E. Hagen, T. Kawasaki, D. Lluch-Beldae, S. E. Lluch-Cota, A. D. MacCall, Y. Matsuura, M. O. Nevarez-Martinez, R. H. Parrish, C. Roy, R. Serra, K. V. Shust, M. N. Ward, and J. Z. Zuzunaga. 1999. Worldwide large-scale fluctuations of sardine and anchovy populations. South African Journal of Marine Science 21:289–347.

Schwing, F. B., M. O'Farrell, J. M. Steger, and K. Baltz. 1996. Coastal Upwelling indices west coast of North America. NOAA Technical Report NMFS SWFSC NMFS SWFSC 231.

Scura, E. D., and C. W. Jerde. 1977. Various species of phytoplankton as food for larval northern anchovy, *Engraulis mordax*, and relative nutritional value of the dinoflagellates *Gymnodinium splendens* and *Gonyaulax polyedra*. Fisheries Bulletin 75:577–583.

Stierhoff, K. L., J. P. Zwolinski, and D. A. Demer. 2019. Distribution, biomass, and demography of coastal pelagic fishes in the California Current Ecosystem during summer 2018 based on acoustic-trawl sampling. U.S. Department of Commerce, NOAA Technical Memorandum NMFS-SWFSC-613.

Sydeman, W. J., S. A. Thompson, J. A. Santora, J. A. Koslow, R. Goericke, and M. D. Ohman. 2015. Climate-ecosystem change off southern California: Time-dependent seabird predator-prey numerical responses. Deep Sea Research II 112:158–170.

Thayer, J. A., A. D. MacCall, P. C. Davison, and W. J. Sydeman. 2017. California anchovy population remains low, 2012–16. California Cooperative Oceanic Fisheries Investigations Reports 58:69–76.

Thompson, A. R., T. D. Auth, R. D. Brodeur, N. M. Bowlin, and W. Watson. 2014. Dynamics of larval fish assembalges in the California Current System: a comparative study between Oregon and southern California. Marine Ecology Progress Series 506:193–212.

Thompson, A. R., C. J. Harvey, W. J. Sydeman, C. Barceló, S. J. Bograd, R. D. Brodeur, J. Fiechter, J. C. Field, N. Garfield, T. P. Good, E. L. Hazen, M. E. Hunsicker, K. Jacobson, M. G. Jacox, A. Leising, J. Lindsay, S. R. Melin, J. A. Santora, I. D. Schroeder, J. A. Thayer, B. K. Wells, and G. D. Williams. 2019. Indicators of pelagic forage community shifts in the California Current Large Marine Ecosystem, 1998–2016. Ecological Indicators 105:215–228.

Thompson, A. R., I. D. Schroeder, S. J. Bograd, E. L. Hazen, M. G. Jacox, A. Leising, B. K. Wells, J. L. Largier, J. L. Fisher, K. Jacobson, S. Zeman, E. P. Bjorkstedt, R. R. Robertson, F. P. Chavez, M. Kahru, R. Goericke, S. McClatchie, C. E. Peabody, T. R. Baumgartner, B. E. Lavaniegos, J. Gomez-Valdes, R. D. Brodeur, E. A. Daly, C. A. Morgan, T. D. Auth, B. J. Burke, J. C. Field, K. M. Sakuma, E. D. Weber, W. Watson, J. Ccoates, R. Schoenbaum, L. Rogers-Bennett, R. M. Suryan, J. Dolliver, S. Loredo, J. E. Zamon, S. R. Schneider, R. T. Golightly, P. Warzybok, J. Jahncke, J. A. Santora, S. A. Thompson, W. J. Sydeman, and S. R. Melin. 2018. State of the Callifornia Current 2017–18: Still not quite normal in the north and getting interesting in the south. California Cooperative Oceanic Fisheries Investigations Reports 59:1–66.

Varoujean, D. H., and D. R. Matthews. 1983. Distribution, abundance, and feeding habits of seabirds off the Columbia River, May–June 1982. Report No. OIMB 83-1, University of Oregon Institute of Marine Biology, Charleston. 28 pp.

Velarde, E., E. Ezcurra, M. H. Horn, and R. T. Patton. 2015. Warm oceanographic anomalies and fishing pressure drive seabird nesting north. Science Advances 1:e1400210.

Wells, B. K., I. D. Schroeder, S. J. Bograd, E. L. Hazen, M. G. Jacox, A. Leising, N. Mantua, J. A. Santora, J. L. Fisher, W. T. Peterson, E. Bjorkstedt, R. R. Robertson, F. P. Chavez, R. Goericke, R. Kudela, C. Anderson, B. E. Lavaniegos, J. Gomez-Valdes, R. D. Brodeur, E. A. Daly, C. A. Morgan, T. D. Auth, J. C. Field, K. M. Sakuma, S. McClatchie, A. R. Thompson, E. D. Weber, W. Watson, R. M. Suryan, J. K. Parrish, J. Dolliver, S. Loredo, J. M. Porquez, J. E. Zamon, S. R. Schneider, R. T. Golightly, P. Warzybok, R. Bradley, J. Jahncke, W. J. Sydeman, S. R. Melin, J. A. Hildebrand, A. J. Debich, and B. Thayre. 2017. State of the California Current 2016–17: Still anything but "normal" in the north. CalCOFI Reports 58:1–55.

Zamon, J. E., E. M. Phillips, and T. J. Guy. 2014. Marine bird aggregations associated with the tidally-driven plume and plume fronts of the Columbia River. Deep Sea Research II 107:85–95.

Zwolinski, J. P., D. A. Demer, B. J. Macewicz, S. Mau, D. Murfin, D. Palance, J. S. Renfree, T. S. Sessions, and K. Stierhoff. 2017. Distibution, biomass and demography of the central-stock of Northern Anchovy during summer 2016, estimated from acoustic-trawl sampling. U.S. Department of Commerce NOAA-TM-NMFS-SWFSC-572.

Zwolinski, J. P., K. L. Stierhoff, and D. A. Demer. 2019. Distribution, biomass, and demography of coastal pelagic fishes in the California Current Ecosystem during summer 2017 based on acoustic-trawl sampling. U.S. Department of Commerce, NOAA Technical Memorandum NMFS-SWFSC-610.

SUPPLEMENTAL FIGURES

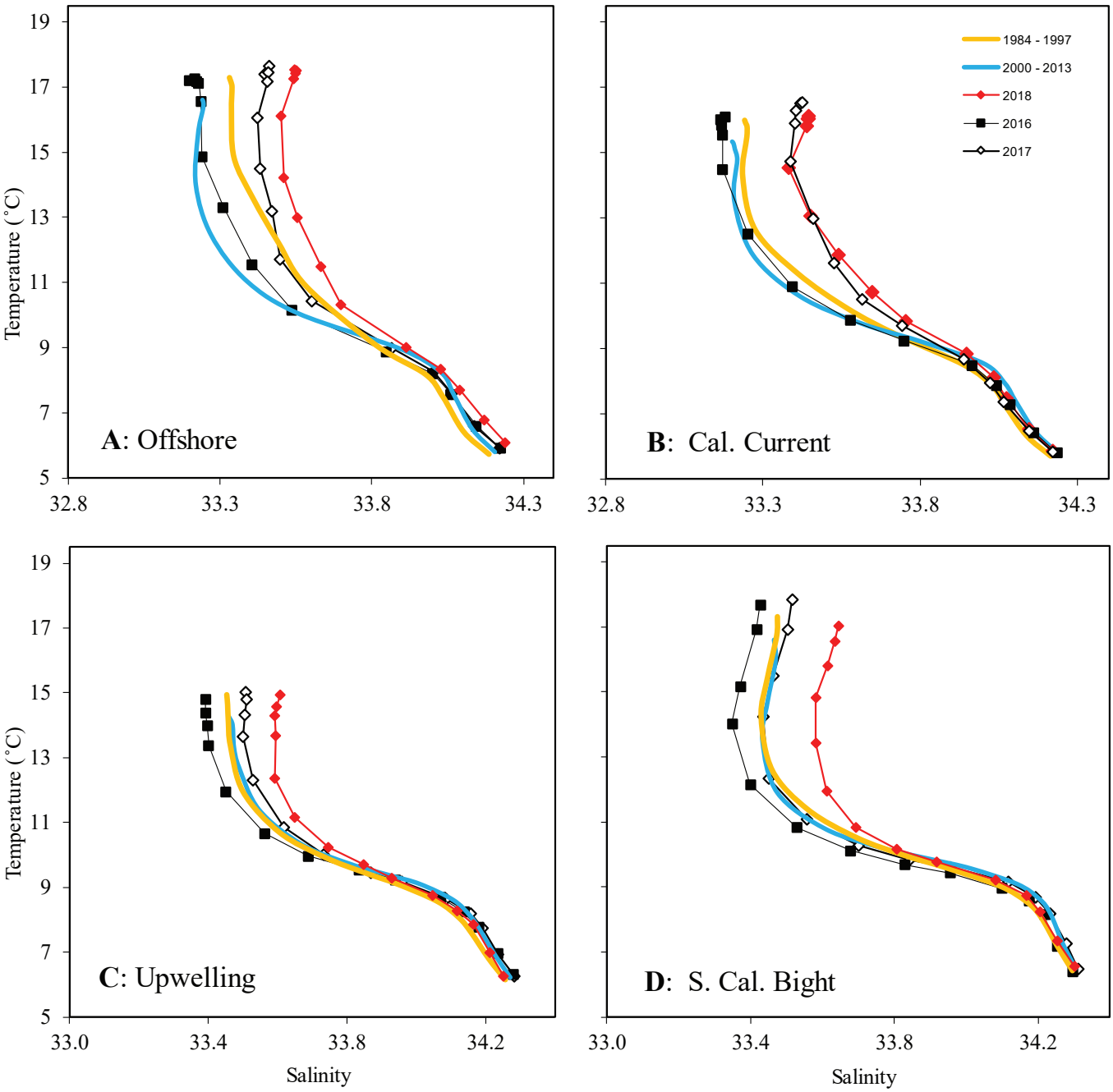

Figure S1. Annual average TS properties for representative areas of the CalCOFI region for different time periods, i.e. 1984 to 1997, 2000 to 2013, 2016, 2017 and 2018. Annual averages are based on ENSO years, i.e., the time from June of the target year until May of the target year plus one. The regions are: A: offshore (CalCOFI Lines 90-93, Stations ≥ 90; L87-77, St ≥ 100), B. California Current region (L90 St 60-80, L87-77 St 70-90), C. upwelling (L87 St 51-60, L82 St47, L77-80 St ≤ 60), and D: Southern California Bight (L 90-93 St ≤ 45, L87 St ≤ 40, L83 St ≤ 42). Each data point represents the average TS characteristic of one standard depth level (0, 10, 20, 30, 50, 75,100, 125, 150, 200, 250, 300, 400, and 500 m) for the specified time period and area.

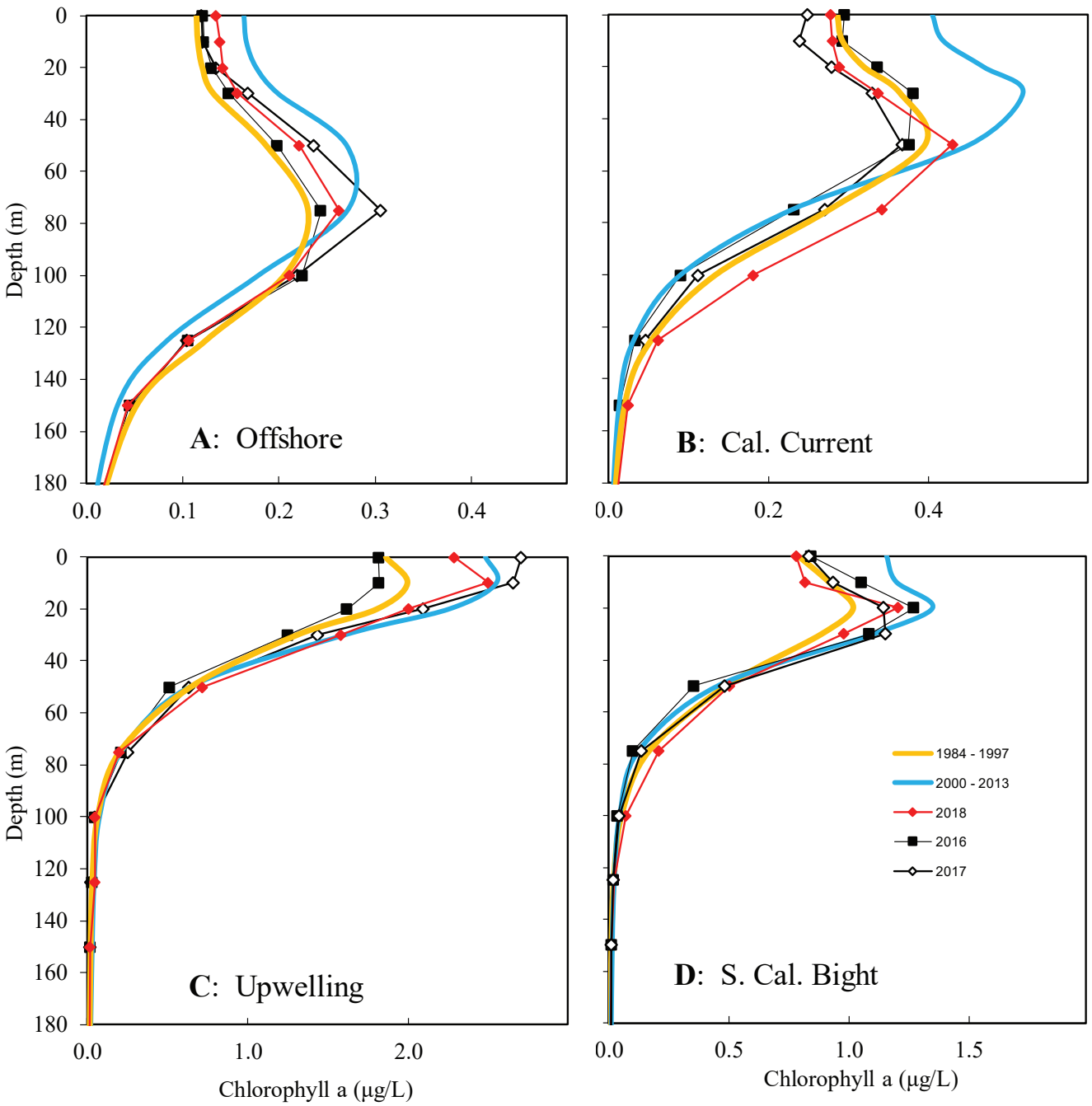

Figure S2. Depth profiles of Chl *a* for the times and four areas of the CalCOFI region that are defined in CalCOFI Fig. S1. Data were derived and are presented as described in CalCOFI Fig. S1.

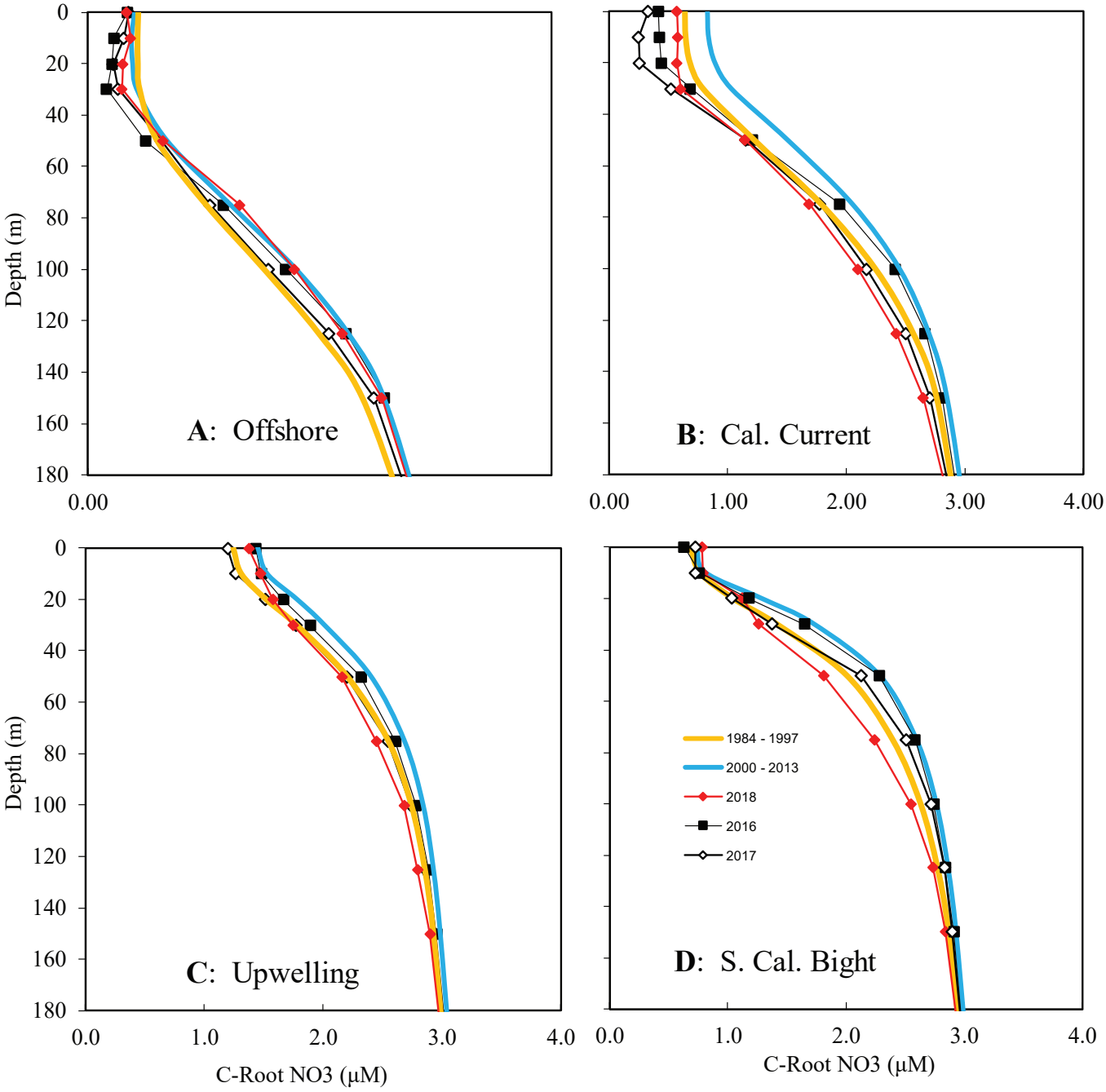

Figure S3. Depth profiles of cuberoot of nitrate for the times and four areas of the CalCOFI region that are defined in CalCOFI Fig. S1. Data were derived and are presented as described in CalCOFI Fig. S1.

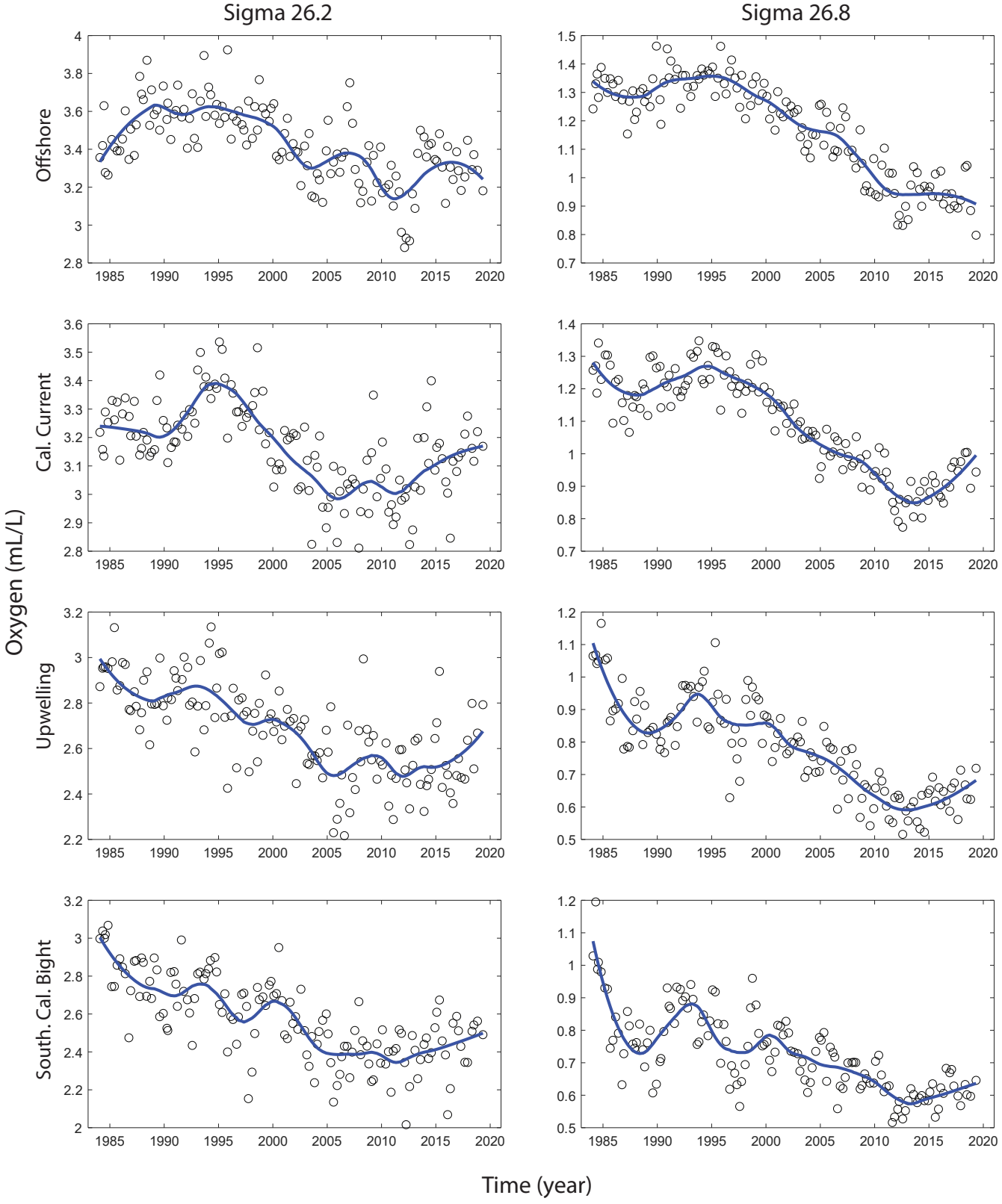

Figure S4. Oxygen concentration anomalies at the σ_t 26.2 and 26.8 isopycnals plotted as described in CalCOFI Fig. 2 for the four regions as defined in the legend of CalCOFI Fig. S1.